NATIONAL TECHNICAL UNIVERSITY OF ATHENS
SCHOOL OF MECHANICAL ENGINEERING
SECTION OF MANUFACTURING TECHNOLOGY

DIPLOMA THESIS

CRASHWORTHINESS BEHAVIOR OF THIN-WALLED BI-TUBES
UNDER AXIAL COLLAPSE

KONSTANTINA D. KARANTZA

Supervisor Professor: D. MANOLAKOS

Athens
February 2020

To my father Dionysios

and my mother Dimitra

Abstract

The aim of current diploma thesis study is to investigate the crashworthiness behavior of circular thin-walled bi-material tubes, oftenly called as bi-tubes, by both conducting experimental tests and carrying out numerical simulations. For the needs of this study, four bi-tube specimens 100 mm long are initially constructed by combining steel and ertalon tubes of different thickness. The four examined bi-tube specimens consist of different thickness and combination of steel/ertalon as internal/external tubes. The variety of combination of examined specimens is selected in order to capture both the effects of single tube components thickness ratio and combination of hard (steel) and soft (ertalon) tubes as internal or external tubes.

The bi-tube specimens are then examined by conducting experimental tests in quasi-static and dry conditions. During each test, the examined specimens are compressed with loading rate of 10mm/min until their final length of 40mm, causing thus a shortening of 60 mm. For each crushed bi-tube specimen, the processing of the recorded data allows the calculation of the crashworthiness response characteristics, such as load-deflection curve, peak crushing force, mean sustained load, amount of absorbed energy and specific energy absorption. Also, the occurred collapse mechanism is observed too by capturing different states of each deformed specimen during its collapse.

Next, numerical simulation are carried out in LS-DYNA software after the development of the examined bi-tube models. The developed models are simulated by adjusting a crushing speed of 0.5 mm/msec. The provided results are both load-deflection curve, followed by the calculation of the appropriate crashworthiness response characteristics, and the occurred collapse mechanism. Following, the results from the experimental tests and the numerical simulations are compared to each other.

It is concluded that increasing bi-tube external diameter results in greater sustained load and energy absorption capability, while greater bi-tube thickness also reacts on higher amounts of absorbed energy. Further, the bi-tube which combines a hard (steel) tube and a softer (ertalon) tube as external and internal ones, is proved to be the more crashworthy structure revealing greater energy absorption capability. Also, in this occasion, the adhesion between the two tubes seems to be almost fully maintained, while in the case of ertalon external tube and steel internal one, the adhesion is lost by keeping the two tubes partially in contact only in the area where convolution have been formulated. Both experimental tests and numerical simulations revealed a mixed collapse mechanism for all four examined bi-tubes, while the matching between experimental and simulation results was more sufficient in the bi-tube specimens

which combine steel external tube and ertalon internal one. Finally, peak crushing force proved to be more complicate to be predicted compared to mean sustained load, which revealed lower relative errors between experimental data and numerical simulation results.

Acknowledgements

I would like to deeply thank my thesis supervisor professor D.Manolakos for entrusting me with such an interesting subject, as well as for his valuable guidance, advice and constant encouragement throughout my diploma thesis study.

I also gratefully acknowledge Dr. P.Kostazos for his continued advice and useful comments and suggestions regarding to the models development and simulation in LS-DYNA software and their provided results assessment, while I would like to express my grateful thanks to the technical staff of the Manufacturing Technology Lab of NTUA for their useful help on specimens productions and experimental tests conduction.

Finally, I would like to specially thank my family for their continued encouragement and support during my studies and throughout my life

Contents

List of Figures

List of Tables

1. Introduction

1.1 Introduction to crashworthiness

The desire of designers and engineers to increase occupant safety in vehicle structures has brought the need of improving the crashworthiness characteristics of structures. Crashworthiness is a design philosophy applied in every vehicle structure of the current transportation field, from automobiles and trains to aircrafts and helicopters. The overall objective of designing for crashworthiness is to reduce the impact of crash on the passengers resulting in increased structure safety levels. The reduction of crash impact aims to eliminate injuries and fatalities in the case of mild impacts, and minimize them in severe collisions. Also, modern crashworthy vehicles are designed to control the extent of crash impact damage by dissipating large amounts of crushing energy, while an adequate space for the passengers has to be maintained in addition. Thus, the design of crashworthy structures targets in absorbing the greater possible amount of energy produced during the crash. However, the energy absorption is preferable to be accomplished with controllable collapse in the event of a collision, and within certain constraints, such as limits on force transmission, permissible deformations and failure.

More specifically, if only small deformations are permitted regarding to occupant space, then large amounts of momentum transfer and force levels will be occurred, which may be unacceptable to be experienced from the passengers. On the other hand, a limit in permanent deformations must be enforced to retain a minimum volume for survival. So, in order to achieve an optimal combination of permitted frame deformation and transmitted forces to passengers, specific energy absorbing devices, strategically placed in the appropriate frame positions, are applied to vehicle structures to improve their crashworthiness behavior. Energy absorbers are mainly constructed by metals (steel, aluminum etc.), polymers, composite or bi-metallic materials. The two latter materials are widely used in current technology, as they provide light structures capable of absorbing large amounts of impact energy under axial crushing, bending and/or combined loading conditions. Further, research studies and experiments propose that thin-walled structures are more beneficial for use as energy absorbers, as they provide devices with high energy absorption capability and reduced total weight. The greater energy absorption capacity of a thin-walled structure is based on the fact that a thin-walled structure requires lower crushing loads to behave plastically and dissipate amounts of energy. In contrast, compact structures require greater loads to receive plastic deformations, which may keep them behaving completely elastic without dissipating any energy, or deform them in low strain levels, reducing the energy absorption capability in every case. As a result, the energy absorbers are preferable to be thin-walled structures.

In general, crashworthiness behavior and survivability can be improved by modifying the structural geometry or by introducing specifically designed energy absorbing devices. Both research directions have been investigated from the designers to produce crashworthy structures which dissipate the kinetic energy of crash in the most effective way. Figure 1 illustrates typical frame positions in which energy absorbers are usually placed for both automobile and aircraft's fuselage cases. As shown, energy absorbers are used in modern structures as collapsible tubular rails in the front end of automobiles, or in the case of aircrafts, as collapsible floor stanchions and beams.

The new design philosophy of crashworthiness has replaced more traditional design approaches, which considered strong, massive and stiff structures as the better ones. Such approaches have been rejected by current design trends as they fail to dissipate energy during impact, conveying it to the occupants and the cargo. In contrast, crashworthy structures are designed to provide a progressive controllable collapse, during of which they ensure a safe dissipation of adequate amounts of kinetic energy.

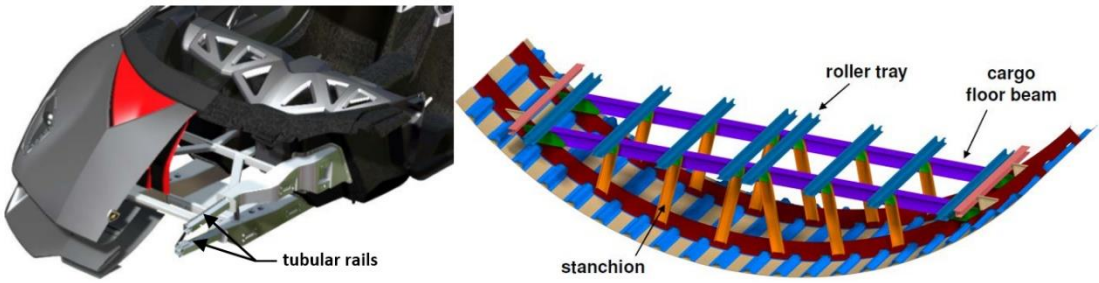

Figure 1 Energy absorbers positions in automobile and aircraft's fuselage structures, [1]

A structure designed to satisfy the main crashworthiness requirements must ensure five conditions for survival which are:

- Maintaining sufficient and survivable occupant space
- Providing adequate occupant restraint
- Limiting acceleration and loads experienced from the occupants by employing energy absorbing devices
- Providing protection from the release of items of mass
- Allowing for a safe post-crash egress from the vehicle

Regarding to aircraft structures, crashworthiness regulations have been set in Advisory Circular (AC) of Federal Aviation Administration (FAA) as suggested in [2]. The regulations were introduced based on experiences gained during actual aircraft operations. In order to set the appropriate regulations, FAA considered the impact response characteristics of the fuselage to examine the crashworthiness efficiency of aircrafts. On the other hand, regarding to automobiles, the crashworthiness regulations are set based on either past experience from incidents and accidents or according to safety rules.

The need of designing for crashworthiness has turned the research interest into investigating how structures response in crushing conditions. The complexity of understanding how factors, such as structure materials, geometry, failure mechanisms and crushing modes, affect the energy absorption capability of the structures, has led the engineering community to carry out several research works. As a result, many studies on crashworthiness behavior and energy absorption capability of structures have been carried out by conducting experimental crash tests and by using finite element analysis (FEA) numerical simulations.

1.2 Aim of this thesis

The aim of this diploma thesis is to analyze and investigate the crashworthiness behavior of thin-walled bi-material tubes (bi-tubes) under axial crushing and compressive loads. At first, thin-walled circular bi-tubes are constructed from the materials of Steel/Ertalon. At next, analysis is carried out by firstly conducting quasi-static experimental crush tests for the constructed specimens, which are next examined in axial crushing by applying compressive loads. Secondly, the LS-DYNA finite element analysis software is utilized as the modelling tool in which FEA numerical simulations are carried out to study the crashworthiness behavior of the four examined specimens. Finally, the experimental results are compared to the numerical ones in order to provide useful conclusions about the crashworthiness response of thin-walled circular bi-tubes under axial crushing and compressive loads. Specifically, the analysis of the present thesis aims to investigate the accuracy of the numerical simulations in predicting the energy absorption capability of the specimens, the maximum presented loads, the predicted load-displacement curves, the failure modes and the mechanisms of collapse for each specimen.

1.3 Scope

In the initial part of this diploma thesis, a short introduction into crashworthiness is presented in a preliminary and theoretical level. The aim of the current chapter is the description of the need of implementing the crashworthiness philosophy in design of vehicle structures. For this reason, the advantages which crashworthiness brings, and some main regulations and requirements which a crashworthy structure must satisfy are described. Finally, this initial part ends with the presentation of the aim of this diploma thesis.

Chapter 2 presents the main characteristics of crashworthiness behavior of structures in more detail and from a more technical point of view. Also, the way many factors affect the energy absorption capability is described, followed by a detailed description of the failure mechanisms and crushing modes which can be observed under crushing conditions. At next, the two main types of experimental crush tests which can be conducted for crashworthiness analysis are described

by presenting the benefits and the drawbacks of each one. Finally, chapter 2 summarizes and reviews a number of research studies on crashworthiness response, presenting a theoretical analysis to calculate the mean crushing force for bi-material thin-walled structures.

Chapter 3 presents a description of bimetallic materials in theoretical level, informing about mechanical properties and their main applications.

Following, the experimental crush tests carried out are described in chapter 4. More specifically, initially, the construction of four examined bi-tube specimens and the machine in which the tests were conducted are described. At next, the experimental results are provided and discussed by assessments and by observations of moments during collapse to obtain the failure mechanism and crushing mode. Finally, critical crashworthiness response characteristics are computed based on the experimental data, while the collapse mechanism is observed and discussed too.

Chapter 5 presents the modelling approach followed to simulate each test case. Initially, a short description of LS-DYNA software is presented, followed by the FEA models development. After that, the numerical results are presented and assessed by both calculating the main crashworthiness characteristics and observing the predicted collapse mechanism for each examined bi-tube specimen.

Chapter 6 presents the respective comparisons between the experimental and the numerical results with the relative errors. The comparison offers the opportunity to provide useful conclusions for the crashworthiness behavior of the examined thin-walled bi-tube structures and to examine the accuracy and validity of the numerical simulations. After the comparison between experimental and numerical simulation results in terms of crashworthiness response characteristics, the occurred collapse mechanisms for each bi-tube is also observed and discussed.

Finally, chapter 7 contains a short summary of the aim of this thesis, the utilized modelling tool and the conducted experiments and numerical simulations with their revealed results too. Critical conclusions are next extracted for both crashworthiness response characteristics and collapse mechanisms, while finally some recommendations about future work are made.

2. Crashworthiness

2.1 Energy absorption characteristics

The main aim of designing crashworthy structures is to improve their capability in absorbing the amount of energy produced during a crush event. A typical response of a crushed structure in terms of applied force versus shortening (or stroke) of the structure is depicted in Figure 2. Some basic terms referring to crashworthiness behavior are pointed-out below.

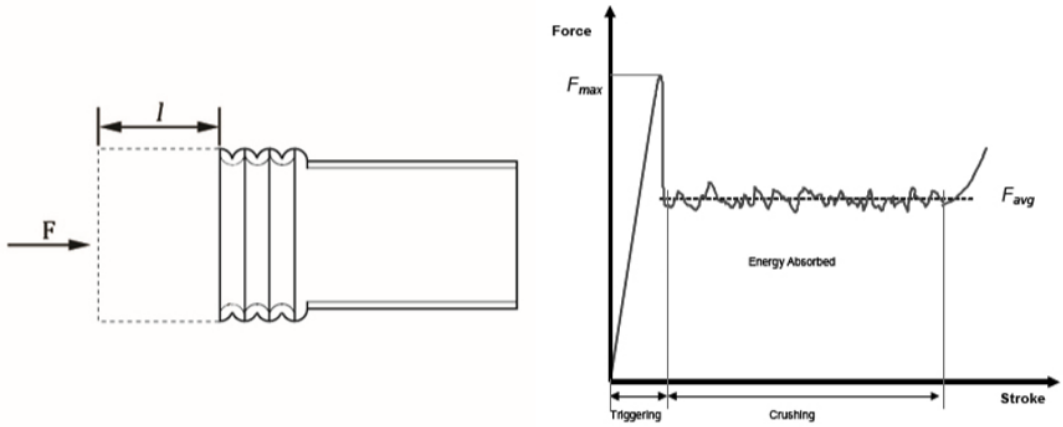

Figure 2 Load-displacement curve of a crushed structure, [3]

- Stroke, or displacement, is the structure length being compressed (shortened) during the crush.
- Peak force (F_{max}), or Peak Crush Force (PCF), is the maximum load observed in the force-stroke (or force-displacement) diagram.
- Average crush force (F_{avg}), or sustained load, is the displacement-averaged or time-averaged value of crush force.

$$F_{avg} = \frac{1}{s} \cdot \int_0^s F \cdot ds \tag{1}$$

1. Crush initiator, or trigger mechanism, is a design feature that causes the start of a progressive collapse of the structure, avoiding the tendency of an unpredictable and unstable collapse which sometimes is possible to be occurred.
2. Crush Force Efficiency (CFE), or Load uniformity (LU), is the ratio of mean sustained load to the peak load. CFE represents the uniformity of applied load considering the displacement.

$$CFE = \frac{F_{avg}}{F_{max}} \tag{2}$$

3. Energy Absorption (EA) is the amount of crush kinetic energy dissipated from the structure. It is equal to the total area under the load-stroke curve (Figure 3).

$$EA = \int_0^s F \cdot ds = F_{avg} \cdot s \tag{3}$$

4. Specific Energy Absorption (SEA) is the absorbed energy per unit mass of crushed structure expressed in J/g.

$$SEA = \frac{\int_0^s F \cdot ds}{m} = \frac{EA}{\rho \cdot A \cdot l} \tag{4}$$

5. Stroke Efficiency (SE) is the ratio of final structure length (l_s) after the crush to the initial one (l_0) before the crush.

$$SE = \frac{l_s}{l_0} \tag{5}$$

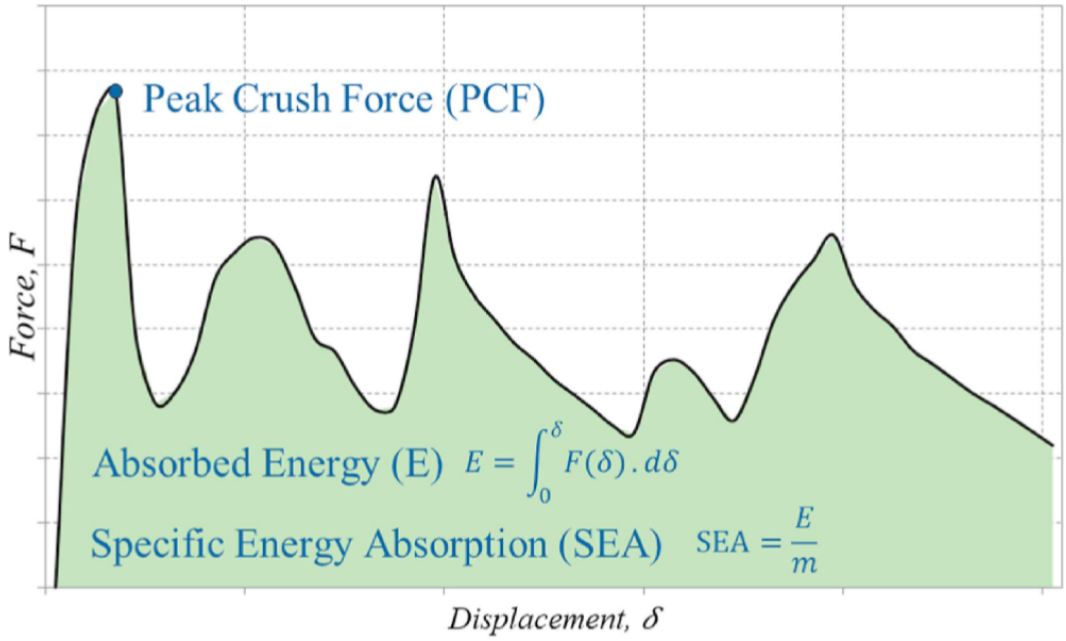

Figure 3 Energy absorption basic terms referring to load-stroke diagram, [4]

Structures of high energy absorption capability can be described as efficient ones in terms of crashworthiness. However, the specific energy absorption (SEA) is the main parameter for the evaluation of material efficiency. As a result, the comparison of two structures in terms of energy absorption capability is made comparing their SEA values. Obviously, the structure with greater SEA is the more efficient one. Additionally, a parameter of high importance is the peak crush force (PCF or F_{max}). PCF must be a reasonable value because if peak load is too great, the crush load may not reach the required force level, which is the F_{max}, to deform the structure plastically, meaning that the structure will retain behaving completely elastic without absorbing any energy. PCF is a function of

geometric (thickness in case of thin-walled structures) and material characteristics of the structure.

Further, the crushing force efficiency (CFE) is an important factor representing the decelerating force which is applied to the passengers as the structure is loaded from maximum load to sustained one. A CFE of 100% is an ideal value as it provides a completely uniform applied load of high energy absorption. Finally, stroke efficiency (SE) is preferred to be as great as possible, resulting in high plastic deformations which increase the energy absorption capability of the structure and make the use of the material efficient in terms of crashworthiness behavior. A representative example of the effect of SE on energy absorption capacity is the comparison between brittle and ductile materials. As shows, ductile materials are characterized by greater SE as they can be deformed plastically without failing, resulting in greater energy absorption capacity compared to brittle.

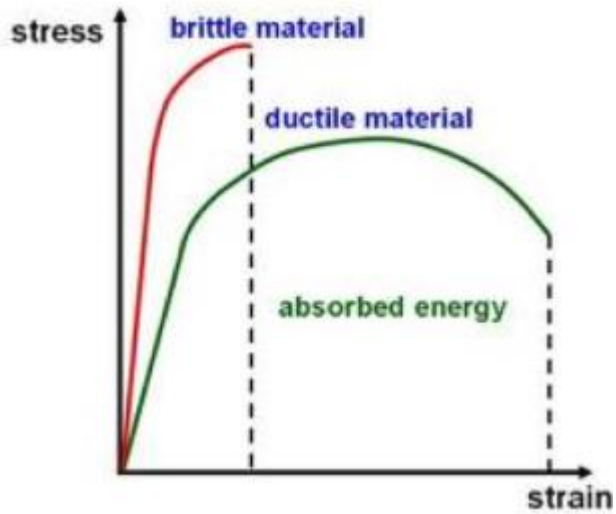

Figure 4 Energy absorption for brittle and ductile materials, [5]

Summarizing, an ideal energy absorber is characterized by high specific energy absorption (SEA), a reasonable peak load, a crushing force efficiency (CFE) of 100% and a stroke efficiency (SE) as closer to 100% as possible. The following figures depict typical energy absorbing devices for frontal longitudinal crushes in case of automobiles.

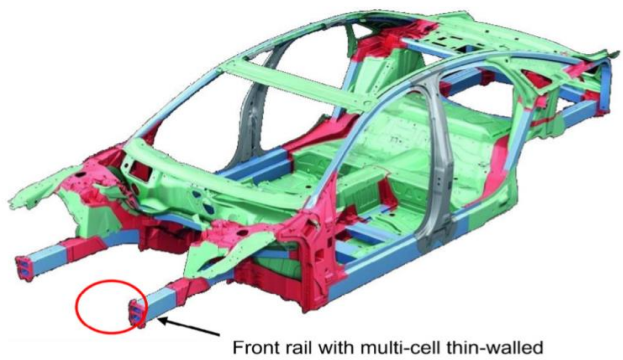

Figure 5 Frontal longitudinal energy absorbers of typical automobile, [6]

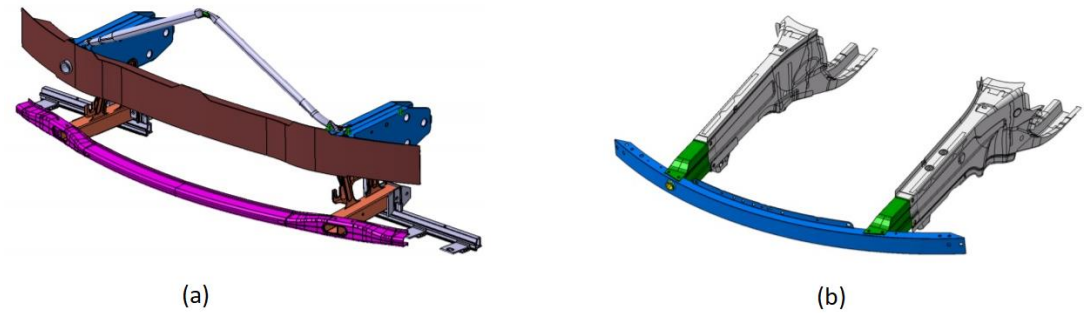

Figure 6 Energy absorbing system of front end of automobiles, (a) BMW 3 series model and (b) Mercedes C Class, [7]

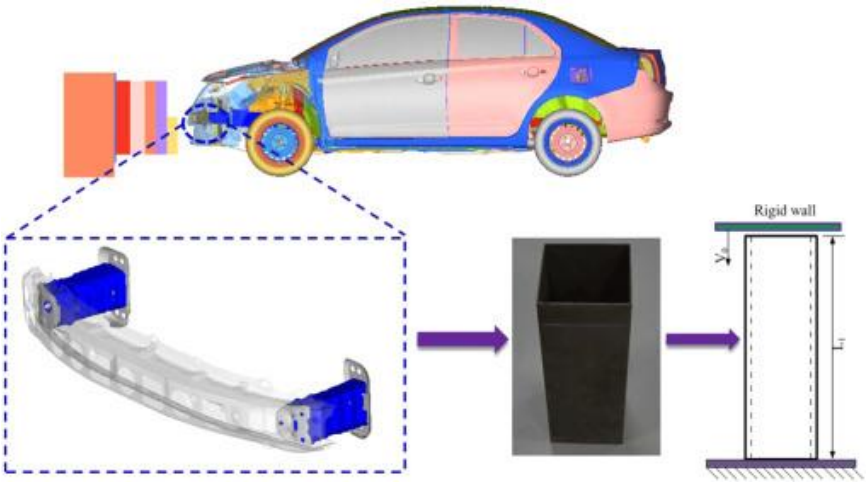

Figure 7 Energy absorbing system of front end of automobiles, [7]

The two next figures show the crashworthiness design of the fuselage of aircrafts, in which energy absorbing devices (beams and stanchions) are located in order to dissipate the necessary amounts of energy under loading, during vertical crushing conditions of the fuselage.

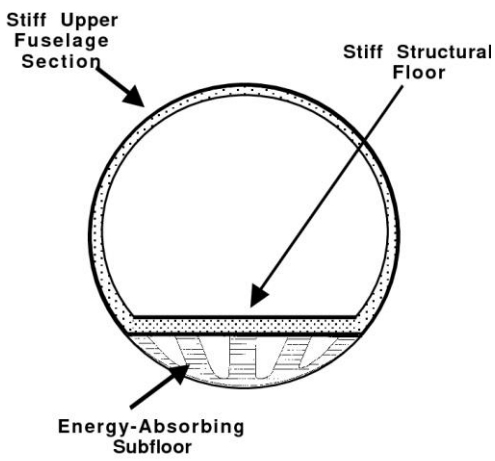

Figure 8 Crashworthiness design of aircraft's fuselage, [8]

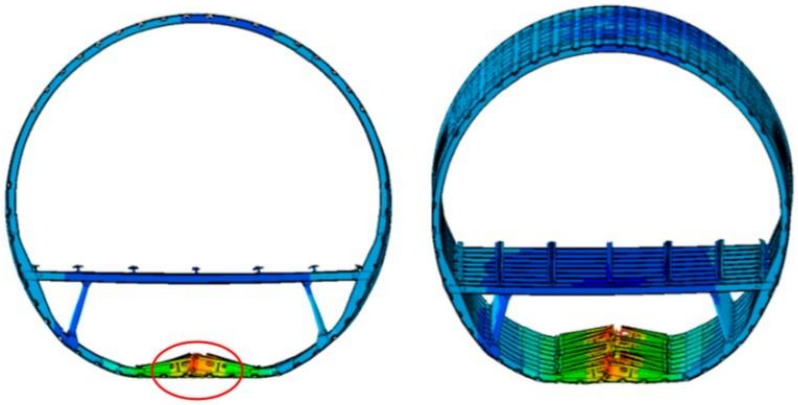

Figure 9 Aircraft's fuselage crushing behavior, [8]

2.2 Energy absorption and failure mechanisms

The specific energy absorption, which is the main parameter characterizing the energy absorption capability of a structure, strongly depends on the mode the structure fails. In fact, two different crushing modes can occur; the catastrophic failure mode and the progressive failure mode.

The catastrophic failure mode occurs when unstable interlaminar crack growth occurs and it is characterized by a sudden increase in load until the peak load, followed by a low post-failure load. This type of failure mode is also described as uncontrollable.

In contrast, the progressive failure mode is controllable and progresses through the material at the loading speed. In this case, a triggering mechanism is provided at the one of the structure ends, as a stress concentrator, and causes the failure initiation. A reduction of peak load is observed down to a lower, almost constant, sustained load, under of which a stable collapse is provided. The advantages of a progressive failure mode are that the energy absorption is larger in a progressive crush compared to a catastrophic failure, while structures designed to response to loads by progressively failing have proved to be lighter than the ones which are designed to react to loads by catastrophically failing. Thus, the progressive failure mode is more beneficial compared to the catastrophic one because it provides lighter structures of higher energy absorption capability, or on other words structures of higher SEA.

According to Farley and Jones [9], the crushing mode is an indicator of how efficiently the structure is being crushed. The prediction of crushing response includes the understanding of how the energy absorption is affected by both material mechanical properties and specimen structure (geometry). Farley and Jones suggest that the crushing speed affects the energy absorption capability of a structure in the same way the strain rate affects the mechanical response of a

material (Figure 10). As a result, the amount of absorbed energy depends on the crushing speed in a proportional way.

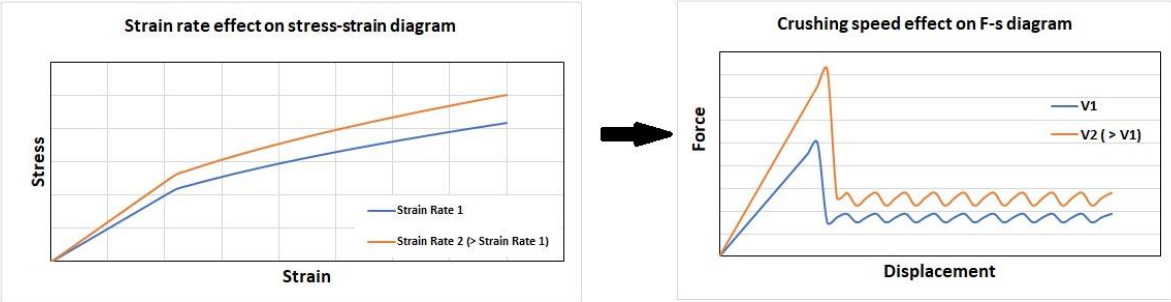

Figure 10 Effect on crushing speed on energy absorption according to [9]

Referring to the studies of Farley and Jones (1989), four different crushing modes have been identified considering composite materials. These four proposed crushing modes are presented below. All of them are exhibited by brittle composite materials, but the last crushing mode is the only one which can be also exhibited by ductile materials.

1. *Transverse shearing and fragmentation mode*
   It is characterized by laminate cross-section with short interlaminar and longitudinal cracks that form partial lamina bundles (Figure 11). The main energy absorption mechanism is the fracturing of lamina bundles; when the fragmentation occurs, the length of interlaminar and longitudinal cracks is lower than that of the lamina. The mechanism is observed when the crushed material length is short. The mechanism that controls the crushing process is the transverse lamina bending strength, which is a function of fiber stiffness and strength in case of composite materials. As Farley and Jones suggested, if the fiber mechanical response depends on the strain rate, then the energy absorption depends on crushing speed in a similar way.

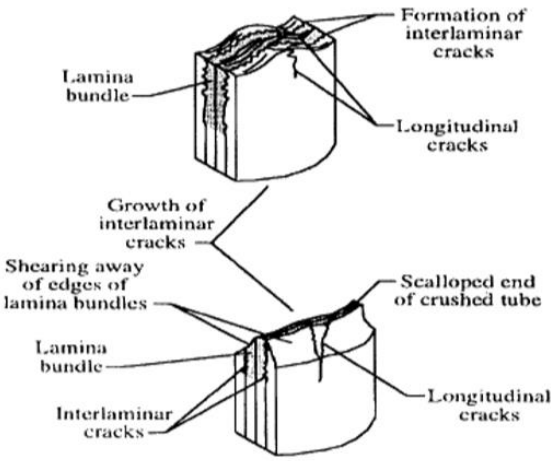

Figure 11 Transverse shearing and fragmentation crushing mode, [3]

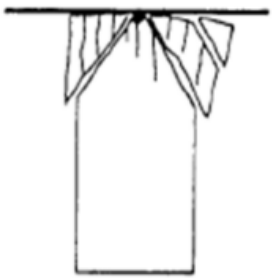

Figure 12 Fragmentation crushing mode, [1]

2. *Brittle fracturing*

The brittle fracturing crushing mode exhibits the same energy absorption mechanism like the fragmentation mode, which is the failure of lamina bundles. However, the length of interlaminar cracks in brittle fracturing lies from one to ten times the lamina thickness. The longer the fractured lamina bundle is, the less efficient the crushing mode is. Lamina bundles in brittle fracturing mode often exhibit some bending and usually fracture near the base. When the first lamina bundles fracture, the load is redistributed resulting in cracks growth and further lamina bundles fracturing. The controlling mechanisms in brittle fracturing mode, for composite materials, are the matrix stiffness and the lamina bundle tensile strength. The first controls the interlaminar and parallel-to-fiber crack growth, while the second controls the fracture of lamina bundle.

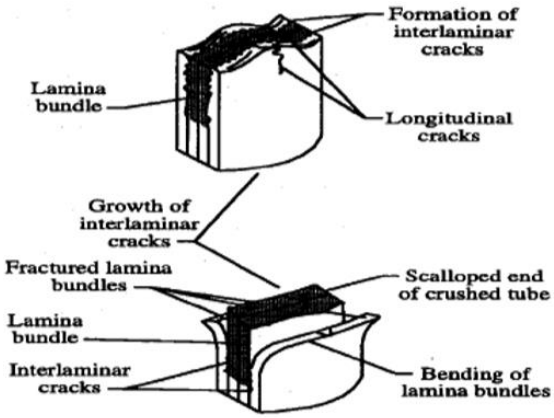

Figure 13 Brittle fracturing crushing mode, [3]

3. *Lamina bending or splaying mode*

Splaying mode is characterized by very long interlaminar and parallel-to-fiber cracks, but the lamina bundle does not fracture. The energy absorption mechanism here is crack growth. The respective cracks length is greater than ten times the lamina thickness. In splaying crushing mode, the lamina bundles exhibit significant bending deformation but do not fracture. The not fractured long lamina bundles result in an inefficient crushing mode. The matrix strength is the controlling mechanism of the splaying mode, as it controls the cracks growth. Once again, the way the strain rate affects the mechanical

response of a material, is the same to the way the crushing speed affects the lamina bending and in consequence the energy absorption.

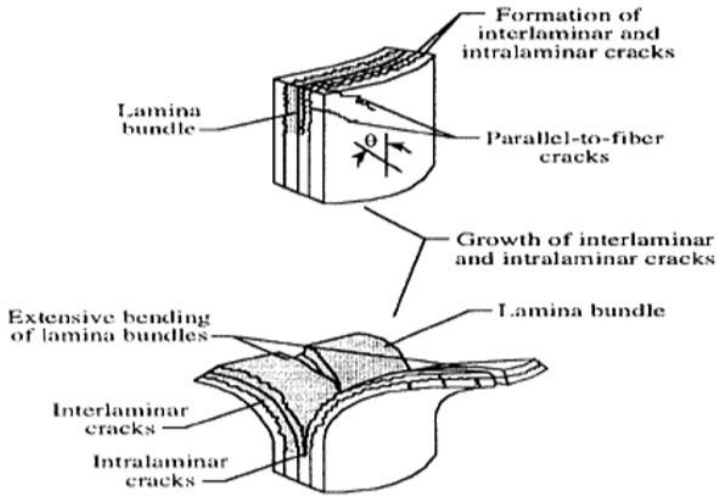

Figure 14 Splaying mode, [3]

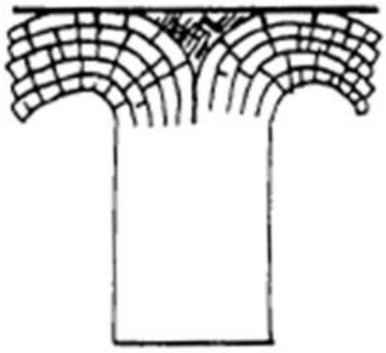

Figure 15 Splaying mode, [1]

4. *Local buckling or progressive folding*

The progressive folding crushing mode is characterized by the formation of local buckles, or folds, by means of plastic material deformation. This mode is exhibited by both brittle and ductile materials. The ductile fiber-reinforced composites remain intact after the crush due to the fiber and matrix plasticity and fiber splitting. In the case of brittle composite materials, the structure collapses in folding mode when matrix has higher failure stress than the one of the fibers. The mechanisms that control the progressive folding crushing mode is the plastic yielding of the fiber and/or the matrix. More specifically, the matrix non-linear stress-strain response controls the local buckling progress in case of brittle materials, while the matrix or fiber stiffness controls the progress of local buckling in case of ductile materials.

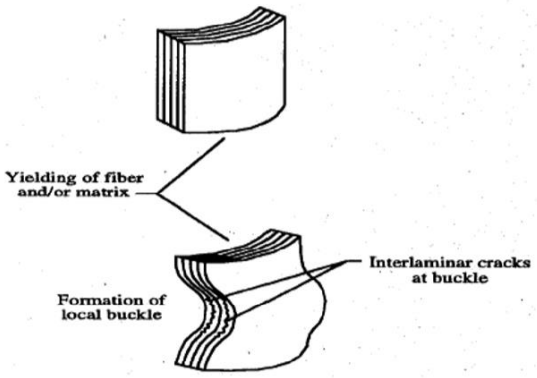

Figure 16 Local buckling or progressive folding mode, [3]

Further crushing modes referring to specific materials and geometries can be found in many studies of open literature, which have examined certain structures. A typical example is the study carried out by Bisagni [10] who observed the failure modes occurred in crushed circular carbon fiber tubes.

The energy absorption capability of a structure is a function of both geometry and material properties. In addition, energy absorption capacity of a structure depends strongly on the failure mechanism (crushing mode) which is observed during the collapse. So, regarding to composite materials, progressive crushing with microfragmentation is associated with the larger amount of absorbed crush energy according to Mamalis et al. [11]. However, when the fragmentation is quite intense providing large debris which have the tendency to concentrate in the interior of the tube, the fragmented and compacted debris limit the available stroke, resulting in lower stroke efficiency and in consequence lower levels of energy absorption capability. Furthermore, structures which collapse according to the crushing mode of progressive folding and hinging, are characterized by medium energy absorption capacity, while brittle fracturing mode results in very little levels of energy absorption providing a catastrophic failure. Finally, in every failure mode, environmental factors react in the same way on crashworthiness behavior. An important factor is the ambient temperature which reduces the amount of energy absorption according to Ptak et al. [12], as the force levels decrease in higher temperatures, moving the force-displacement curve downwards, reacting on lower energy absorption. The same paper underlined also the effect of crushing speed concluding that increased crushing speeds increase in turn the energy absorption as Figure 10 shows.

More emphasis will be given to local buckling and progressive folding crushing mode, as different types of folding modes can be occurred in the case of an axial crushed structure. The progressive folding and hinging is an oftenly observed failure mode. The four main types of progressive folding crushing mode are:

1. Concertina mode or ring mode
2. Diamond mode (3 lobes, 4 lobes etc.)
3. Mixed mode
4. Euler-type buckling mode

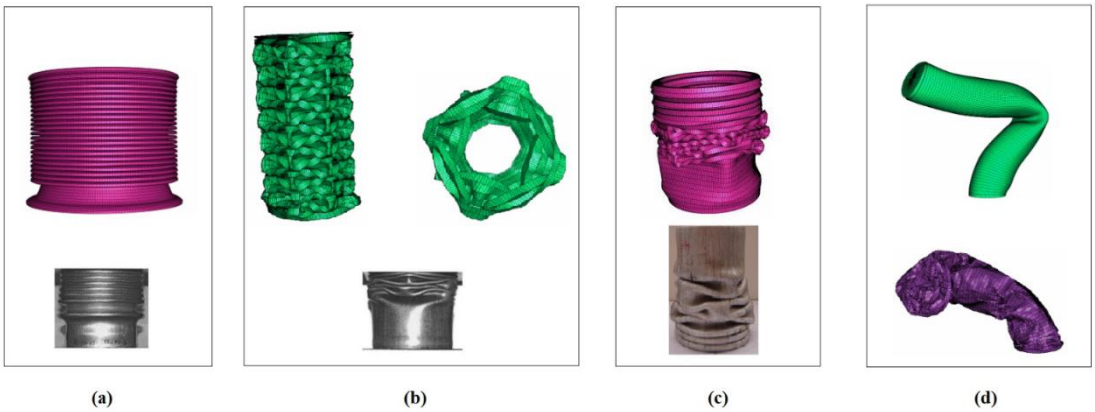

Figure 17 Progressive folding crushing mode, (a) concertina mode, (b) diamond mode, (c) mixed mode and (d) Euler-type buckling mode

The type of folding crush mode in which a structure is expected to collapse strongly depends on geometric characteristics. Specifically, a thin-walled tube will collapse under axial crushing load either axisymmetrically or non-asymmetrically, depending on the ratio of diameter to thickness (D/t) and the ratio of the length to the diameter (L/D). The axisymmetric mode is often called as concertina mode (or ring mode), while the non-symmetric one as diamond mode. For a certain D/t ratio, a tube may start collapsing in concertina mode and switch to diamond mode, exhibiting in that way a mixed crushing mode. Finally, a tube can also collapse in Euler-type buckling mode, which is a catastrophic and uncontrollable collapse provided by large bending of the tube resulting in significant loss in energy absorption capacity.

As mentioned before, the energy absorption capability strongly depends of failure mode. In case of folding and hinging crushing mode, research studies and experimental works have shown that concertina mode seems to be the best folding mode providing the highest energy absorption levels. A little lower energy absorption capability is provided by diamond mode, while the Euler-type buckling mode is characterized by very low energy absorption levels due to its catastrophic and unstable collapse progress.

Regarding to geometric characteristics which have a strong influence on expected type of folding, Florent et al. [13] examined aluminium tubes, suggesting that thick and short tubes are expected to collapse in concertina mode. As the tube thickness reduces and the length of the tube increases, a mixed mode is more expected to be observed, while even thinner and longer tubes may collapse in diamond mode. However, for extremely thin and long tubes, Euler-type buckling mode may be occurred. So, the length of the crushed structure or specimen must be very carefully selected in order to avoid the uncontrollable and catastrophic collapse of Euler-type buckling mode. For this reason, extremely long tubes must be avoided. Figure 18 illustrates the expected type of folding for aluminium tubes according to [13].

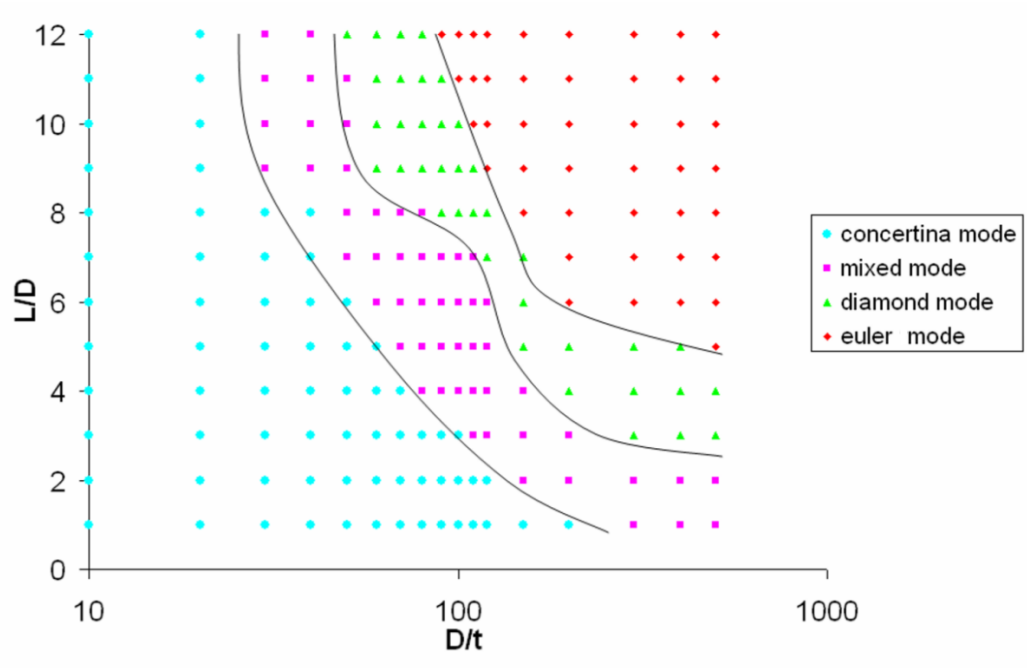

Figure 18 Folding mode classification for aluminium tubes, [13]

In addition, an important parameter in designing energy absorbers is their cross-section. Recent studies have examined single cross-sectioned tubes, concluding that circular tubes provide the highest energy absorption capability. A little lower levels of energy absorption capability are provided by square cross-section, and even lower by rectangular ones. In general, for cross-sections with corners (square, hexagonal, octagonal etc.), the energy absorption levels increase as the number of corners is getting higher. For example, the energy absorption capability of a circular tube is higher than an octagonal, which in turn is higher than a hexagonal one, which in turn is higher than a square one etc.

Finally, Florent et al. [13] investigated the effect of the type of support applied at structure ends. Specifically, the examined support types were tie constraint, roller and fixed, while four different boundary conditions were examined; (1) tie constraint-roller, (2) fixed-fixed, (3) fixed-roller and (4) roller-roller. The first support type refers to the bottom of the tube, while the second one refers to the top of the tube. For an examined specimen which was expected to collapse in concertina folding mode, the four types of support which were examined affected the folds formation as the next figure shows. A key-factor is that at symmetric supports, (2) and (4), the folds formation was also symmetric, as folds appeared at both ends of the specimen (aluminium tube).

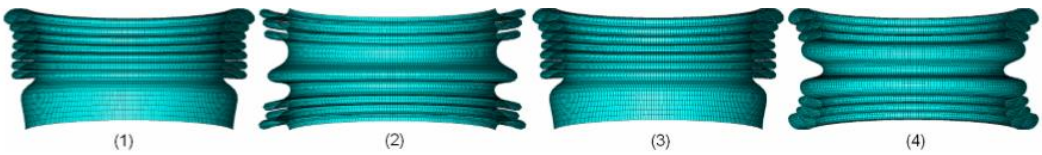

Figure 19 Effect of support types on specimen expected to collapse in concertina mode, (1) tie constraint-roller, (2) fixed-fixed, (3) fixed-roller and (4) roller-roller, [13]

Following, a examined specimen in [13], expected to collapse in mixed folding mode, in fact collapsed in concertina mode for fixed-roller supports as shown in next figure, suggesting that when the one of two tube ends is fixed, the concertina folding mode is occurred.

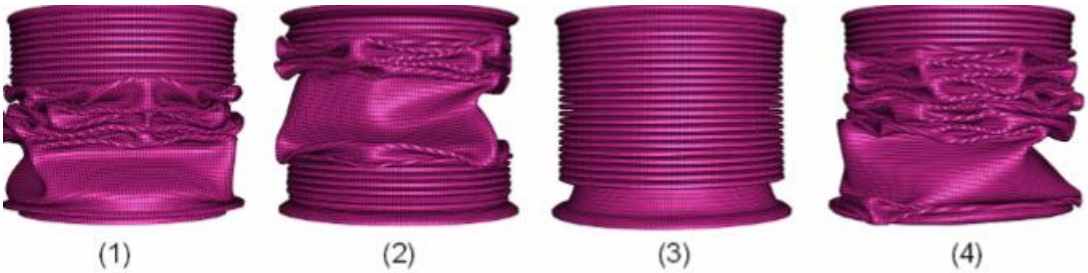

Figure 20 Effect of support types on specimen expected to collapse in mixed mode, (1) tie constraint-roller, (2) fixed-fixed, (3) fixed-roller and (4) roller-roller, [13]

Finally, the same study, [13], examined a specimen expected to collapse in Euler-type buckling mode. It was concluded that the end of specimen which was fixed or tied to the plate, was remained in contact to the plates after the collapse, while the end in which a roller boundary conditions was applied, was losing its contact to the plate by sliding over it.

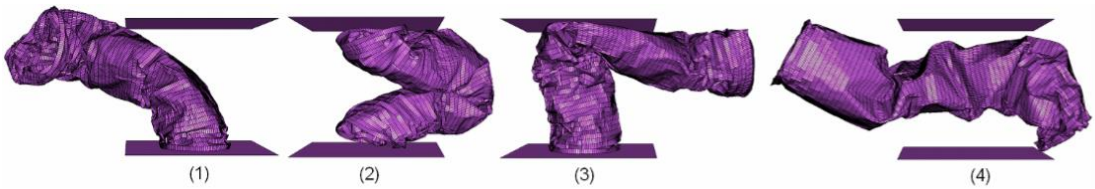

Figure 21 Effect of support types on specimen expected to collapse in Euler-type buckling mode, (1) tie constraint-roller, (2) fixed-fixed, (3) fixed-roller and (4) roller-roller, [13]

Summarizing on the effect of support types on folding collapse mode, when at least one end is fixed, more axisymmetric folds are created, providing so the best supported structure in terms of energy absorption capability which is at the higher levels. In contrast, when both ends are free, the energy absorption is significant low.

2.3 Crush tests

The crashworthiness behavior of a structure and its main characteristics can be studied through numerical simulations or experimental tests. The experimental tests often provide more accurate results in every aspect; prediction of energy absorption capability, maximum load, maximum specimen shortening, force-displacement curve, failure mode etc. The experiment tests, oftenly called

as crush tests, can be conducted in two different ways: quasi-static and impact conditions.

Figure 22 Impact crush test of aircraft's fuselage, [8]

In quasi-static conditions, the specimen is crushed at constant speed. However, quasi-static conditions do not represent a true simulation of crush conditions, because in real crush conditions the structure is subjected to a decrease in crushing speed, from the initial impact to rest. Given that many materials are strain rate sensitive and the energy absorption capability depends on crushing speed according to Farley and Jones [9], the quasi-static tests may not lead to an accurate prediction of the amount of absorbed energy. Although, the advantages of quasi-static tests are that they are simple and easy to control without requiring expensive equipment to record the crush events.

On the other hand, the impact tests represent a true simulation of real crushing conditions, as the crushing speed decreases from the initial impact velocity to rest because of the energy absorption by the specimen. The benefit of impact tests is their accuracy in predicting the collapse mode and the main crashworthiness characteristics (energy absorption capability, maximum load, maximum specimen shortening, force-displacement curve, failure mode etc.). Their major disadvantage though is that they require expensive equipment, such as high-speed cameras, data recorders of very high frequency etc., as the crushing process takes place in a fraction of second.

2.4 Previous research studies

A plenty of research studies on crashworthiness have been carried out through the recent years by either numerical simulations with finite element analysis software or experimental crush tests. The main emphasis has been paid

on investigating different materials (aluminium, composite materials etc.), different cross-section designs or different support types. The metrics used by the major of the studies to evaluate the crashworthiness efficiency is parameters such as specific energy absorption (SEA), mean crush force (MCF) or known as sustained load, peak crush force (PCF) and crushing force efficiency (CFE) or known as load uniformity. Some of these studies are presented below.

Mamalis et al. [14] (2004) conducted experimental tests on thin-walled carbon fiber reinforced plastic (CFRP) composite square tubes. The results provided conclusions according to which the energy absorption is depending to the collapse mode, which in turn is a function of tube thickness. In addition, it was concluded that the maximum load (PCF) increases as the number of fiber reinforcing layers, fiber volume and tube thickness increase. Finally, when the load was equal to PCF, cracks were observed at the corners of the squared cross-section specimen, due to stress concentration. The cracks growth was parallel to tube axis, while the load was reduced as the crush continued.

Florent et al. [13] (2007) examined the impact of support types and foam filling on the crashworthiness behavior of aluminium thin-walled tubes, and more specifically on exhibited crushing modes. The study utilized as modelling tool the LS-DYNA software. The examined support types were tie-constraint end of tube, fixed end and roller in the tube end. The boundary conditions (support types combination for the two tube ends) have been referred to previous subsection of this chapter (2.2). It was concluded that for a specimen expected to collapse in concertina failure mode, both shell elements model and solid elements model predicted correctly the failure mode. However, given that a certain initial tube length can be formed in a standard number of folds, the shell elements model predicted more accurately the number of folds compared to the solid elements model (Figure 23). Additionally, the impact of boundary conditions in terms of support type of each tube end was examined providing the conclusions referred to subsection 2.2 of this chapter. Finally, the aluminium foam filled tubes showed higher energy absorption levels. However, the aluminium foam filling resulted in shortening the folding length (Figure 24), while a change in collapse failure mode from diamond mode to concertina or Euler-type was occurred. The last observation is considered to be disadvantageous as it may cause unstable collapse (Euler-type buckling mode).

Figure 23 Bare tube folds prediction (shell elements model, experimental specimen, solid elements model), [13]

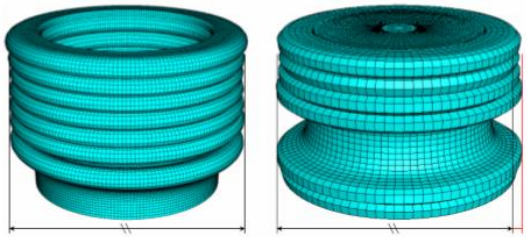

Figure 24 Effect of aluminium foam filling on exhibited number of folds, [13]

Mamalis et al. [11] (2009) studied square tubes of vinyl-ester and fiberglass composite material, internally reinforced with aluminium or polyurethane foam. Both experimental tests and numerical simulation in LS-DYNA software were conducted to observe and analyze the collapse mechanisms. The numerical simulations in LS-DYNA predicted correctly the failure mode, while mean deviations in predicted F-s curve of 20% and 15% were observed in the case of bare tube and tube reinforced with foam (both aluminium and polyurethane cases), respectively. It was concluded that the energy absorption was higher for the foam filled tubes compared to the bare ones. In fact, the aluminium foam filled tube was the one of higher SEA. Also, filling with aluminium foam provided better stabilization of the collapsed specimen and the crush energy was absorbed in completely plastic way in form of heat energy. In contrast, polyurethane foam filling provided an elastoplastic behavior during energy absorption, retransferring the amount of absorbed energy back to the crushing system.

Suzhen et al. [6] (2016) examined the effect of multi-cell cross-section designs on the crashworthiness characteristics of aluminium square tubes. The finite element analysis models which were developed for the needs of the study were initially validated by both quasi-static experimental tests. A typical representation of the study results is shown in the next two figures, where the collapsed specimens are depicted in the first figure, and the influence of multi-cell cross-section on energy absorption is depicted in the second figure. As Figure 26 shows, all SEA, PCF and MCF parameters increase as the number of cells increases too.

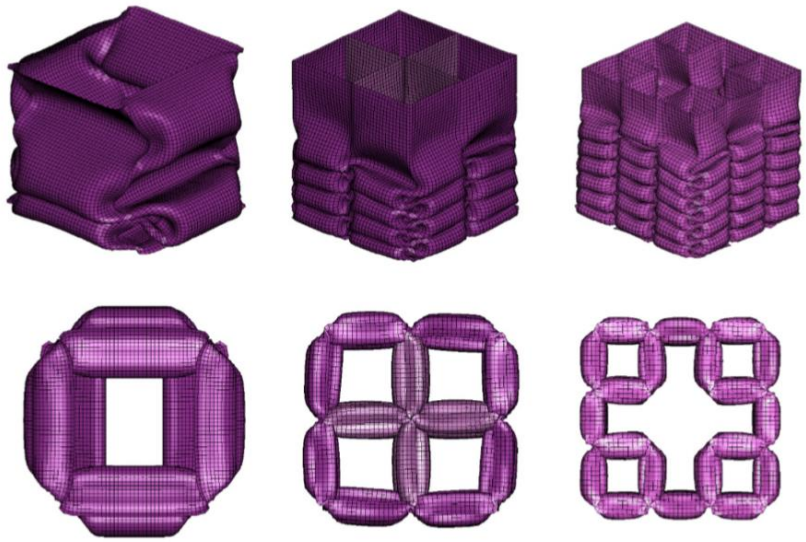

Figure 25 Collapsed specimens (single-cell, four-cell and five-cell cross-sectioned square tubes), [6]

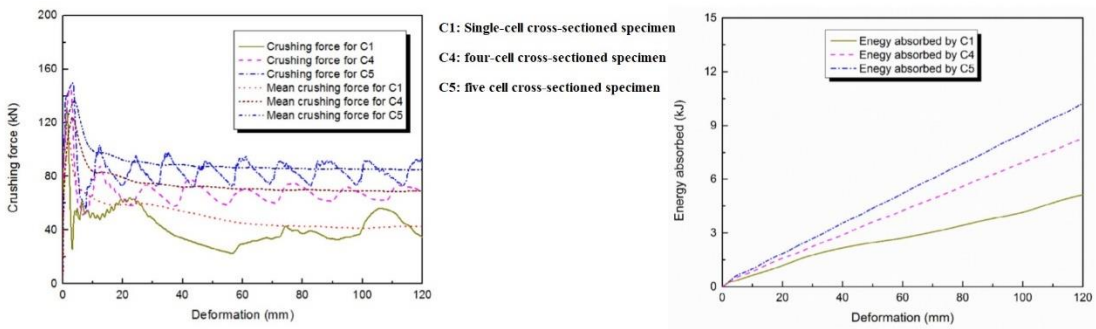

Figure 26 Effect of multi-cell cross-sections on energy absorption, [6]

Nikkhah et al. [4] (2019) studied the crashworthiness behavior of thin-walled windowed tubes made of aluminium. Different multi-cell cross-section designs were also considered in this research work too. It was concluded that the windowed thin-walled tubes were characterized by lower peak crush force (PCF) and lower specific energy absorption (SEA). The first consequence is positive, considering that PCF must be a reasonable value in order to the specimen be able of being deformed plastically absorbing energy. However, low SEA means in turn reduced energy absorption capability.

Acar et al. [15] (2019) examined different designs of multi-cell cross-sectioned thin-walled aluminium tubes, too. An optimization of crashworthiness response considering the CFE and SEA parameters was performed. The finite element models which were developed for the needs of the study were initially validated with experimental results. For the optimization, the same weighting factors were considered in the objective function for both CFE and SEA, paying in that way the same importance on maximizing both parameters. It was concluded that designs of thinner and larger in diameter tubes were provided for CFE maximization compared to the ones provided for SEA maximization.

Although most research works have been performed on crashworthiness analysis of simple composite structures such as tubes, Mamalis et al. [16] (1991) studied the effect of specimen geometry of thin-walled conical shells on energy absorption capability. Specifically, geometry characteristics like thickness, shell length and apical angle were investigated both experimentally and analytically. A standard crushing speed of 10mm/min was applied at all test cases until a deformation of 63mm being reached. The examined specimens were fiber-reinforced thin-walled composite conical shells with the semi-apical angle lying in the region of 5° to 30°. The failure mode of collapse and the effect of geometry characteristics (shell length, thickness of thin-walled shell, apical angle, diameter) on energy absorption capability were obtained. In general, thin-walled shells revealed a more efficient crashworthy behavior compared to thin-walled tubes. The experimental data provided that the specific energy absorption is a linear function of diameter to thickness ratio, or SEA (kJ/kg) = $1469.4 \cdot t/D - 6.8$. For axial compression of thin-walled composite shells, it was concluded that catastrophic brittle fracture and elastic instability must be prevented in order to achieve stable collapse during crushing conditions. In case of conical shells, stable collapse may be developed with absence of external trigger mechanism, as conical shells develop self-triggering mechanism with fracture initiating at regions of highest stress. The transition from stable to unstable collapse mode regarding to semi-apical angle was found to be in the region of 15° to 20°. Finally, the results showed that specific energy absorption decreases as semi-apical angle of shell increases, as thickness increases or as diameter decreases. In fact, though, large diameter shells may collapse under catastrophic failure.

In the field of crashworthiness of bi-material structures, which is the topic of the present diploma thesis, the research work has not been expanded too much yet. Two research works on crashworthiness of bi-material tubes are following. Mamalis et al. [17] (1991) studied the crashworthiness response of bi-material tubes. The examined bi-material tubes consisted of the following materials; aluminium-mild steel (Al-St), PVC-high strength steel (PVC-St), aluminium-copper (Al-Cu) and aluminium-PVC (Al-PVC). All the examined specimens were of 127mm initial length and were axially crushed in quasi-static conditions. The experiments were conducted in dry conditions. Also, in that paper an analytical calculation of crushing load is presented for the case of bi-material structures. The conclusions of that research work are associated with both deformation characteristics and load-displacement curve. Regarding to deformation characteristics, the following conclusions were provided:

- Concertina, diamond or mixed failure mode were observed for the examined bi-material tubes. The exhibited failure mode which will be occurred depends on the yield stress ratio of the two materials of the bi-material structure and on the collapse mode of the harder component when the thickness ratio is around 0.5.
- When the two components of the bi-material structure are of highly different yield strengths ($Y_1 >> Y_2$), the collapse mode of the harder component determines the mode in which the bi-material structure will fail.

- When concertina mode is occurred for bi-material specimens, and the outter tube is the softer material, the softer component is trapped and extruded severely in the convolutions of the harder, inner, component. Full adhesion is maintained at the internal edge of the convolution, while the adhesion is lost at the outer edge (Figure 27).

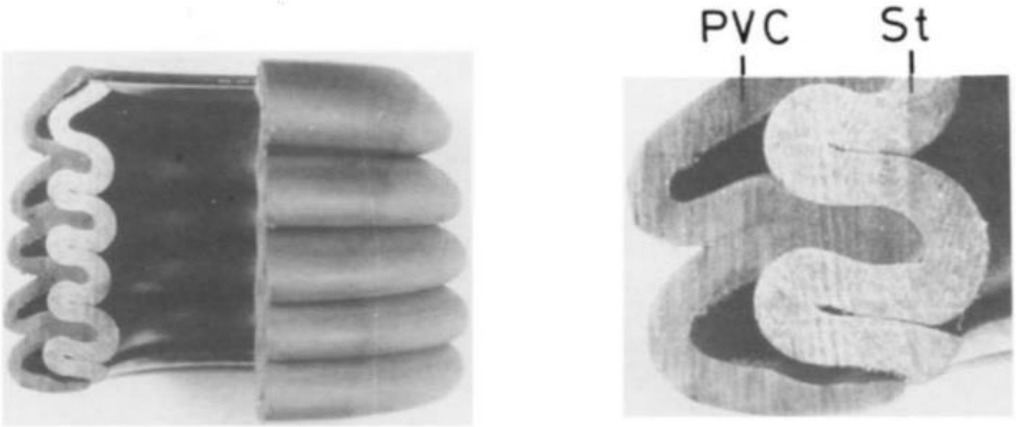

Figure 27 Loss of adhesion in outer edges of convolutions and maintained adhesion in internal edges, [17]

- For medium yield stress ratio of the two tube components, adhesion is lost at both internal and outer ends of a convolution, due to slight relative sliding between the two materials at the beginning of the convolution formation (Figure 28).
- Less separation (adhesion loss) is observed between the components of a bi-material structure which collapses in diamond mode compared to one which collapses in concertina mode.

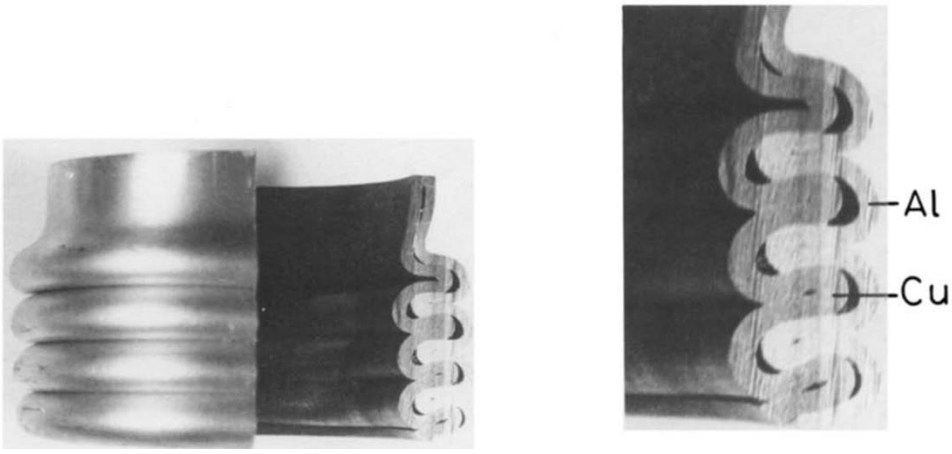

Figure 28 Loss of adhesion in both internal and outer edges of convolutions, [17]

Further, the conclusions regarding to load-displacement curve, as were provided by Mamalis et al. [17] from comparison between the F-s curve of the bimetallic specimen and the superposition of the F-s curves of the two components, are presented below:

- The peak load F_{max} of the bimetallic F-s curve is greater than that of the superposition, demonstrating higher strength for the bimetallic tubes.
- The inclination of the elastic load-deformation line of bimetallic curve is closer to that of the harder component and appears to be the same to the one of the superimposed curve.
- The initial post-buckling region (first lobe) of the bimetallic F-s curve, is represented by a load drop, the rate of which is lower than that of the superimposed curve and significantly affected by the initial post-buckling F-s region of the harder component.
- The peaks and drops of the load response in post-buckling bimetallic F-s curve, are affected by the ones of the harder component's F-s curve.
- When bimetallic tubes of components with very different strength are compressed and collapse in concertina mode, the post-buckling peaks show a gradient increase which may be caused by the loss of adhesion. This tendency is not appeared in diamond collapse mode.
- The energy absorption capability of a bimetallic structure (area under the F-s curve) is greater than that of the superposition of its two components.

Finally, Umer et al. [18] (2018) studied the crashworthiness behavior of bi-material tubes considering different cross-section for the internal and the external tube. The two materials examined were low carbon steel ASTM A36 and aluminium alloy AA6060. The numerical simulations were carried out in ABAQUS software. A variety of combinations of cross-sections for internal and external tubes were examined (circular, rectangular, hexagonal and square). The provided conclusions were that peak crush force (PCF), average crush force (MCF) and specific energy absorption (SEA) do vary in accordance with the cross-section. Specifically, geometries which have polygon as the outer tube showed better results in PCF, MCF and SEA compared to geometries which have circular outer tube. The maximum values of SEA and MCF were obtained in the case of the bi-material specimen which had an outer tube of the polygon cross-section with the higher number of sides. Finally, all examined bi-material tubes revealed greater PCF, MCF and SEA compared to a single, not bi-material, tube.

2.5 Analytical calculation of mean crushing load for bi-materials

Efforts during the past have been made in order to calculate an analytical and theoretical expression of the mean crushing load of a bimetallic structure. One of the first works is the one of Alexander [19] made in 1960. That research work was carried out for thin-walled cylindrical shells which were expected to collapse in concertina mode. The mean collapse load is calculated by equating the internal work to the mean collapse load multiplied by the total. From that study, Alexander suggested the following expression for mean collapse load.

$$\bar{P} = 6.08 \cdot Y \cdot t^{1.5} \cdot \sqrt{D} \tag{6}$$

In the above equation, let Y be the yield stress, t the thickness and D the diameter.

Another study which provided an analytical expression of mean collapse load is the one of Mamalis et al. [17]. Below, the analytical theoretical calculation procedure is presented as reported in [17].

Consider a bi-material plate consisting of two fully adhering different materials of thicknesses t_1, t_2, and yield stresses Y_1, Y_2 respectively. Examining a full yielding of the cross-section, the stress distribution in which is depicted in Figure 29, and applying the force equilibrium equation, the location of the plastic neutral axis (x) can be obtained.

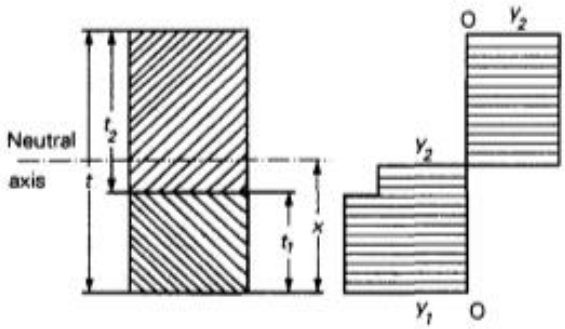

Figure 29 Stress distribution in fill yielded bimetallic cross-section, [17]

$$x = \frac{Y_2 \cdot (t + t_1) - Y_1 \cdot t_1}{2 \cdot Y_2} \quad , \qquad Y_1 \cdot t_1 < Y_2 \cdot t_2 \tag{7}$$

The required moment to bend plastically the entire section M_p (moment of full plasticity) can be calculated by taking moments about the plastic neutral axis.

$$M_p = Y_2 \cdot \frac{(t-x)^2}{2} + Y_2 \cdot \frac{(x-t_1)^2}{2} + Y_1 \cdot t_1 \cdot (x - \frac{t_1}{2}) \tag{8}$$

By introducing the dimensionless ratios of yields stress and thicknesses respectively, $k = Y_1/Y_2$ and $t_r = t_1/t_2$, the moment which bends plastically the entire section becomes:

$$M_p = \frac{1 + 2 \cdot k \cdot t_r + 2 \cdot k \cdot t_r^2 - k^2 \cdot t_r^2}{(1+t_r)^2} \cdot \frac{Y_2 \cdot t^2}{2} \tag{9}$$

So, expressing the full plastic bending moment M_p in relation to an equivalent yield stress $\bar{Y}$ in the form of $M_p = \bar{Y} \cdot t^2/4$, we have:

$$\bar{Y} = \frac{1 + 2 \cdot k \cdot t_r + 2 \cdot k \cdot t_r^2 - k^2 \cdot t_r^2}{(1+t_r)^2} \cdot Y_2 \tag{10}$$

2.5.1 Extensible plastic collapse of bi-materials

Considering the collapse mode proposed by Alexander [19] which is depicted in Figure 30, and taking into account the formation of external or internal convolution, the mean crushing load can be obtained by equating the external work (W_e) to the internal work of deformations (W_i). The internal work is divided to the one dissipated in bending the tube wall (W_1) and the one dissipated in stretching the tube wall to become a convolution (W_2), giving so that $W_e = W_i = W_1 + W_2$.

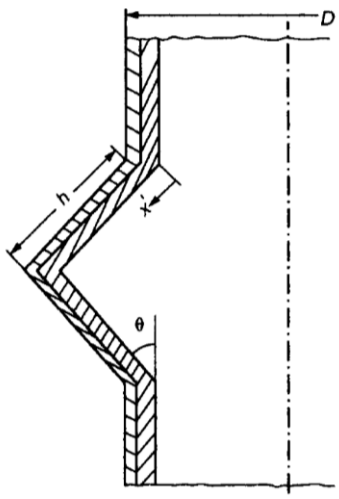

Figure 30 Assumed deformation mode for the extensible collapse, [19]

Thus, in more detail, we have the following expressions for each work:

$$W_1 = 2M_p\{\pi D\frac{\pi}{2} + \int_0^{\frac{\pi}{2}} \pi(D \pm 2h \cdot sin\vartheta)\,\delta\vartheta\} = 2M_p\pi(\pi D \pm 2h) \tag{11}$$

$$W_2 = \sum_{i=1}^{2} 2\int_0^h Y_i\pi D_i\, t_i\, \frac{2x \cdot sin\vartheta}{D_i} \cdot dx = 2\pi h^2(Y_1t_1 + Y_2t_2) \tag{12}$$

$$W_e = \bar{P} \cdot 2h = W_i = W_1 + W_2 \tag{13}$$

The combination of the three above equations yields to the calculation of the mean crushing load $\bar{P}$.

$$\bar{P} = M_p\pi(\frac{\pi D}{h} \pm 2) + \pi h(Y_1t_1 + Y_2t_2) \tag{14}$$

In equations (11) and (14), the sign of minus refers to the internal convolution, while the positive sign to the external convolution. Minimizing $\bar{P}$ with respect to h, or $\partial\bar{P}/\partial h$=0, we find:

$$h = \sqrt{\frac{\pi M_p D}{Y_1 t_1 + Y_2 t_2}} = \frac{1}{2}\sqrt{\frac{1 + 2kt_r + 2kt_r^2 - k^2 t_r^2}{(1 + kt_r)(1 + t_r)}}\sqrt{\pi D t} \qquad (15)$$

Since it is not known a priori if the convolutions will form internally or externally (the external formulation is the more possible one), we consider the mean crushing load as the average of the two provided by equation (14). Replacing h with the above expression, we finally calculate the mean crushing load $\bar{P}$.

$$\bar{P} = 2\pi\sqrt{\pi D M_p (Y_1 t_1 + Y_2 t_2)}$$
$$= \pi^{1.5} t^{1.5} D^{0.5} Y_2 \frac{\sqrt{(1 + 2kt_r + 2kt_r^2 - k^2 t_r^2)(1 + kt_r)}}{(1 + t_r)^{1.5}} \qquad (16)$$

For similar materials, not considering a bi-material structure, i.e. Y_1=Y_2=$\bar{Y}$, we have that:

$$\begin{cases} h = 0.886\sqrt{Dt} \ \ and \\ \bar{P} = 5.6Yt\sqrt{Dt} \end{cases} \qquad (17)$$

The predicting mean crushing load for a single material (not bi-material) satisfactorily agrees with what Alexander proposed in [19]. In both studies, Tresca yield condition is considered.

2.5.2 Inextensional plastic collapse of bi-materials

The present theoretical analysis of inextensional plastic collapse mode of bi-material tubes uses the model developed from Johnson et al. [20]. An equivalent tube of thickness t and yield stress $\bar{Y}$, computed from equation (10), is considered. The necessary assumptions which were made to use the model of Johnson, are presented below:

- The rigid-perfectly plastic material has infinite ductility.
- A frictionless compression with both ends of the tube free to deform.
- Only the terminal deformation mode is taken into account, neglecting the history of possible exhibited collapse modes.
- Direct and shear stresses are neglected, as only the vertical crush load is considered.

Applying the travelling mechanism of hinging as proposed from Johnson et al., the mean post-buckling load is computed as:

$$\bar{P} = 2\pi M_p \frac{D/r - n\,cot(\pi/2n) + 1 + n\,cosec(\pi/2n)}{1 - 2r/h_1} \tag{18}$$

In the above expression of mean crushing load during an inextensional plastic collapse mode, n is the number of lobes per layer and r is the below parameter.

$$r = \frac{D}{A}\left(\sqrt{1 + \frac{A}{2}\frac{\pi}{2n}tan(\pi/2n)} - 1\right) = \frac{D}{A}\left(\sqrt{1 + \frac{Ah_1}{2D}} - 1\right) \tag{19}$$

$$A = 1 + n \cdot cosec(\pi/2n) - n \cdot cot(\pi/2n) \tag{20}$$

In the above analysis, when Mises yield condition is used, the full plastic bending moment M_p must be multiplied by $2/\sqrt{3}$ in equation (9), while the lobe length h and the mean calculated load $\bar{P}$ must be multiplied by the value of $\sqrt{\frac{2}{3\sqrt{3}}}$ in equations (15) and (16).

3. Bimetallic Materials

3.1 Introduction

Nowadays, the current interest of industries and research community has been emphasized on developing and using materials which provide advanced properties (mechanical, chemical, electrical, thermal etc.). Specifically, in the field of crashworthiness, modern crashworthy structures have to be as light as possible and absorb the impact energy in the most plastic, progressive and safe way for the passenger or the protected substance in general. In order to achieve such constructions, new highly efficient materials, such as composite ones, are used. Composite materials are widely used in crashworthy structures designs, as they have considerable potential for absorbing huge amounts of kinetic energy during a crash, under the constraint of low weight levels.

Composite materials consist of two (or more) components; the reinforcing component and the matrix. The two components are selected and combined in order to achieve the desirable properties and material characteristics which cannot be achieved by only using a single material. The reinforcing component strengthens the overall material with the appropriate properties, while the matrix is oftenly a lower density material whose aim is to secure a solid structure of the expected characteristics. Depending on the reinforcing component, the composite materials can be divided into:

- Fibrous composites
- Particulate composites
- Laminar composites

The materials of last category, laminar composites, include a wide range of material combinations and they can in turn be divided into:

- Thin or thick coated materials
- Bimetallic materials
- Multilayers materials
- Sandwich materials

The present diploma thesis studies the crashworthiness behavior of thin-walled circular bi-tubes. So, for the purpose of this thesis, only the bi-metallic materials will be described further in more detail. Bimetallics are called the materials which are produced by the combination of two metals strongly connected to each other, providing a solid structure. Thus, a bimetallic material is obviously described by properties and characteristics of both components from which is consisted of. The examined specimens of present work are four circular thin-walled bi-tubes of steel and ertalon.

The bimetallics have the following advantages for use against the single metallic materials:

- Minimized thermal expansion
- Reduced stresses in overall structure
- Increased thermal conductivity
- Lower temperature operating levels for the structure
- Reduced metal corrosion, oxidization and friction levels
- Higher fatigue strength
- Reduced structure weight
- Capability of continuous production
- Lower needs for structure maintenance and increased lifetime

Considering the above benefits, it is easily understood that the bimetallic materials are widely used for a range of application cases which are presented in the next section of this chapter. Finally, regarding to main mechanical properties, Uscinowicz [21] suggested that the yield stress, the tensile strength and the Young's modulus of the bimetallic is a function of the respective parameters of its single metallic components in a proportional way to their volume fractions. So, for a bimetallic (BM) which consists of the metal A and the metal B, with Y_A, Y_B the respective yield stresses, σ_A, σ_B the respective tensile strengths and E_A, E_B the respective Young's modulus, the yield stress Y_{BM}, the tensile strength σ_{BM} and the Young's modulus E_{BM} of the bimetallic material are expressed as the following equations suggest.

$$Y_{BM} = f_A \cdot Y_A + f_B \cdot Y_B \tag{21}$$

$$\sigma_{BM} = f_A \cdot \sigma_A + f_B \cdot \sigma_B \tag{22}$$

$$E_{BM} = f_A \cdot E_A + f_B \cdot E_B \tag{23}$$

In the above equations, f_A and f_B are the volume fractions (percentage) of each metallic component respectively. Uscinowicz concluded that the Young'modulus of the bimetallic is lower compared to the alloy of the same components of the same volume fractions, while the tensile strengths of the bimetallic and the alloy are almost the same. For example, comparing a bimetallic of 20% Al and 80% Cu to an alloy of 20% Al and 80% Cu, the second one is characterized by considerably higher Young's modulus and almost the same tensile strength.

Finally, M. Abbasi et al. [22] suggested that the specific electrical resistivity (ρ_{BM}) of a bimetallic material can be expressed as a volume fraction weighted value of the specific electrical resistivities of the two metallic components from which the bimetallic is consisted of (ρ_A, ρ_B).

$$\frac{1}{\rho_{BM}} = f_A \cdot \frac{1}{\rho_A} + f_B \cdot \frac{1}{\rho_B} \tag{24}$$

3.2 Applications

The many advantages of bimetallics which were presented in the previous section, have made their use very common in industries and other various applications. As mentioned before, bimetallics combine characteristics and properties of both their components. So, for example, bimetallics materials, and more specifically tubes, are widely used in oil refining systems in which high pressures and temperatures result in highly oxidizing and corrosive environment. In these applications, bimetallic tubes are used for oil transfer, which have an outer tube material (component) of high corrosive resistance like titanium (Ti). For the same reason, bimetallic tubes with the appropriate materials are selected to be used for oil transfer, oil refining systems and generally liquid transfer systems which provide high pressures and stresses under highly oxidizing and corrosive conditions.

In addition, bimetallic tubes occur a widely use in electrical, chemical and nuclear industries, where high pressures and stresses are applied to liquids transfer systems with the need of high electrical conductivity by the materials.

Bimetallics have been also widely used in electrical and electronic components construction, such wires, cables etc., as Figure 31 shows, providing devices of extremely low cross-section area and very high electrical conductivity levels.

Figure 31 Bimetallic cable

Further, shipbuilding constructions oftenly use bimetallic thin-walled shells for ship body structures which are characterized by high resistance against corrosion combined with high strength requirement.

Bimetallic materials are selected in automobile industries for devices such as voltage meters and regulators, thermostats or rolling bearings (Figure 32). Further applications of bimetallics are special thermostats (Figure 33), or generally temperature regulators which operate under special conditions, such as dusty environment or water plunged.

Figure 32 Bimetallic rolling bearings

Figure 33 Bimetallic thermostat

High pressure vessels, steam boilers and tubes for water/steam transmission in steam-generators use bimetallic materials of the appropriate properties for such structures. High temperatures and pressures are applied to the system, while the phase alternation of water provides highly oxidizing and corrosive conditions. High strength demands against oxidizing and corrosion are also observed in hydraulic systems, in which bimetallic tubes are used too.

Figure 34 Steam boiler

Finally, bimetallics have been applied for shape memory structures constructions. A shape memory structure is capable of regaining its initial shape and geometry when is heated above a critical temperature. The heat energy during the heating is then transmitted to mechanical work as the material is contracted regaining its initial shape. Shape memory devices and structures have been used in aerospace technology and biomedical or dentistry applications.

Summarizing, the many advantages of bimetallics have made them being widely used in a range of different applications in current technology. Typical examples are:

- Shipbuilding
- Oil refining and transfer systems (tubes, filters etc.)
- Electrical, chemical, nuclear and automobile industries
- Electrical and electronic devices (wires, cables, electrodes, power switches etc.)
- Thermostats and temperature regulators
- High pressure vessels and steam boiler tubes and shells (tubes, boilers, heat transfer elements, heat exchangers etc.)
- Hydraulic liquid transfer systems
- Aerospace and biomedical applications (shape memory structures)
- Food industry

3.3 Bimetallics Production

The construction of bimetallic structures can be executed with many different processes. The four main production ways of bimetallic structures are:

- Cold rolling welding
- Friction welding
- Explosive welding
- Extrusion

In many occasions, the welding of two metals is many times not recommended as the two metallic components may be incompatible. The reason is that a high affinity may be observed between the two metals at temperatures greater than 120° C. As a result, fusion-welding processes are rejected in such circumstances as brittle intermetallic connections of low strength and high electrical resistance will be produced in the welding zone. In these occasions, solid state welding processes are recommended such as explosion, friction or cold roll welding.

Cold roll welding processes (Figure 35) are conducted at room temperatures and evidence of no solidified and cast structure at the interface has indicated that no liquid or melted phase is formed. Thus, a direct bond at solid state is produced.

The external pressure, mechanical work and plastic deformation applied on the interface zone provide the necessary energy needed for cold roll welding. The main steps which must be followed in cold welding processes are to initially remove surface contamination by treating the metallic surfaces, to align and fix the metallic strips in pack and finally execute the cold rolling process by adjusting the appropriate pressure and distance to the rollers.

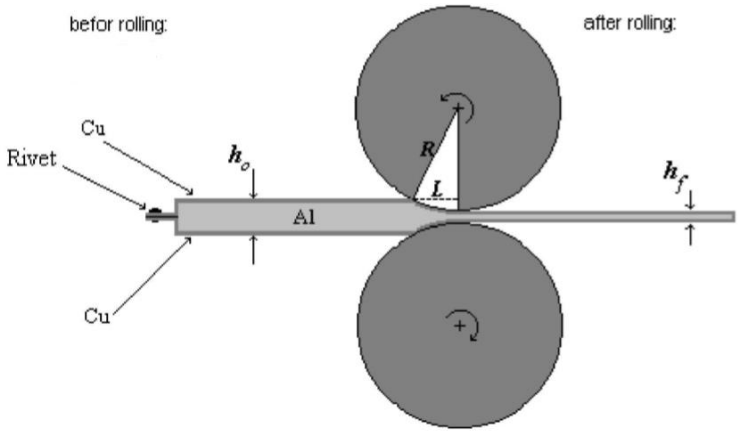

Figure 35 Cold roll welding process, [22]

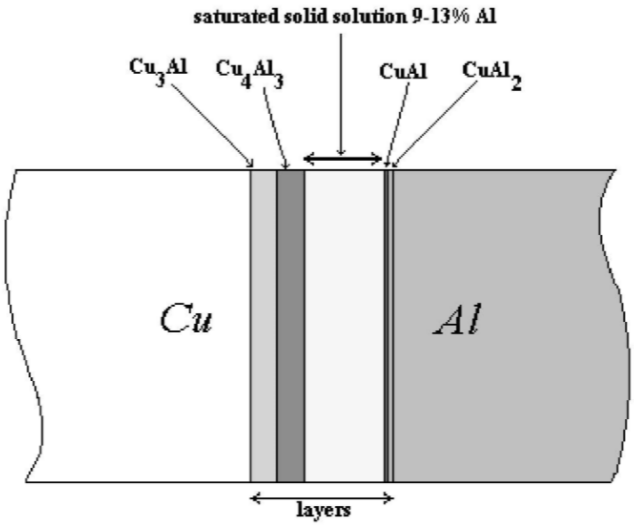

Figure 36 Typical example of welding zone composition at the interface of Al/Cu cold roll welding, [22]

The friction welding process is also a solid-state welding process but the welding mechanism differs from the one of cold roll welding. Specifically, in friction welding, the interface temperature is highly elevated by the developed friction providing transient viscous phase formations. The transient viscous phase is forced out of the bonding zone by the applied pressure.

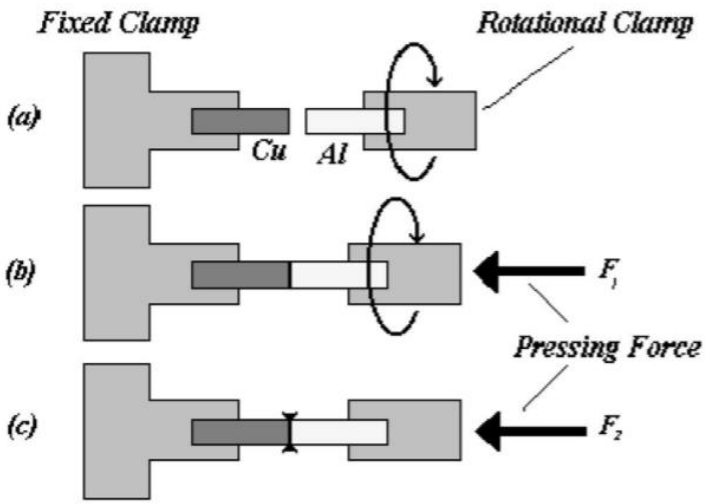

Figure 37 Friction welding of Al-Cu, [22]Figure 37

Explosive welding processes produce the appropriate heat to create a melted zone in the interface by explosion. The advantage which explosive welding offers is that bimetallic joints of high strength are provided even if the two metals are quite different to each other in terms of composition. The productions of explosive welding are characterized by high resistance against corrosion and by sufficient mechanical properties even under the influence of high temperature conditions. An explosive welding process can be conducted in two different ways; with the two metallic plates in parallel or with the two metallic plates in angled formation. In both occasions, an explosive layer is detonated producing very high temperatures and pressures resulting in stresses higher than the yield stress of both metals. This fact makes the two metals behave as fluids in the interface, providing a welding zone of high strength. The first metal is called flyer plate as it is melted by the explosion, covering the second metallic plate which is stable (parent plate). Finally, a thin elastic layer is oftenly placed for protecting the two metals from fracture due to extremely high-pressure waves of the explosion.

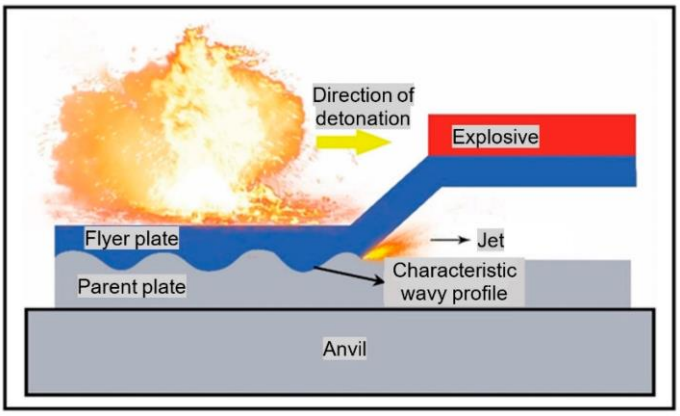

Figure 38 Explosive welding

Finally, regarding to the production of bimetallic structures by extrusion, the two metals are placed in the matrix interior. High pressures are applied by a moving piston, while the two metals are slightly heated. As a result, the two metals are strongly compressed and extruded. The high pressures and friction levels provide stresses which create a strong bimetallic joint in the interface of the two metals, producing in that way the desirable bimetallic structure.

4. Experimental Investigation of Bi-tubes Crashworthiness

4.1 Introduction

This study investigates the crashworthiness behavior of thin-walled circular bi-tubes under axial crushing loading. In order to assess the response characteristics of the crushed structure, both experimental and numerical simulation research studies are carried out. The aim in both cases is to observe the occurred collapse mode and estimate critical parameters of crashworthiness behavior, such as maximum crushing load, mean sustained load, specific energy absorption and/or the amount of absorbed energy.

4.2 Production of Bi-tube Specimens

Current chapter presents the experimental investigation of crashworthy response under axial loading. Four different bi-tube specimens are initially constructed and then tested. Two of the bi-tube specimens consist of an ertalon (PA6) single outter tube and a steel inner tube, while the other two ones contain an ertalon inner tube and a steel outter one. All constructed specimens are 100 mm long, while each one is described by different single tube thickness and diameters (inner and outter diameters). Two different thickness options are considered for each combination of steel and ertalon as the inner tube and the outter one. In particular, the four constructed and finally tested bi-tube specimens are depicted in Figure 39. Also, the dimensions of each bi-tube specimen and its single tube components are reported in Table 1 in more detail.

Each bi-tube specimen is constructed by initially producing its single tubes (bi-tube components) with turning process, and then pressing the one into another by enforcing the appropriate pressure, resulting in achieving a tight fit between the two tubes. In the case of ertalon outter tube (specimen C), the outter tube thickness is selected in order to ensure the necessary strength against shearing, which occurs due to the pressure enforcement during the bi-tube production process.

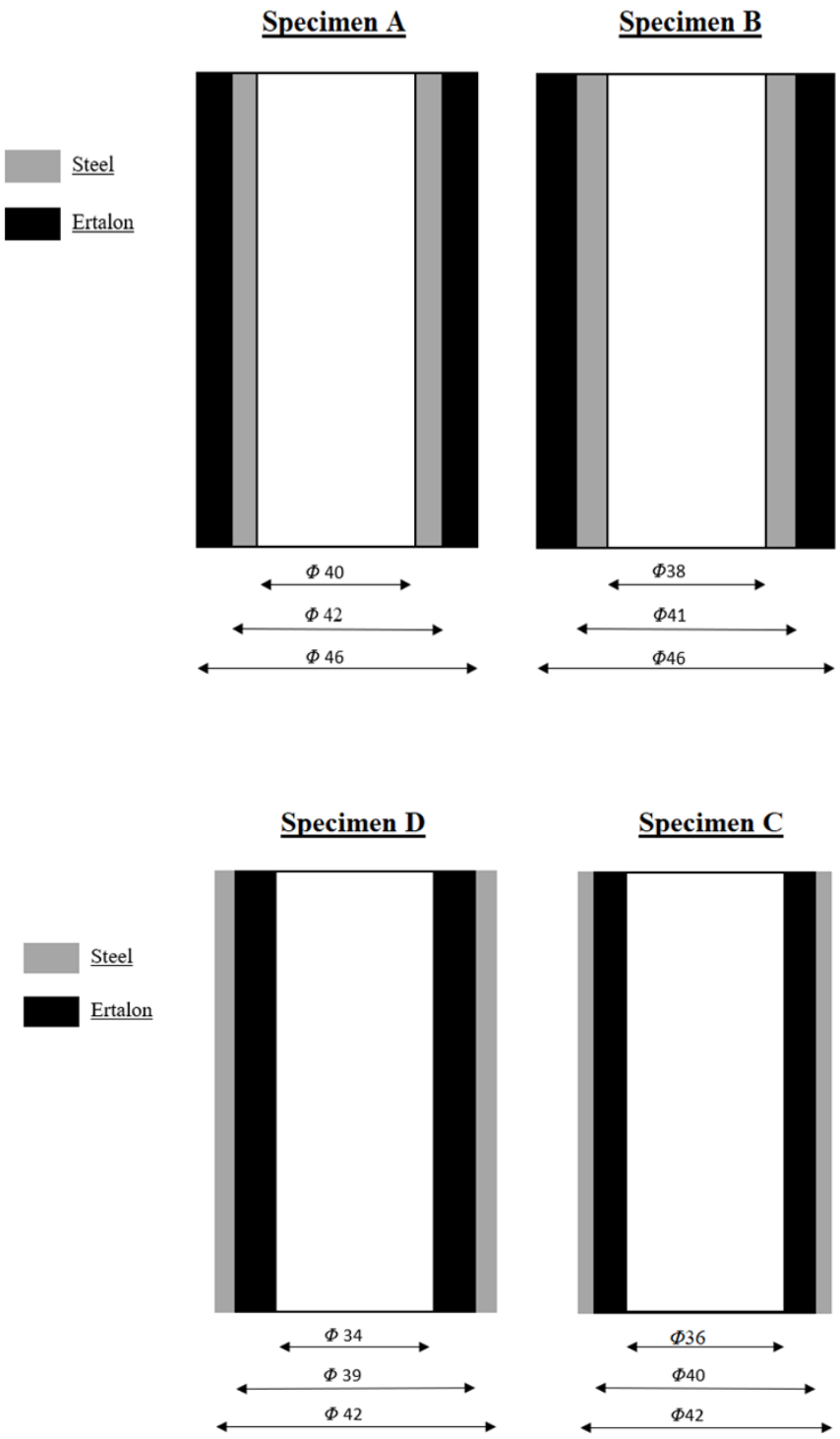

Figure 39 Constructed bi-tube specimens for experimental testing

Specimen	Length (mm)	Outter Diameter (mm)	Inner Diameter (mm)	Thickness (mm)
Specimen A				
Bi-tube	100	46	40	3
Inner tube (steel)	100	42	40	1
Outter tube (ertalon)	100	46	42	2
Specimen B				
Bi-tube	100	46	38	4
Inner tube (steel)	100	41	38	1.5
Outter tube (ertalon)	100	46	41	2.5
Specimen C				
Bi-tube	100	42	36	3
Inner tube (ertalon)	100	40	36	2
Outter tube (steel)	100	42	40	1
Specimen D				
Bi-tube	100	42	34	4
Inner tube (ertalon)	100	39	34	2.5
Outter tube (steel)	100	42	39	1.5

Table 1 Dimensions of each developed model (bi-tube specimens and single tubes)

4.3 Experimental Tests

This study carries out both experimental tests and numerical simulations in order to assess the response of bi-tube structures under axial crushing loads. The main goal of each analysis is to obtain the main response characteristics of a crashworthy structure and observe the crushing mode occurred during the collapse. Peak crushing load, mean sustained load, load uniformity, specific energy absorption and the amount of absorbed energy are some critical key parameters. These parameters together with the appeared collapse mechanism are considered as the appropriate metrics for comparisons between the provided experimental and numerical results. The conducted experimental tests can be used for two main reasons; the first one is to observe the crashworthy behavior

of the structure during the collapse and extract critical conclusions for key response characteristics, while in addition, the results from experimental tests can be utilized as validation source to assess the accuracy of developed numerical models. The last ones are widely used as they provide useful results in predicting the collapse mode and response characteristics of a crushed structure when they have been validated and their accuracy has been proved by sufficient matching against experimental data. The important advantage of carrying out numerical simulations is that they require less cost than conducting experimental tests where the necessary equipment (machine, high-frequency data recorders and high-speed cameras) is oftenly of high cost.

As reported previously in subsection 2.3, the experimental tests which can be conducted are either quasi-static or dynamic tests. The first ones require less expensive equipment but they provide less accurate results, as they are conducted at lower loading speeds than the appeared conditions in real crushes. In contrast, the dynamic crush tests represent more real crushing conditions and provide more accurate results as they are conducted at high loading speeds. However, the cost of such tests is quite higher and they are rarely preferred due to that.

For the purposes of the study of current thesis, the four constructed bi-tube specimens are tested to assess their crashworthy behavior. The experimental tests are conducted in quasi-static conditions by compressing each specimen in a pressing machine with a loading rate of 10 mm/min. All examined specimens are compressed until the final length of 40 mm (60 mm shortening). For each one of the tested bi-tube specimens, different states are captured during their axial collapse, while stress and strain measurements are recorded providing the experimental force-stroke curve. From the provided diagram, parameters which characterize the structure response in crashworthiness - such as peak crushing force (PCF), mean sustained load (F_{avg}), amount of absorbed energy (EA) and specific energy absorption (SEA) - can be computed. The following sections present the results for each bi-tube specimen separately, as the experimental tests revealed them.

4.3.1 Test Case of Specimen A

The bi-tube specimen A is 100 mm long and consists of an ertalon (PA 6) outter tube (Φ46/Φ42) and a steel inner tube (Φ42/Φ40). In the conducted experimental test, the bi-tube specimen is compressed with 10 mm/min loading speed, until its final length of 40mm causing a shortening of 60mm. The recorded data during the test revealed the F-s curve as Figure 40 depicts. Regarding to the provided F-s curve, a summary of previous studies on crashworthiness behavior of thin-walled structures, suggest that each peak of the curve refers to the

formulation of outter folds, while each locally minimum point of the curve refers to the formulation of inner folds. Table 2 presents critical parameters as the experimental data processing revealed for specimen A. Finally, Figure 41 depicts the states of axial collapse as revealed from the experimental test for bi-tube specimen A.

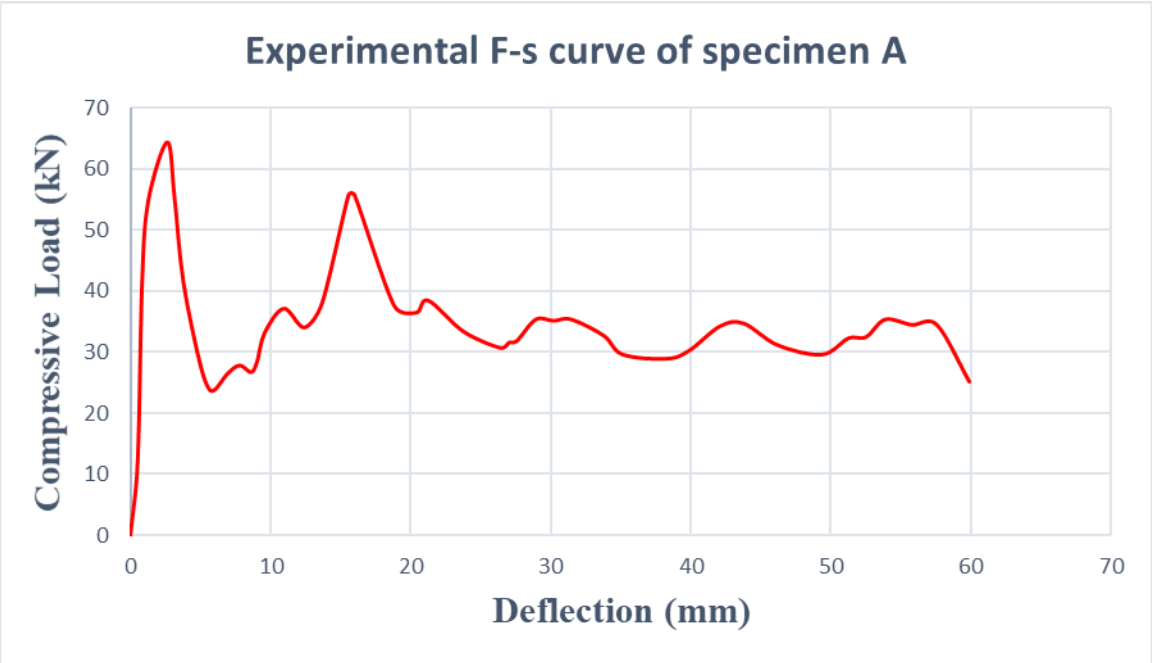

Figure 40 Experimental load-deflection curve of specimen A

Experimental Results	
Bi-tube Specimen A	
Peak Crushing Force (kN)	64.46
Mean Sustained Load (kN)	34.69
Energy Absorption (J)	2081.11
Specific Energy Absorption (J/kg)	15689.01

Table 2 Critical response parameters for crashworthiness behavior of bi-tube specimen A

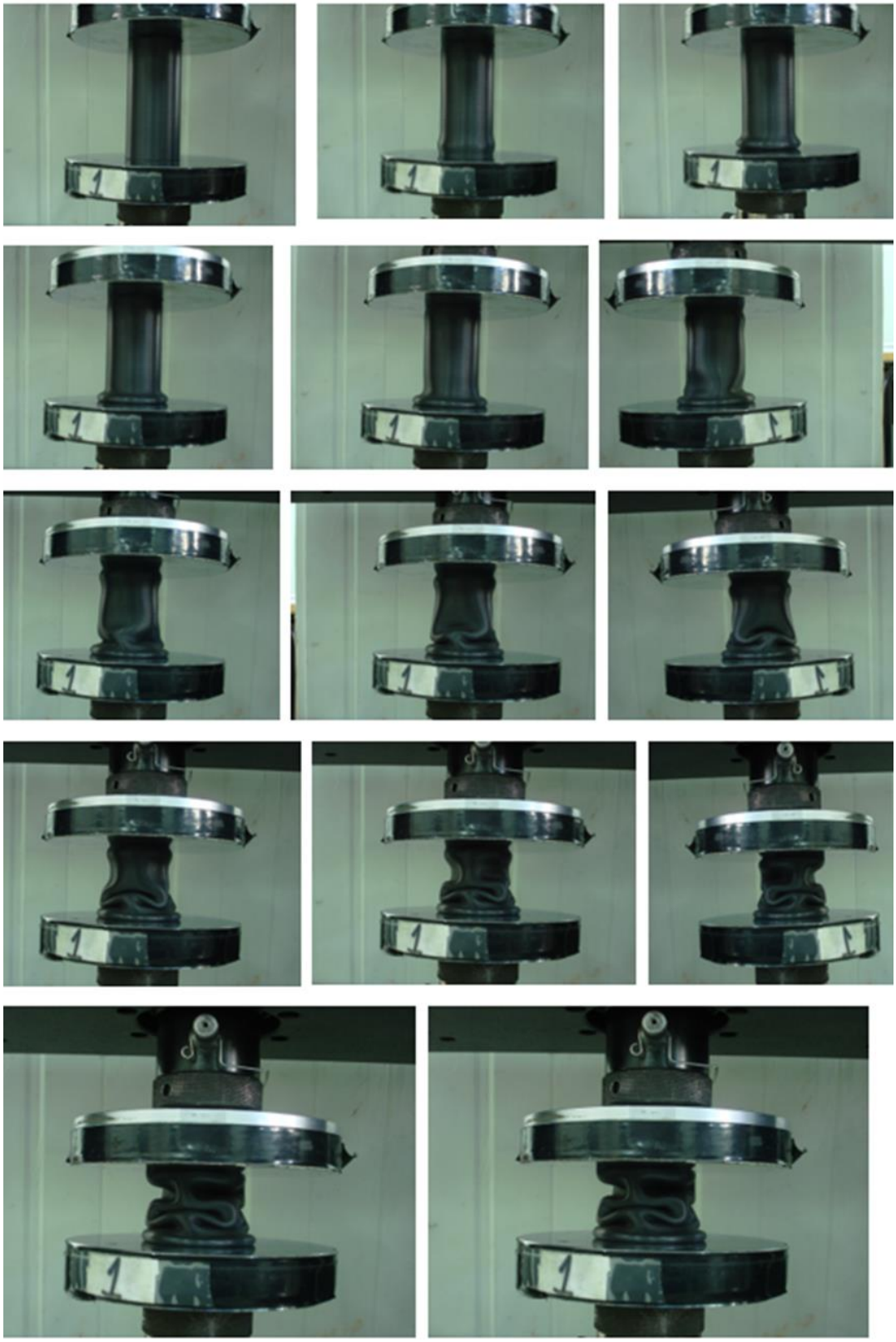

Figure 41 States of specimen A axial collapse

As Figure 41 shows, the bi-tube specimen A is initially folding in concertina mode at its bottom edge by developing one fold, while diamond mode of folding is then occurred with diamond folds to be formulated. As a result, the collapse of bi-tube specimen A can be described as a mixed crushing mode combining both concertina and diamond collapse mechanisms. Finally, Figure 43 and Figure 43 show the final crushed structure of bi-tube specimen A. As observed from the cut structure, the adhesion between the two tube components - inner and outter ones – has been partially lost. In particular, the adhesion has been fully maintained in the internal edge of some convolutions or has been fully lost. Also, it is observed that the softer material of external ertalon tube is oftenly trapped and extruded severely in the convolutions of the harder internal steel tube.

Figure 42 Crushed structure of bi-tube specimen A

Figure 43 Cut structure of crushed bi-tube specimen A

4.3.2 Test Case of Specimen B

The bi-tube specimen B is 100 mm long too and contains an ertalon (PA 6) outter tube (Φ46/Φ41) and a steel inner tube (Φ41/Φ38). In fact, bi-tube specimen B dimensions are selected considering increased thickness for both inner and outter tubes compared to specimen A ones. The specific dimensions are selected in order to assess the impact of thickness on crashworthiness behavior and energy absorption capability. In the conducted experimental test, the bi-tube specimen is compressed with 10 mm/min loading speed, until its final length of 40mm causing a shortening of 60mm. The recorded data during the test revealed the respective following F-s curve, shown in Figure 44, the processing of which provides the response characteristics of structure crashworthiness behavior as Table 3 depicts. Finally, Figure 45 depicts the states of axial collapse as revealed from the experimental test for bi-tube specimen B.

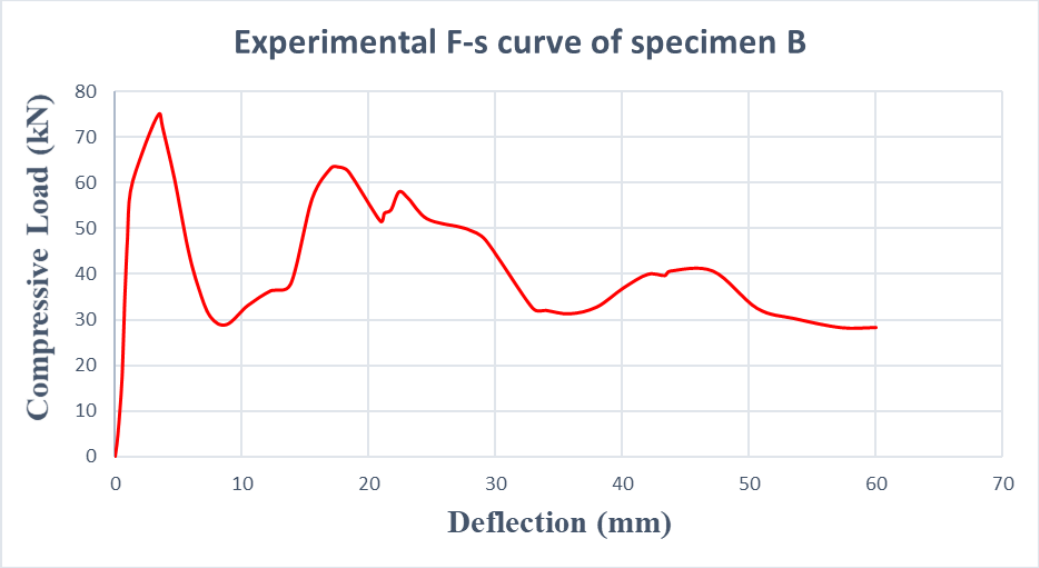

Figure 44 Experimental load-deflection curve of specimen B

Experimental Results	
Bi-tube Specimen B	
Peak Crushing Force (kN)	75.28
Mean Sustained Load (kN)	41.78
Energy Absorption (J)	2507.06
Specific Energy Absorption (J/kg)	13548.70

Table 3 Critical response parameters for crashworthiness behavior of bi-tube specimen B

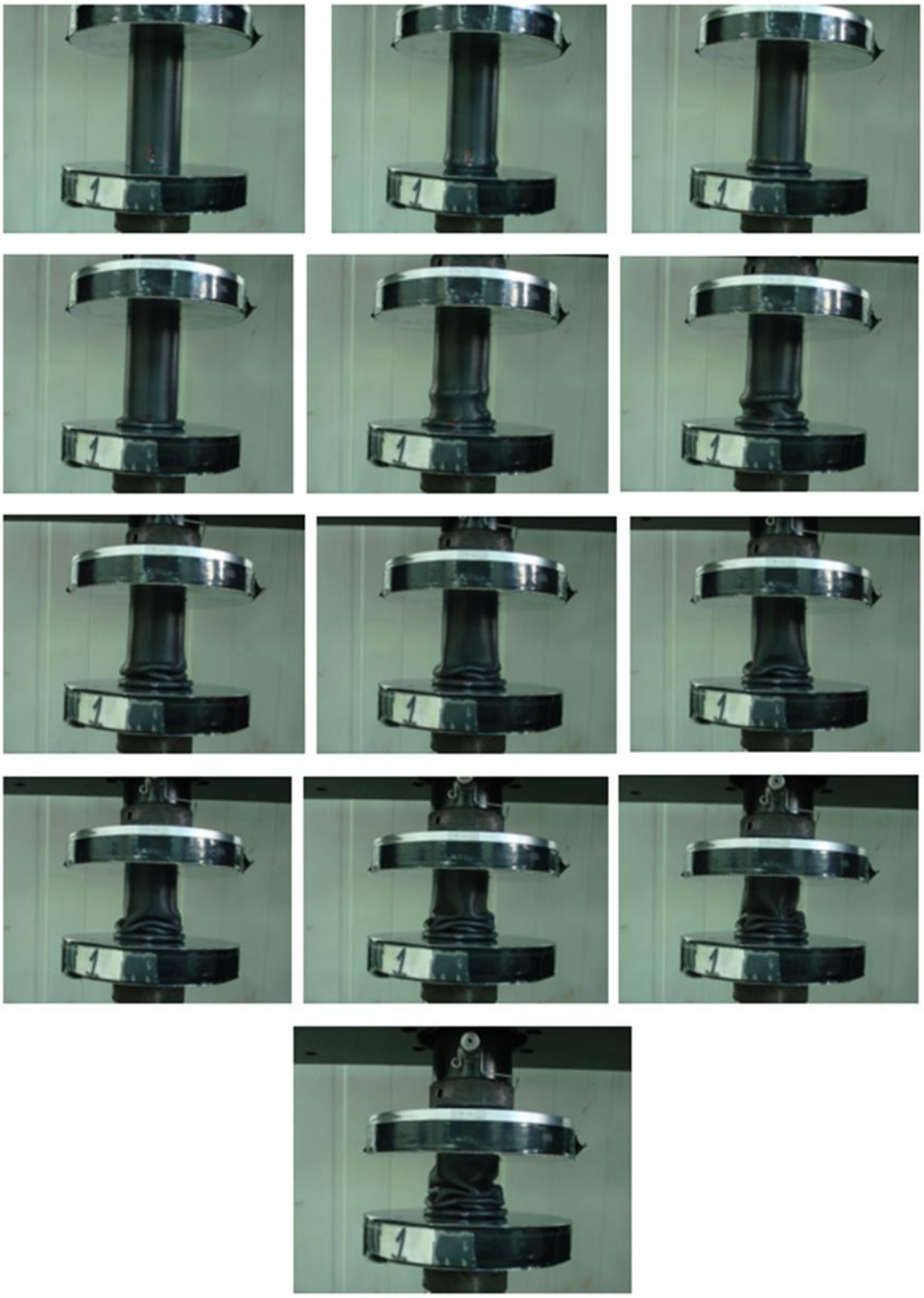

Figure 45 States of specimen B axial collapse

As Figure 45 shows, the bi-tube specimen B is initially folding in concertina mode at its bottom edge, while diamond mode of folding is then occurred, resulting in developing a mixed mode of collapse mechanism for bi-tube specimen B. Finally, Figure 46 and Figure 47 show the final crushed structure of bi-tube specimen B. As observed from the cut structure, the adhesion between

the two tube components - inner and outter ones – has been partially lost. In particular, the adhesion has been fully maintained in the internal edge of some convolutions or has been fully lost as a large convolution of external ertalon tube often contains two small folds of internal steel tube without although maintaining their contact.

Figure 46 Crushed structure of bi-tube specimen B

Figure 47 Cut structure of crushed bi-tube specimen B

4.3.3 Test Case of Specimen C

The bi-tube specimen C is 100 mm long and consists of an ertalon (PA 6) inner tube (Φ40/Φ36) and a steel outter tube (Φ42/Φ40). In the conducted experimental test, the bi-tube specimen is compressed with 10 mm/min loading speed, until its final length of 40mm causing a shortening of 60mm. The recorded data during the test revealed the respective following F-s curve which is depicted in Figure 48, while the progressive collapse mechanism according to which bi-tube specimen C fails is illustrated in Figure 49. Finally, the experimental data processing allows the computation of the response characteristics referring to crashworthiness behavior as Table 4 reveals.

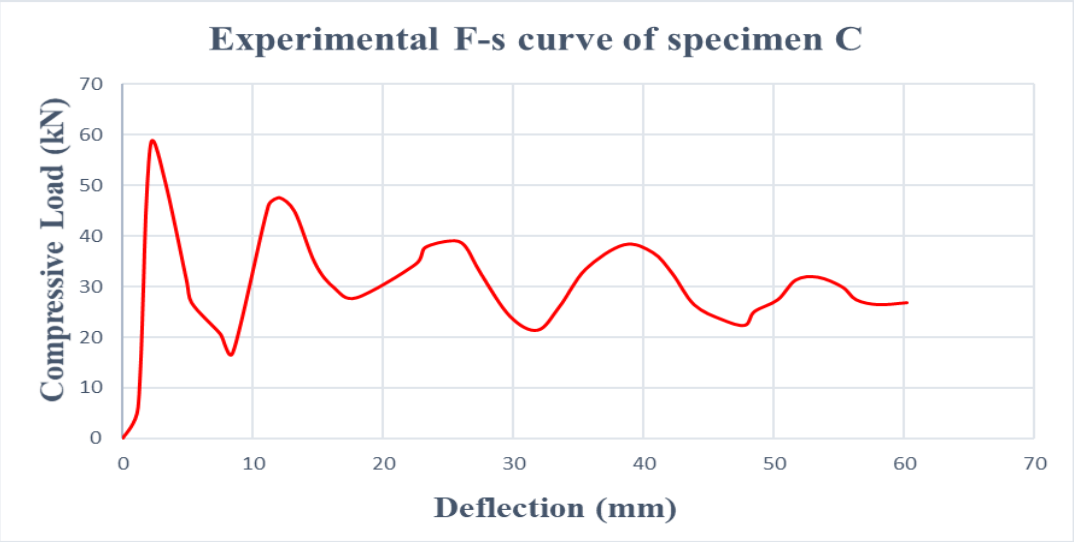

Figure 48 Experimental load-deflection curve of specimen C

Experimental Results	
	Bi-tube Specimen C
Peak Crushing Force (kN)	58.83
Mean Sustained Load (kN)	30.98
Energy Absorption (J)	1858.73
Specific Energy Absorption (J/kg)	14485.99

Table 4 Critical response parameters for crashworthiness behavior of bi-tube specimen C

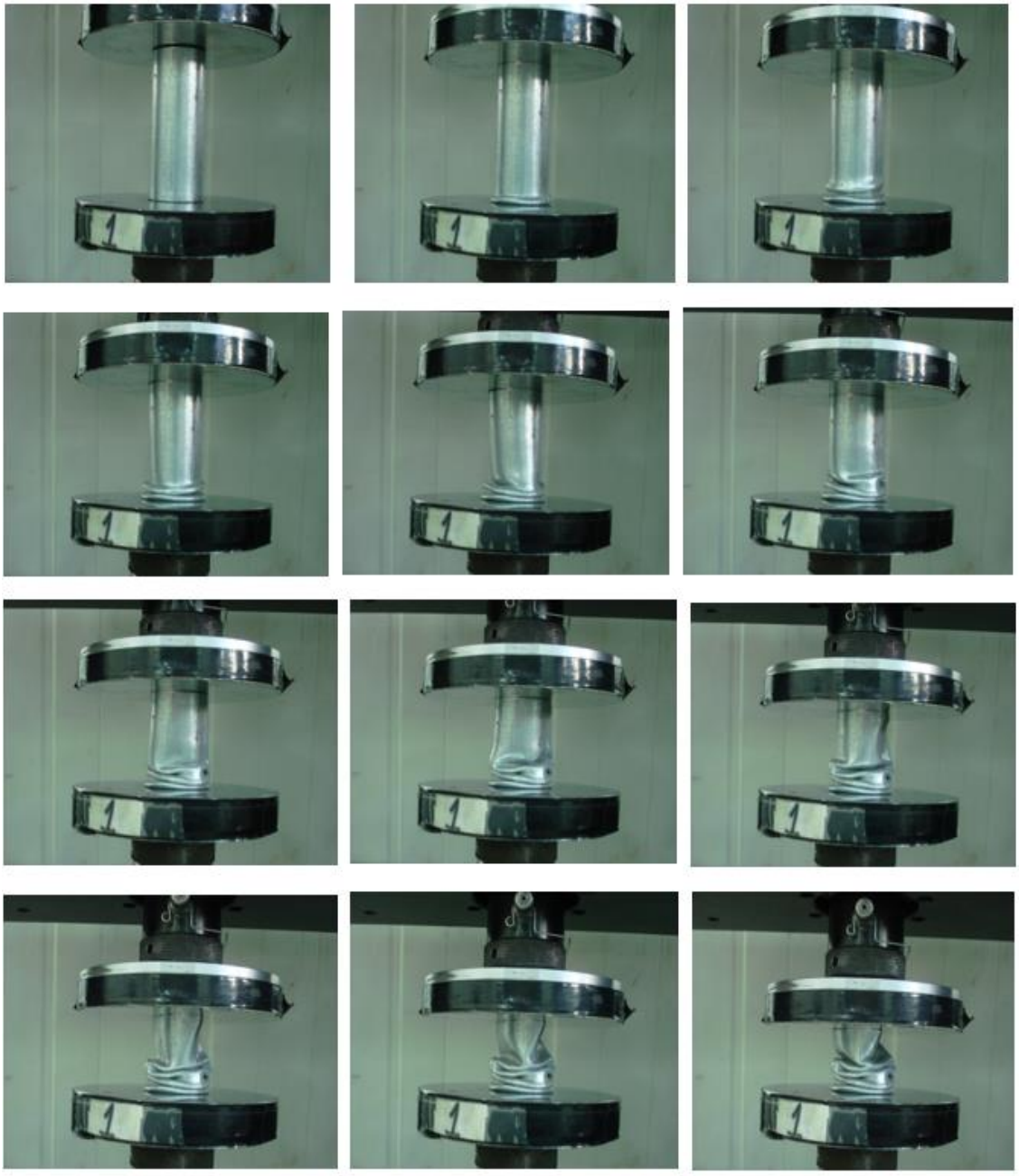

Figure 49 States of specimen C axial collapse

As depicted above in Figure 49, bi-tube specimen C begins collapsing under concertina mode by formulating two folds, while it continues to collapse under diamond mode until its final compression. So, a mixed collapse mechanism is occurred as the bi-tube specimen C is compressed, because both concertina at initial stage and diamond folds at following stages are formulated. Finally, Figure 50 and Figure 51 show the final crushed structure of bi-tube specimen C. As observed from the cut structure, the adhesion between the internal and external tubes is fully maintained in the section of bi-tube specimen where the convolutions are formulated as the developed folds of softer inner tube are penetrate into the developed folds of harder external tube. In contrast, the

adhesion is lost in the section where the bi-tube is simply compressed without formulating any fold yet.

Figure 50 Crushed structure of bi-tube specimen C

Figure 51 Cut structure of crushed bi-tube specimen C

4.3.4 Test Case of Specimen D

The bi-tube specimen D is 100 mm long and contains an ertalon (PA 6) inner tube (Φ39/Φ34) and a steel outter tube (Φ42/Φ39). In fact, bi-tube specimen D dimensions are selected considering increased thickness for both inner and outter tubes compared to specimen C ones. The specific dimensions are selected in order to assess the impact of thickness on crashworthiness behavior and energy absorption capability. In the conducted experimental test, the bi-tube specimen is compressed with 10 mm/min loading speed, until its final length of 40mm causing a shortening of 60mm. The recorded data during the test revealed the respective following F-s curve, shown in Figure 52, the processing of which provides the response characteristics of structure crashworthiness behavior as Table 5 depicts. Finally, Figure 53 depicts the states of axial collapse as revealed from the experimental test for bi-tube specimen D.

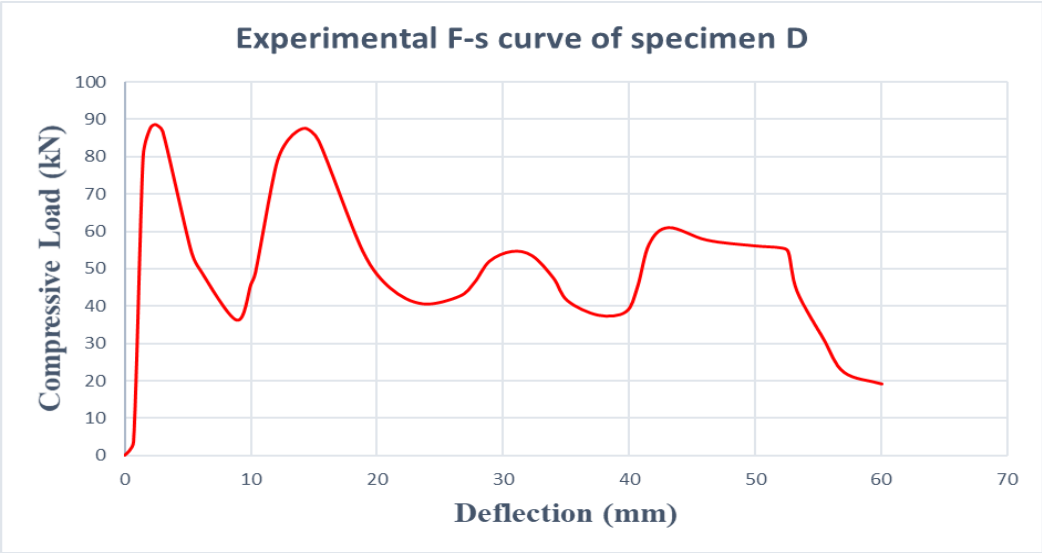

Figure 52 Experimental load-deflection curve of specimen D

Experimental Results	
Bi-tube Specimen D	
Peak Crushing Force (kN)	88.51
Mean Sustained Load (kN)	51.09
Energy Absorption (J)	3065.62
Specific Energy Absorption (J/kg)	16806.77

Table 5 Critical response parameters of crashworthiness behavior of bi-tube specimen D

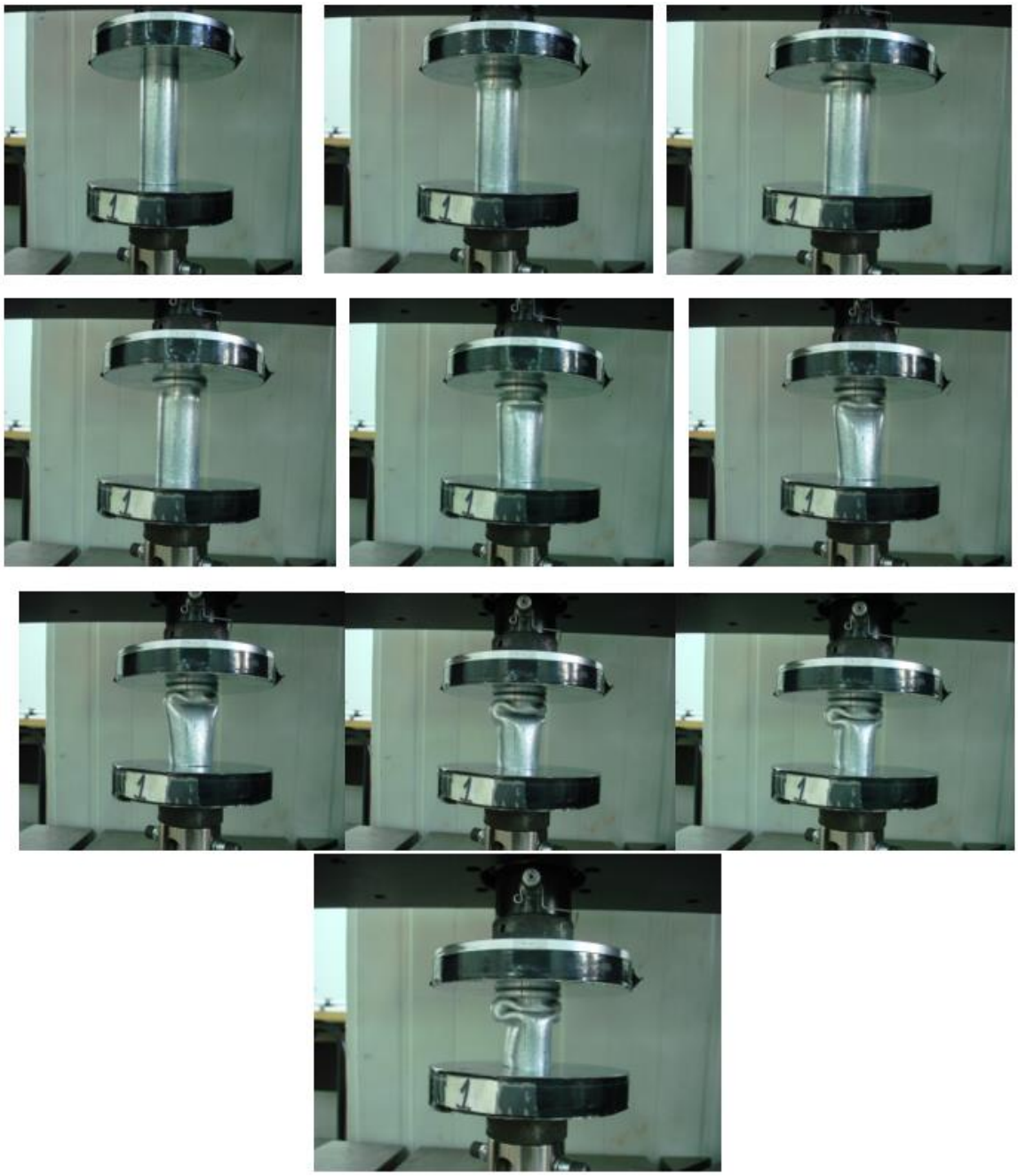

Figure 53 States of specimen D axial collapse

Looking at Figure 53, it is observed that bi-tube specimen D starts collapsing in concertina mode by formulating one circular fold, while it continues to deform under diamond collapse mode. Thus, a mixed collapse mode seems to be occurred as the bi-tube specimen D is deforming during its compression. Finally, Figure 54 and Figure 55 show the final crushed structure of bi-tube specimen C. As observed from the cut structure, the adhesion between the two tubes – internal one and external one – is almost fully maintained, especially in the section of bi-tube where convolutions have been formulated.

Figure 54 Crushed structure of bi-tube specimen D

Figure 55 Cut structure of crushed bi-tube specimen D

4.4 Conclusions

By summarizing the revealed results from the experiments, critical conclusions can be extracted for the crashworthiness response of examined bi-tube structures. More specifically, the results revealed that in both occasions of ertalon/steel (specimens C and D) or steel/ertalon (specimens A and B) as

internal and external tubes respectively, the specimens of larger thickness (B and D) provided greater peak crushing force and mean sustained load (Figure 56) compared to the ones of smaller thickness (specimens A and C). In addition, specimens C and D revealed greater energy absorption capability and specific energy absorption (Figure 57 and Figure 58). The above experimental results suggest that as the bi-tube thickness increases, the energy absorption capability of the structure gets greater too, as the sustained load, the peak load, the amount of absorbed energy and the specific energy absorption are all increasing. This conclusion totally agrees with the suggestion made by both Alexander [19] and Mamalis et al. [17], according to which as the thickness of a bi-tube structure gets larger, the sustained load increases resulting in an energy absorption capability increment. Further, considering that the sustained load, and thus the mount of absorbed energy, varies proportionally to the external diameter of the bi-tube, the bi-tube structure which consists of a harder external tube (steel) and a softer internal one (ertalon), is the one which appears to behave in a more crashworthy way. Especially, the sustained load and the absorbed energy are expected to be even higher compared to the ones of specimens A&B when the specimen D is of the same external diameter. Also, in fact, specimen D is characterized by the higher energy absorption capability as is the one with the greatest SEA, which is considered as the one of the most appropriate metrics to assess the crashworthiness of different structures.

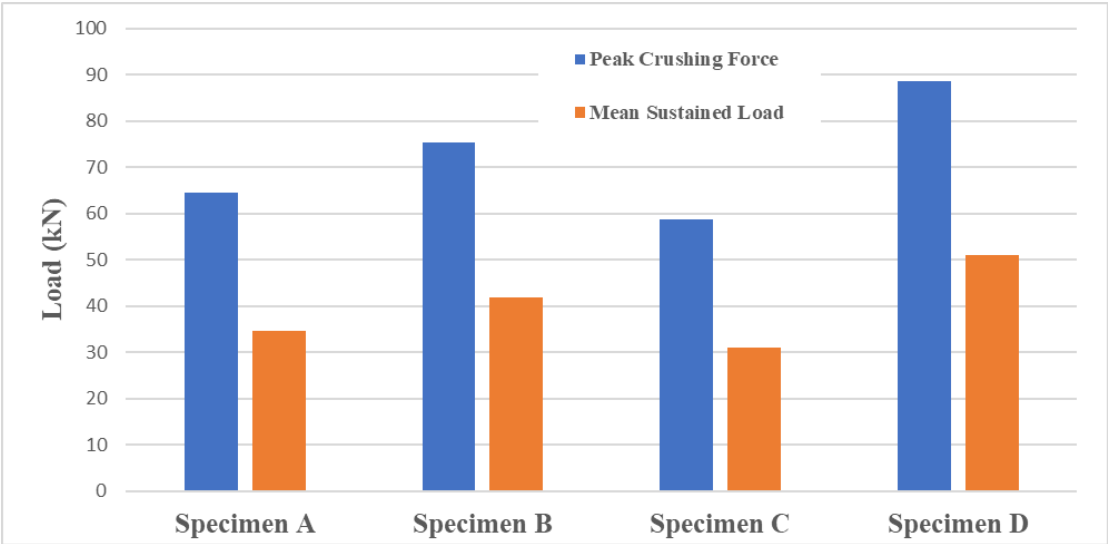

Figure 56 Experimental results for peak crushing force and mean sustained load of examined bi-tube specimens

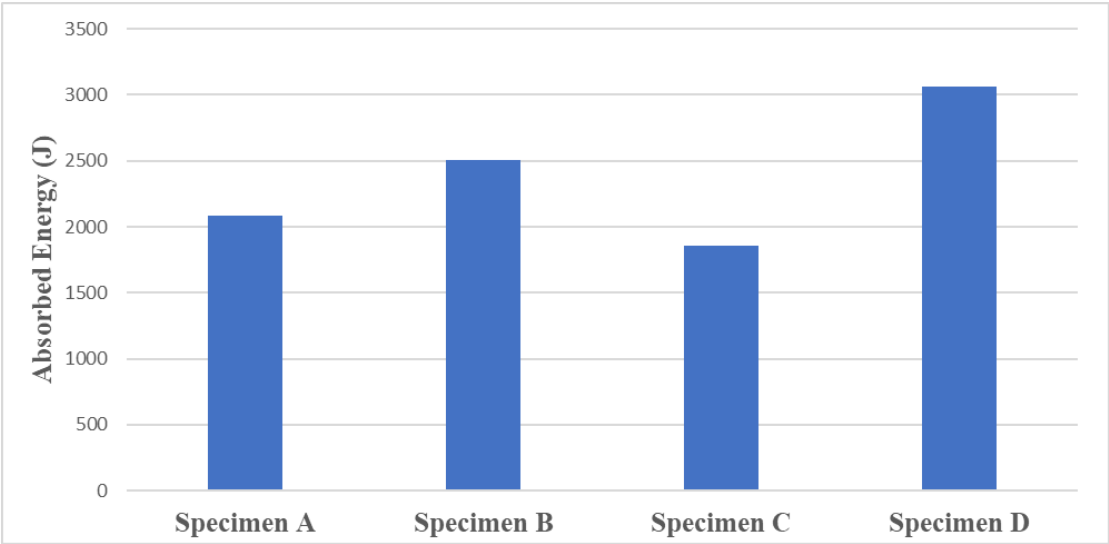

Figure 57 Experimental results for energy absorption capability of the examined bi-tube specimens

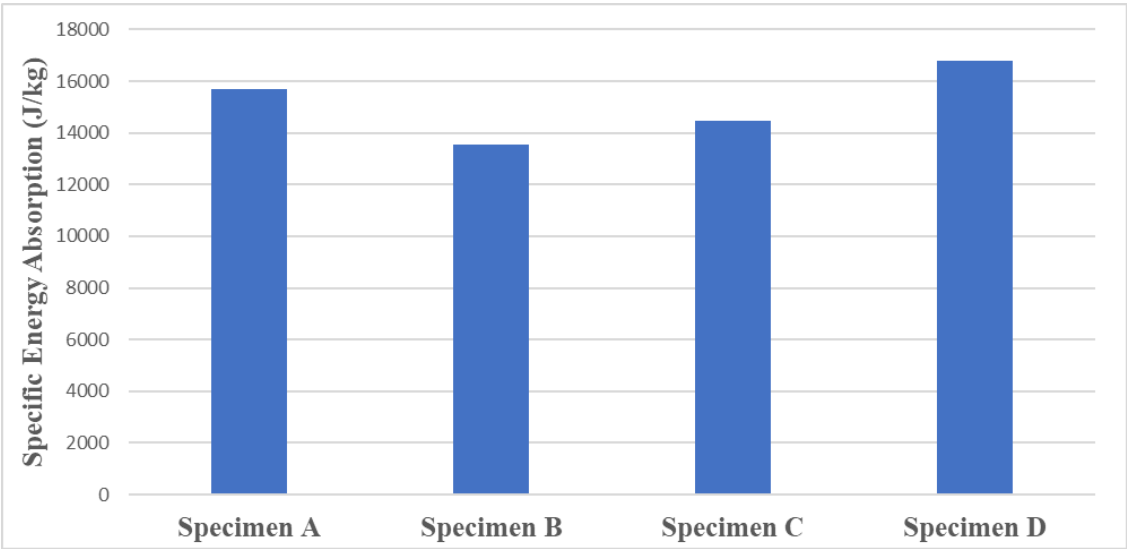

Figure 58 Experimental results for specific energy absorption of the examined bi-tube specimens

Further, all examined bi-tube specimens started collapsing in concertina mode by initially formulating a ring fold at their bottom edge, except from bi-tube specimen D which developed a ring fold at its top edge. Following, all specimens continue collapsing in diamond mode by formulating 2-lobes or 3-lobes folds. So, the occurred collapse mechanism is described as a mixed mode for all tested specimens.

Finally, in the case of softer external tube (ertalon) the adhesion between the two tubes is partially lost during collapse, as the larger convolutions of softer external material oftenly contain smaller folds of harder internal tube, without

although maintaining any contact. However, when bi-tube thickness increases, the adhesion is slightly maintained as the softer external tube folds are trapped and partially extruded by the harder internal tube folds. In contrast, in the case of harder external tube (steel), the adhesion between the two materials is fully maintained in the bi-tube section where convolutions have been formulated. This trend is getting stronger as the bi-tube thickness increases.

So, by concluding, the increased bi-tube thickness seems to affect positively the energy absorption capability of a structure by increasing it and making in that way the structure able of behaving in a more crashworthy way. Further, the combination of a harder external tube with a softer internal one seems to provide a better structure in terms of crashworthiness. Finally, the bi-tubes of greater thickness seem to maintain in larger percentage the adhesion between their tube components.

5. Finite Element Modelling Approach of Bi-tubes and Simulation Results

5.1 Introduction

The aim of this study is to investigate crashworthiness behavior of circular thin-walled bi-tubes by both conducting experimental tests and numerical simulations. The development of appropriate models in software offers the capability to obtain the crashworthiness response characteristics, the failure mode and the type of collapse without spending high costs for experimental equipment. Also, simulations can be carried out in order to investigate how different parameters affect the response and the characteristics of the crushed structure. Such important and interesting to analyze parameters can be related to structure, like dimensions (length, diameter, thickness), the combination of materials in case of bi-tubes, special structure configurations (edges etc.), type of supports etc., or can be related on loading characteristics like crushing speed. However, an important step before carrying out simulation cases, is the comparison of developed models with experimental data in order to assess their validity and accuracy.

The study of present diploma thesis utilizes Finite Element Analysis (FEA) for the needs of model development. In particular, a finite element modelling approach is used in this study in order to create the appropriate models of bi-tubes. LS-DYNA software [23] is utilized as the modelling tool for the purposes of current study. In general, the first step of modelling procedure with FEA is the geometry determination of the structure by defining the structure shape and the appropriate dimensions. Next, mesh generation usually follows by properly distributing the finite element nodes. Many softwares offer an automatic mesh generation, but they allow users to select the preferable mesh density and type of finite elements. Also, the material properties of the created structure are defined too, by giving information about physical and mechanical properties, like yield stress, Young modulus, Poisson ratio, density and finally the stress-plastic strain curve. After that, the support characteristics must be enforced, while the last stage of modelling is to define the loading characteristics.

The above modelling steps are made in the pre-processor of LS-DYNA. So, by summarizing, the pre-processing procedure includes the following steps:

- ✓ Geometry determination

- ✓ Mesh generation
- ✓ Material properties
- ✓ Support characteristics
- ✓ Loading characteristics

As soon as the model is developed, LS-DYNA solver computes the response of the examined structure under the defined loading, by solving the equations provided from the implementation of FEA. Finally, when the numerical solution by the solver ends, LS-DYNA post-processor allows to observe the response of crushed structure under loading conditions. Further, post-processor provides critical data for the crushed structure like crashworthiness characteristics, observed failure mode, load-deflection diagram (F-s curve) etc. Thus, the modelling and calculating procedure in LS-DYNA includes the following three stages as Figure 59 depicts. The first and the last stage of the illustrated procedure can be both conducted in LS Pre-Post. LS Pre-Post includes both pre-processor and pro-processor of LS-DYNA, but not the solver which is provided by ANSYS software.

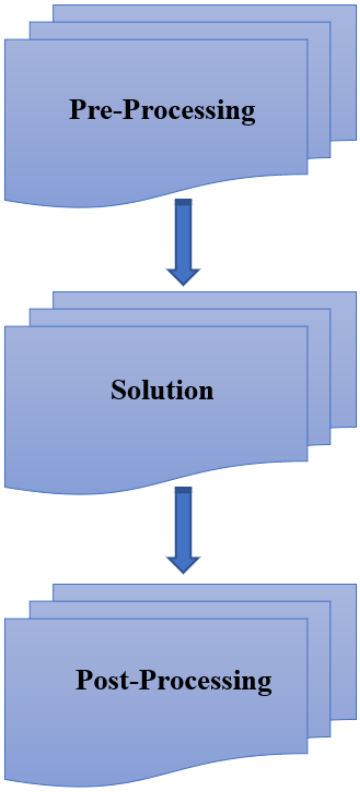

Figure 59 Modelling and calculating procedure of FEA in LS-DYNA

Finally, the unit system which LS-DYNA uses is shown in Table 6. Each produced variable is also expected to be described by the respective units, as for example the unit of N·mm=mJ for energy.

Variable	Units
Mass	gr
Length	mm
Time	msec
Velocity	mm/msec
Force	N
Stress	N/mm^2
Density	gr/mm^3

Table 6 Units system in LS-DYNA software

5.2 Modelling of Bi-tube Specimens in LS-DYNA

For the needs of this study, four different bi-tube specimens are modelled and examined. Each bi-tube specimen consists of one inner tube and one outter tube. The single tubes are constructed by steel or ertalon (PA 6). All examined specimens are 100 mm long. The first two bi-tube specimens (specimen A and specimen B) consist of a steel inner tube and an ertalon outter tube, while the last two bi-tube specimens (specimen C and specimen D) consist of an ertalon inner tube and a steel outter tube. The four examined bi-tube specimens, which are modelled, are presented in Figure 39. Further, the dimensions of each bi-tube specimen and its single tube components are also depicted in Table 1. For each bi-tube specimens, the models of its single tubes are also developed and simulated in order to observe the difference between the crashworthiness response of bi-tube structure and the one of the superposition provided from the two single tubes. So, 12 models are developed overall in LS-DYNA software, 4 of them for the bi-tube specimens and 8 of them for the single tubes. The modelling procedure as it was conducted in the pre-processor of LS-DYNA (LS Pre-Post) is presented in detail below.

Each examined configuration is consisted of the bi-tube specimen, an upper plate and a down plate. The upper plate is the one which moves down, compressing the bi-tube specimen with a constant speed, while the down plate is stationary. Also, both plates are considered as rigid bodies compared to the bi-tube specimen. A typical illustration of the examined configuration is depicted in Figure 60.

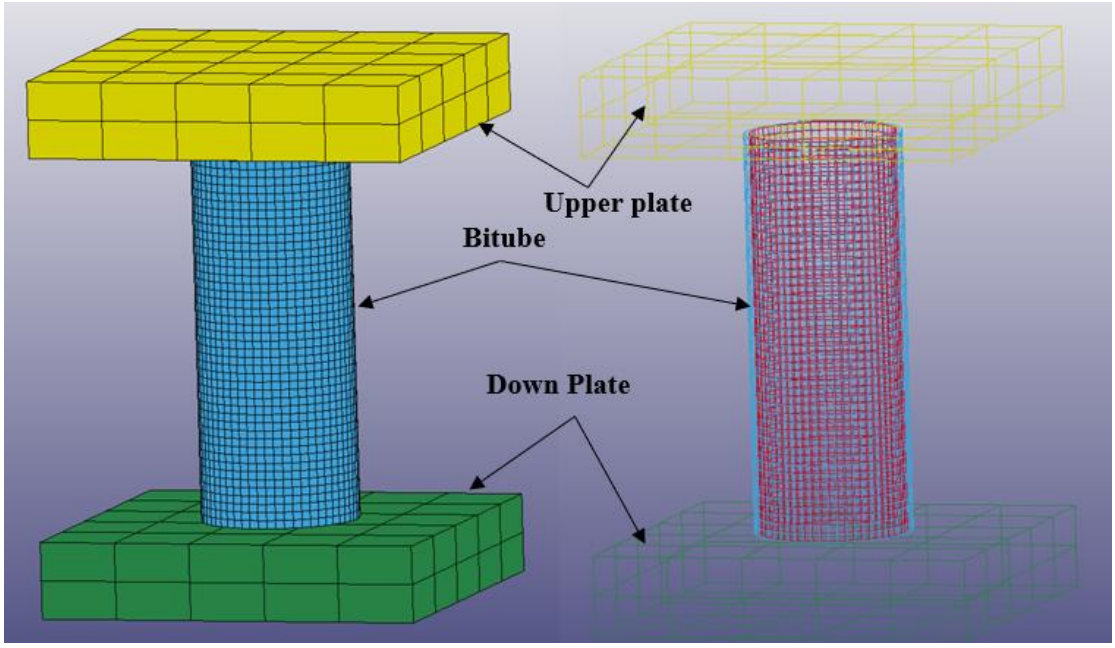

Figure 60 Examined configuration for modelling in LS-DYNA

The basic steps of the modelling procedure are to initially define the desirable specimen geometry (shape and dimension) and select a mesh density. After that, each created body is characterized by an individual section which describes the finite elements from which the body is consisted of. For the needs of this study, shell elements (*Section_Shell*) are selected for the single tubes and solid elements (*Section_Solid*) are selected for the two plates. Next, the material of each body is selected according to its physical and mechanical properties. After that, the appropriate considerations for each contact between two surfaces are following. This study considers the contacts between the two plates and the bi-tube specimen and the contacts of bi-tube folds which are developed during the collapse. Finally, the loading characteristics are selected by adjusting a constant speed to the upper plate. All four examined specimens are compressed until the deflection reaches 60 mm, or in other words until the final length of 40 mm, while the crush velocity is adjusted at 0.5 mm/msec in every case. In the following sections, the modelling procedure is described in more detail.

5.2.1 Geometry determination

In the first stage, the specimen shape and the appropriate dimensions are adjusted for each bi-tube specimen, by initially defining the shape and the dimensions of its single tubes (inner and outter ones). Especially, all developed tube models refer to circular thin-walled tubes with length of 100 mm. Because of their thin-walled structure, tube models are created with use of 2D plane finite elements, usually called as *shell elements*. In contrast, the two plates which are considered compact bodies, are modelled with 3D finite elements, usually called

as *solid elements*. In each case, the tube models use shell elements as the size of thickness compared to the diameter or the length of the tube, is negligible. So, shell elements provide less nodes, resulting in lower computational time and cost. However, for the tube models appropriate dimensions, the use of shell elements means that each tube model is developed considering the mean diameter $d_m=(d_{in}+d_{out})/2$.

Thus, in LS Pre-Post environment, the two first defined geometries are for the inner and outter tubes. As soon as the two single tube models are created, they are set as a common part by selecting them and creating a new entity (FEM→Model and Part→Create Entity→Set Data →Set Part). Each single circular tube model is created by selecting the *Cylinder Shell* choice which is included in the *Shape Mesher* of LS Pre-Post. So, for each tube, the mean diameter and its length are adjusted properly. As mentioned before, the length is equal to 100 mm in every case. As soon as the two single tube models are created and set as a common part, the two plate geometries are defined. For the plates, the *Box Solid* choice of *Shape Mesher* is selected. There, the dimensions of the plate are defined which are the same for every examined case. In particular, each plate is 50mm in width and length, and 20mm in thickness.

5.2.2 Mesh Generation

In the second stage, without in fact having finished within *Shape Mesher* yet, the mesh density is selected properly. More specifically, the mesh density is adjusted by introducing the size of finite elements. A key parameter in problems like the one studied in this thesis, is that the size of the finite elements of tube models must be greater than the thickness of the single tube in order to predicting accurately the type and number of folds. Further, the number of finite elements in the circumferential direction, is selected the same for the inner tube and the outter one. So, in the cases that the maximum thickness of single tubes is 2 mm, the mesh is generated for providing finite elements of 2.1 mm width, while for maximum single tubes thickness 2.5mm, the mesh is generated for providing elements of 2.6mm width. For the plates, a more arrow mesh is generated with 5 elements in width, 5 elements in length and 2 elements in thickness. The arrow mesh generation of the plates is reasonable considering that they are treated as rigid bodies.

After mesh generation, the type of elements which each part uses must be defined by making the appropriate selection in *Section* tab of *Keyword Manager*. Thus, a *shell section* is selected to describe the single tube parts, in which the tube thickness is introduced. Also, the number of through shell thickness integration points (NIP) is set equal to 3, while the parameter ELFORM is kept equal to 2 which is its default value. The ELFORM parameter of 2 suggests that the shell formulation is computed according to Belytschko-Lin-Tsay. The proposed mode of formulation is then based on Reissner-Mindlin kinematic assumption providing 5 degrees of freedom (DOF) in local coordinate system

which are the displacements of three axis (u_x, u_y, u_z) and the two rotations (θ_x, θ_y) from bending moments, constraining in that way only torsional rotation (θ_z). Finally, ELFORM option equal to 2 has been proved extremely effective as it takes into account the strain rate effect and the Cauchy stresses distribution, while it enforces a bi-linear interpolation between the element nodes. Additionally, for the modelling of bi-tube specimen B in specific, the ELFORM parameter is adjusted at 16 introducing a fully integrated shell element formulation for specimen B model. This specific option is selected because the model does not behave during collapse according to an appropriate mode, and so different element formulation needs to be introduced. On the other hand, a *Solid Section* is selected for the plates as they are modelled with solid elements. For the plates, the respective ELFORM parameter of *solid section* is kept equal to 1 as the default option. The modelling procedure of defining the appropriate geometry and mesh characteristics is depicted in the following figures.

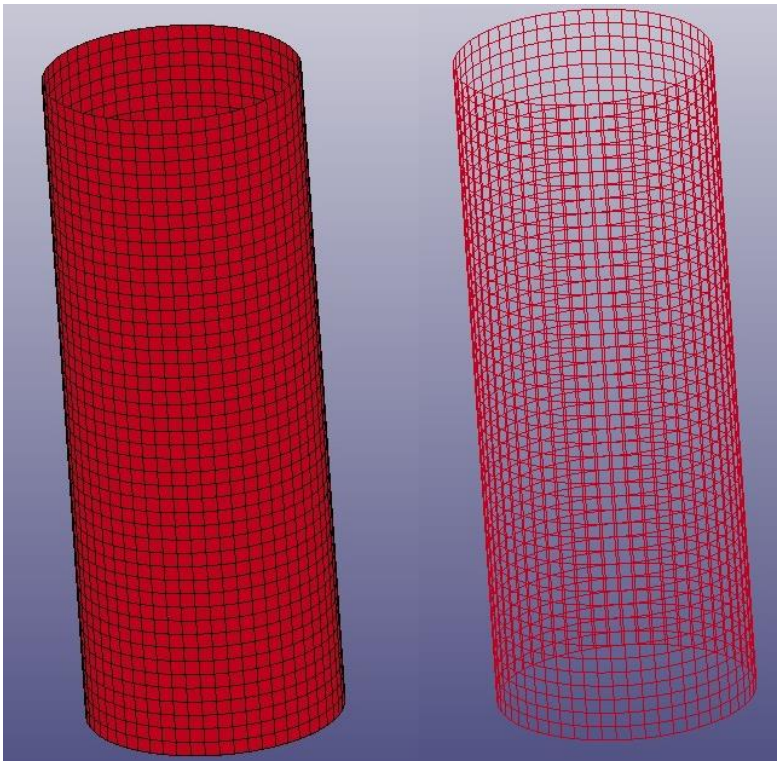

Figure 61 Inner tube geometry and mesh generation

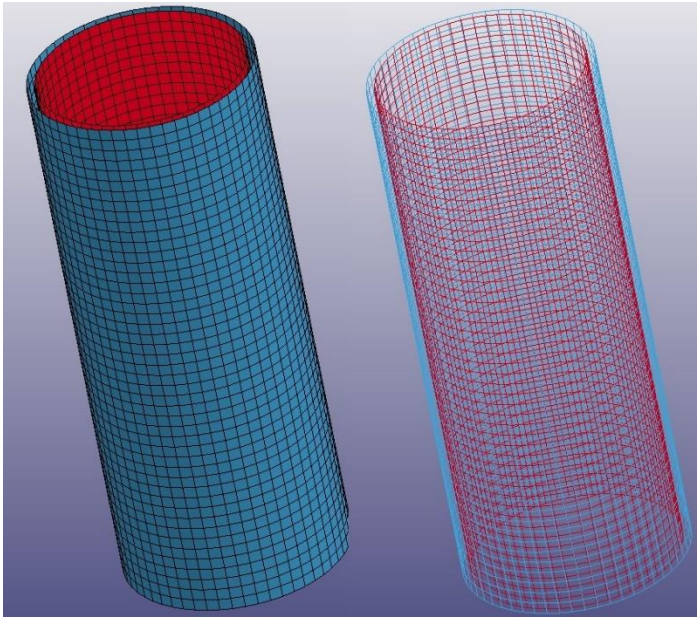

Figure 62 Bi-tube specimen model geometry and mesh generation

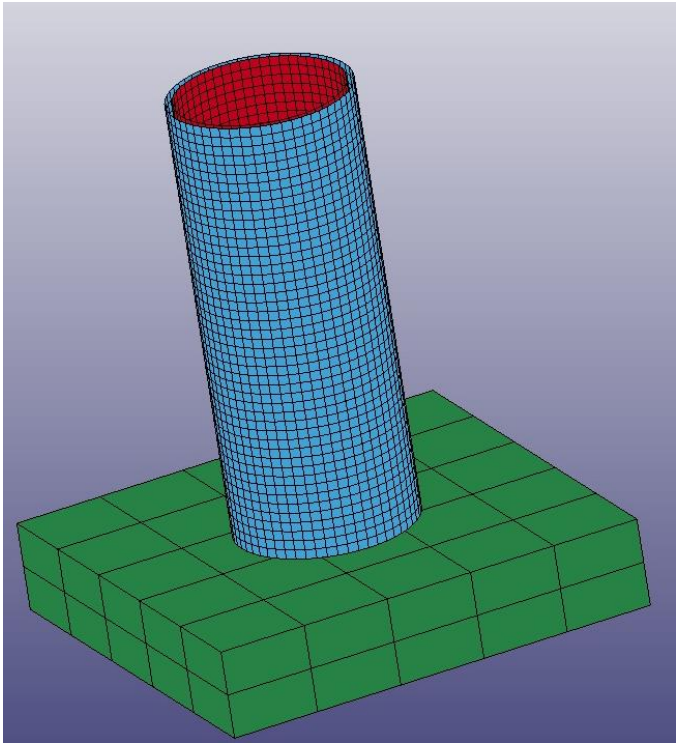

Figure 63 Bi-tube specimen with down plate

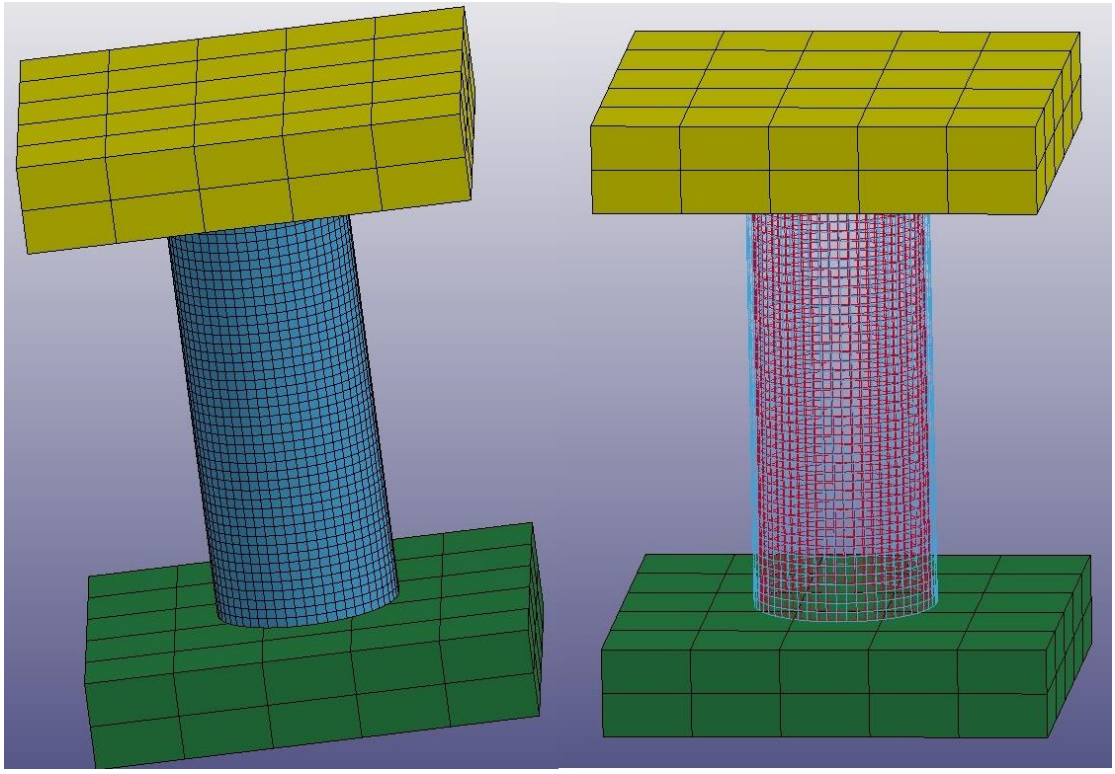

Figure 64 Final developed model. Bi-tube specimen with upper/down plates

5.2.3 Material Selection

In the third stage, the appropriate material properties are introduced into the pre-processor. In particular, the material *MAT024_Piecewise Linear Plasticity* is selected for both inner and outter tubes. *MAT024* describes the material behavior by introducing its density, Young Modulus, Poisson Ratio and yield stress, while it describes the hardening curve of plastic region with 8 points of stress and plastic strain (σ, ε_p). For each modelled material, which is either steel or ertalon (PA 6), Poisson ratio and density is found according to open literature data as Table 7 shows. On the other hand, Young Modulus, yield stress and σ-ε_p curve are calculated according to experimental data by conducting experimental tensile tests for both materials. Both tensile tests are conducted in a pressing machine in which the tensile load is forced with the velocity of 10 mm/min.

	Steel	**Ertalon (PA 6)**
Density (gr/mm^3)	0.00783	0.00115
Poisson Ratio (-)	0.30	0.39

Table 7 Density and Poisson ratio of steel and ertalon

The experimental tensile test of a steel specimen provided the following stress-strain curve as Figure 65 depicts. Table 8 presents the experimental data from steel tensile test as the measurements processing revealed.

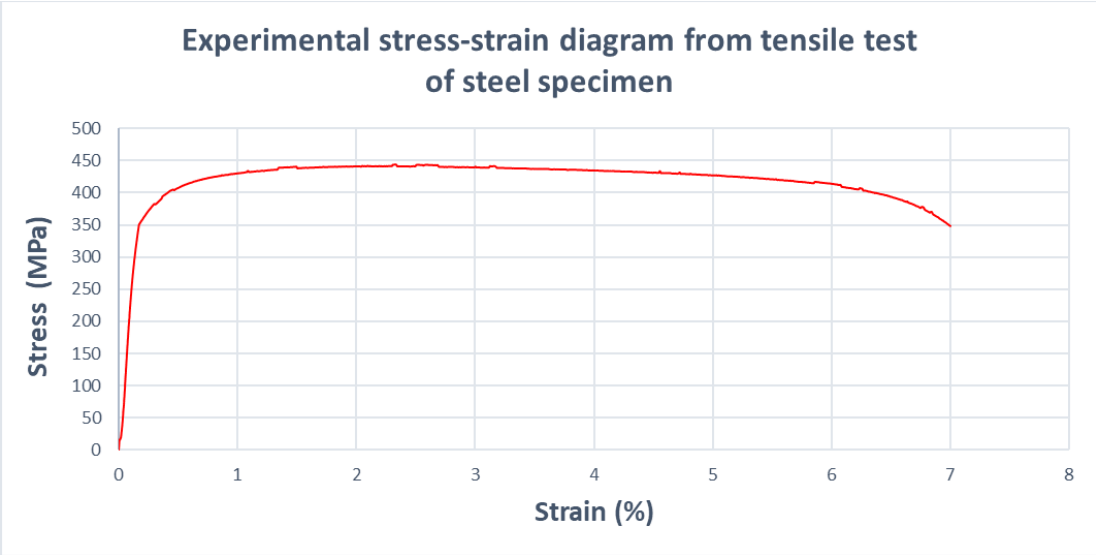

Figure 65 Stress-strain curve from experimental tensile test of steel

Steel		
Young Modulus (MPa)		198532
Yield Stress (MPa)		339
Points	*Plastic strain ε_p (-)*	*Stress σ (MPa)*
1	0	339.0
2	0.001761	400.0
3	0.004350	420.0
4	0.008182	434.7
5	0.017710	442.3
6	0.037080	436.7
7	0.051160	425.0
8	0.063690	388.0

Table 8 Experimental data from steel tensile test

The respective results have been computed for ertalon too. Following, Figure 66 and Table 9 show the σ-ε_p curve and the respective results for ertalon (PA 6).

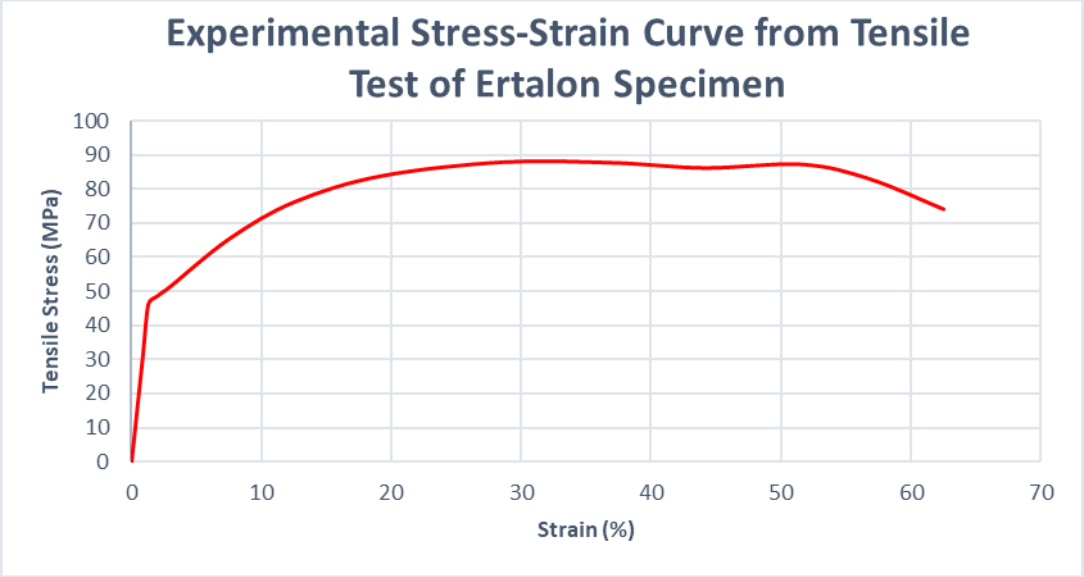

Figure 66 Stress-strain curve from experimental ertalon test of steel

Ertalon (PA 6)		
Young Modulus (MPa)		3600
Yield Stress (MPa)		45.57
Points	*Plastic strain ε_p (-)*	*Stress σ (MPa)*
1	0	45.57
2	0.0257	55.29
3	0.0682	69.87
4	0.1252	79.60
5	0.2113	86.60
6	0.3142	87.50
7	0.4327	86.42
8	0.4842	87.69

Table 9 Experimental data from ertalon tensile test

In addition, the material *MAT020_Rigid* is selected to simulate plates behavior. Both plates are considered to be made of steel with a typical Young Modulus of 205000 MPa, Poisson ratio of 0.3 and density of 0.00783 gr/mm^3. *MAT020* also requires the constrained degrees of freedom for each plate, and for this reason CMO parameter is set equal to 1. Further, parameters CON1 and CON2 represent the constrained displacements and rotations respectively. Thus, for the stationary down plate, CON1 and CON2 parameters are both set equal to 7, which means that the displacements and rotations in every axis are not permitted. However, for the upper plate, CON1 was set equal to 4 and CON2

equal to 7, representing a plate which is only permitted to move alongside z-axis, compressing the bi-tube specimen.

Finally, four different parts are created, containing the two tubes (inner and outter), the upper plate and the down plate, while the bi-tube specimen model is created from the two single tubes by setting them a common part. At its part, the appropriate part ID (PID), section ID (SECID), and material ID (MID) are adjusted, while a viscous and stiffness *hourglass* control for shell elements is selected for the two tubes with respect to Flanagan-Belytschko stiffness form (IHQ=4), except from the model of specimen B in which such a selection does not result in an appropriate collapse mode.

5.2.4 Contacts Definition

After justifying each part properties and characteristics, next step of modelling is to define the type of contact between interface surfaces. For this reason, a *nodes-to-surface contact* and an *automatic single surface contact* are applied to the examined configuration.

In particular, the *nodes-to-surface contact* does not allow the penetration of tube nodes into the surface of the plate, and so this type of contact is applied twice to the developed model; the first time between the bi-tube nodes and the upper plate surface and secondly between the bi-tube nodes and the down plate surface. In each case, the bi-tube specimen is described as the slave segment because it is considered as the deformable body in the interface, while the examined plate (upper or down) is described as the master segment. The master segment is stated by its part ID by selecting the MSTYP parameter equal to 3, while the slave segment is stated by its part set ID by selecting the SSTYP parameter equal to 2. Thus, the appropriate part ID of each plate and the part set ID of the bi-tube are adjusted properly to MSID and SSID respectively. Finally, at each type of contact a static friction coefficient (FS) of 0.2 and a dynamic friction coefficient (FD) of 0.15 are also applied to estimate the occurred resistances from the relative motion of the two interface surfaces.

Additionally, *automatic single surface* type of contact is applied in order to avoid the penetration between the developed folds. In this type of contact, only slave segment is defined by selecting a SSTYP parameter of 2, and adjusting the part set ID of the bi-tube specimen to the SSID parameter. A static friction coefficient of 0.2 and a dynamic friction coefficient of 0.15 are applied in this case too.

5.2.5 Loading Curve Definition

The following step of modelling procedure is to define the loading curve characteristics. The crashworthiness response of the examined specimens is simulated by adjusting a constant crushing velocity of 0.5 mm/msec to the upper plate, which is moving down crushing the bi-tube specimen and providing a

shortening of 60 mm until its final length of 40 mm. Initially, the velocity profile u(t) is defined for 60/0.5=120 msec in *define curve* option of keyword manager. Finally, this velocity profile is adjusted to the upper plate by selecting a scaling factor (SF) of -1 to consider that the moving upper plate crushes the bi-tube specimen.

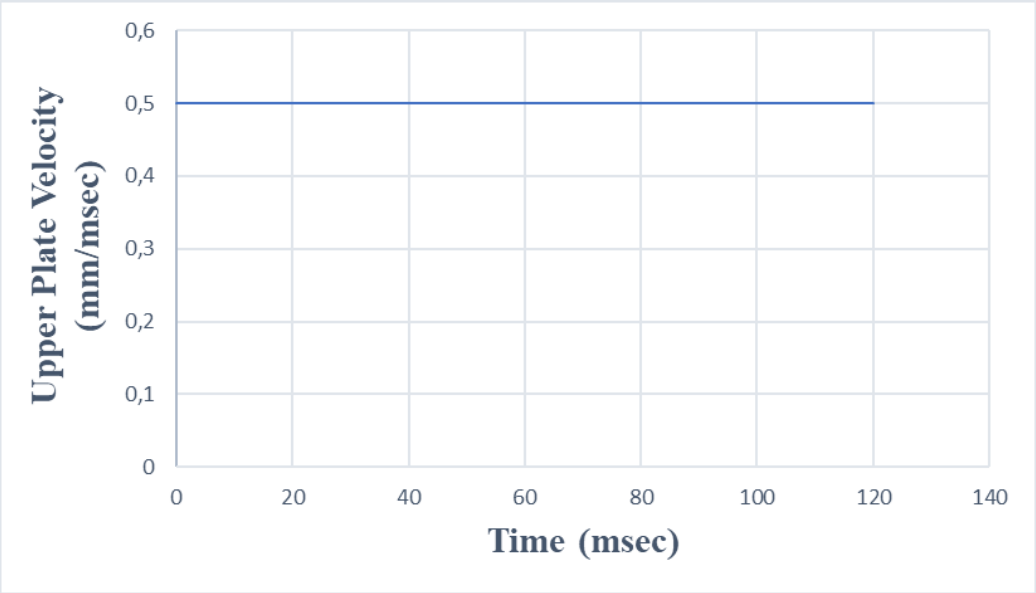

Figure 67 Loading curve

5.2.6 Database and Termination

As soon as the model is developed, the database timestep is defined at 2 msec. The selected data which solver returns are the forces in the contact surfaces (*rcforc*) and the upper plate movement (*rbdout*). Thus, a load-deflection diagram is produced from the post-processor by combining the z-force (crushing load or axial compressive load) in the interface between upper plate and bi-tube, and the z-displacement of upper plate. Finally, the termination time is adjusted at 120 msec. The developed model is saved as a keyword file and after the simulation ends from the solver, a *d3plot* file is created and then fed to post-processor where data processing is available, observing different stages of collapse in the same time.

5.3 Simulation Results

The provided results from the simulations are presented and discussed in this section for each examined configuration of bi-tube specimen. For each examined case, both inner and outter single tubes and bi-tube specimen are simulated to assess their crashworthiness response under the axial compressive loading of 0.5 mm/msec crushing speed. The revealed load-deflection curve consists of the one

of the bi-tube and the ones of the two single tubes (inner and outter). Finally, expect from obtaining the appropriate response characteristics such as peak force (PCF), sustained load, energy absorption (EA) and specific energy absorption (SEA), the collapse mode is also observed. Following, the results of numerical simulations, which are carried out in LS-DYNA software, are presented below for each developed model of examined bi-tube specimen.

5.3.1 Bi-tube Specimen A

The model of bi-tube specimen A is simulated under axial compression with 0.5 mm/msec crushing speed. Additionally, the internal and external tubes, from which the bi-tube consists of, are also simulated. The provided load-deflection curves of bi-tube specimen and its internal/external tubes are illustrated in Figure 68. As observed in the same figure, the bi-tube F-s curve is greater than the ones of the two tubes, while the steel F-s curve is placed upper than the one of ertalon as expected. For the numerical simulation results processing, the response characteristics of bi-tube crashworthiness behavior can be computed. Specifically, peak crushing force, mean sustained load, specific energy absorption and amount of absorbed energy are the computed parameters to assess the crashworthiness behavior of the bi-tube structure. Table 10 presents the values of critical parameters for crashworthiness assessment as the numerical F-s curve data processing revealed them.

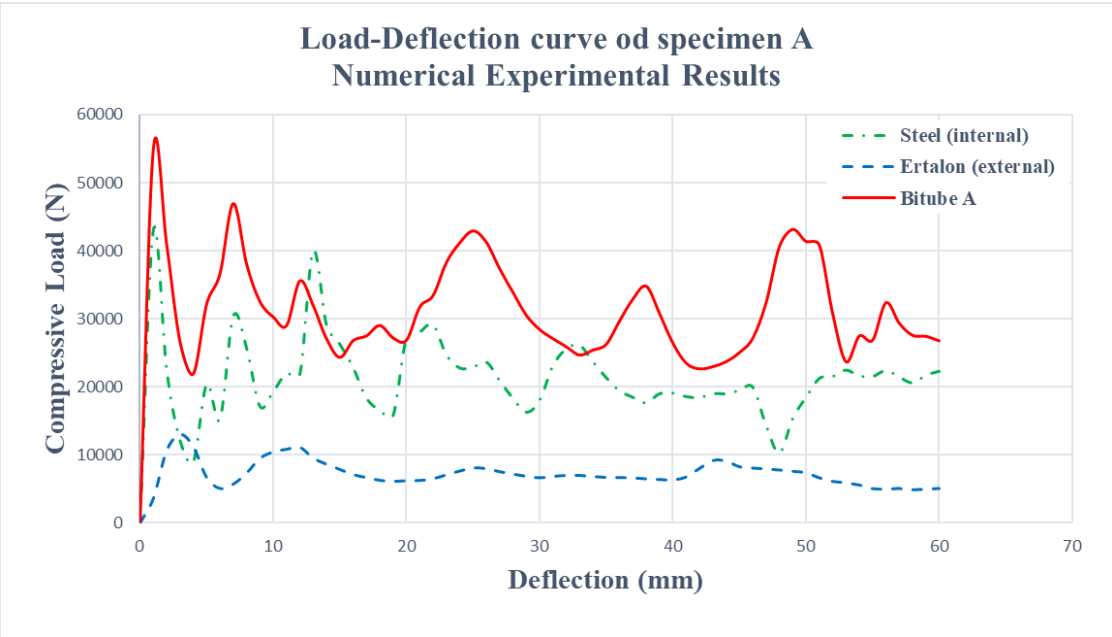

Figure 68 Numerical results for load-deflection curve of bi-tube A and its tube components

Numerical Simulation Results	
Bi-tube Specimen A	
Peak Crushing Force (kN)	56.80
Mean Sustained Load (kN)	32.20
Energy Absorption (J)	1872.23
Specific Energy Absorption (J/kg)	14114.30

Table 10 Numerical Simulation Results for bi-tube A crashworthiness assessment

Apart from the response characteristics calculation, the simulated model of crushed bi-tube specimen provides also critical conclusions for the occurred collapse mechanism which the simulation revealed for the examined bi-tube structure. As Figure 69 depicts, the developed model of bi-tube A crushes by initially formulating a concertina fold at the edge of its bottom and continuing by being formulated in 3-lobe diamond mode. In fact, both internal steel tube and external ertalon tube deform by initially formulating a ring fold and continue to collapse by formulating 3-lode diamond folds, as Figure 70 and Figure 71 show.

Thus, the numerical simulation study reveals that a mixed collapse mode appears to be the dominant failure mechanism during the collapse of the examined bi-tube specimen, while both internal and external tubes collapse in mixed mode too. In addition, Figure 72 illustrates the fully collapsed bi-tube A as the numerical simulation reveals it, while Figure 73 shows a cut view of previous figure. As shown, the simulation predicts the collapse mechanism of bi-tube A, and also it reveals that the adhesion is lost in general, except from two specimen areas where the convolution of external softer tube (ertalon) partially maintains the adhesion with the developed folds of internal harder tube (steel).

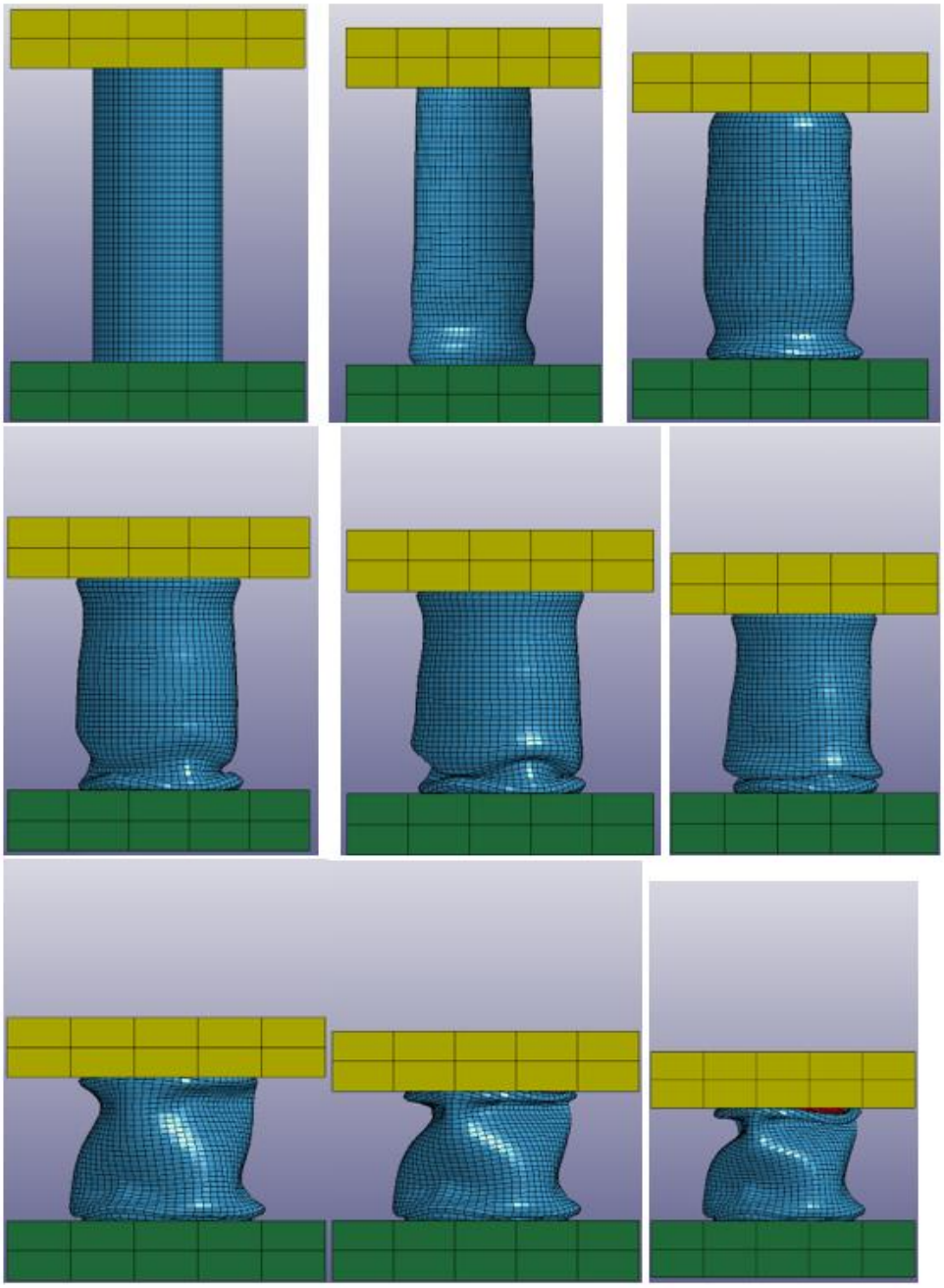

Figure 69 States of axial collapse from numerical simulations of bi-tube A

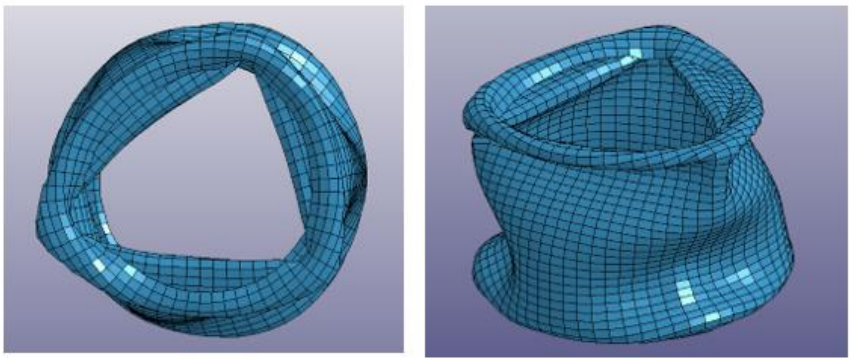

Figure 70 Fully collapsed external ertalon tube of bi-tube A

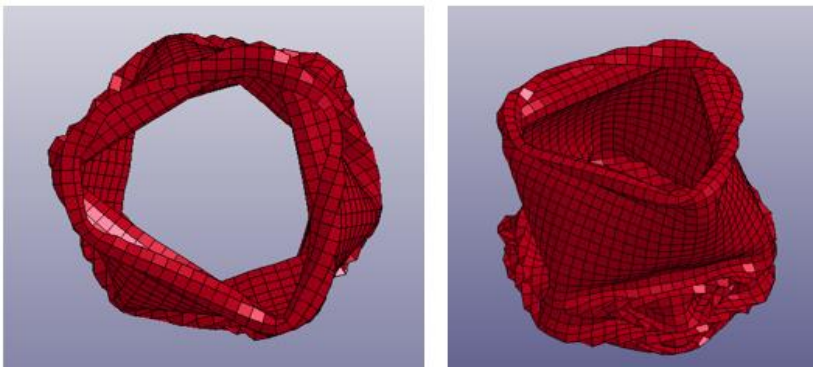

Figure 71 Fully collapsed internal steel tube of bi-tube A

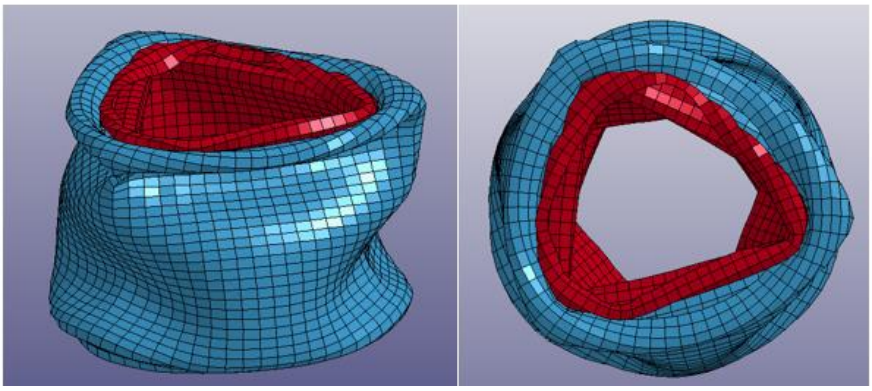

Figure 72 Fully collapsed bi-tube A

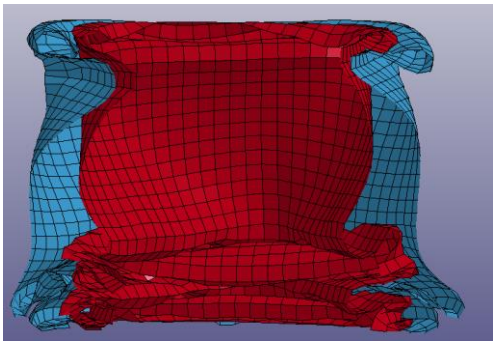

Figure 73 Cut structure of fully collapsed bi-tube A

5.3.2 Bi-tube Specimen B

The model of bi-tube specimen B is simulated under axial compression with 0.5 mm/msec crushing speed. Additionally, the internal and external tubes, from which the bi-tube consists of, are also simulated in this case too. The provided load-deflection curves of bi-tube specimen and its internal/external tubes are illustrated in Figure 74. As observed in the same figure, the bi-tube F-s curve is greater than the ones of the two tubes, while the steel F-s curve is placed upper than the one of ertalon as expected. For the numerical simulation results processing, the response characteristics of bi-tube crashworthiness behavior can be computed. Specifically, peak crushing force, mean sustained load, specific energy absorption and amount of absorbed energy are the computed parameters to assess the crashworthiness behavior of the bi-tube structure. Table 11 presents the values of critical parameters for crashworthiness assessment as the numerical F-s curve data processing revealed them.

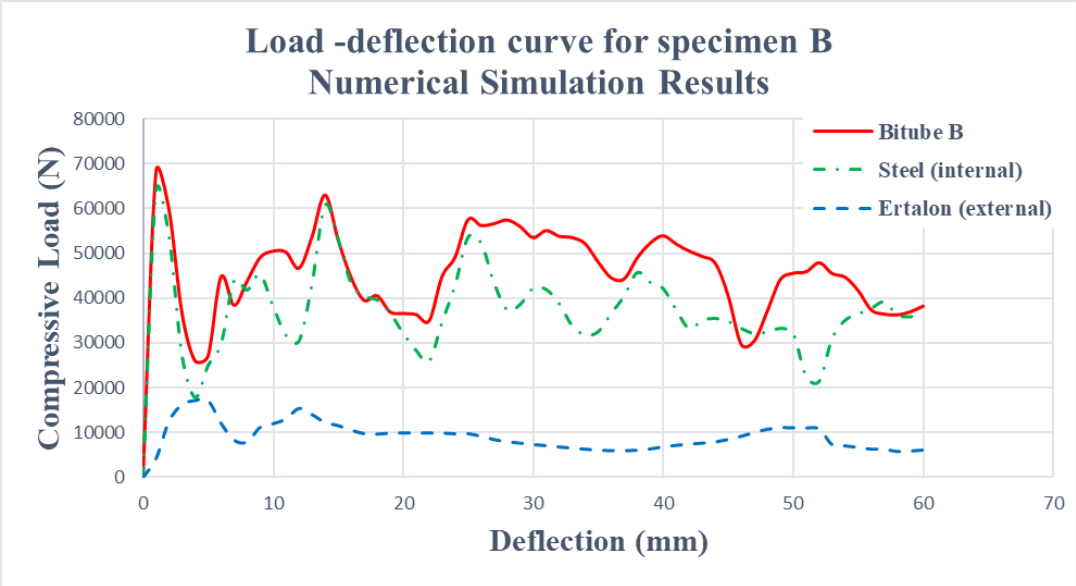

Figure 74 Numerical results for load-deflection curve of bi-tube B and its tube components

Numerical Simulation Results	
Bi-tube Specimen B	
Peak Crushing Force (kN)	68.20
Mean Sustained Load (kN)	45.66
Energy Absorption (J)	2739.78
Specific Energy Absorption (J/kg)	14806.70

Table 11 Numerical Simulation Results for bi-tube B crashworthiness assessment

Except from the response characteristics calculation, the simulated model of crushed bi-tube specimen provides also critical conclusions for the occurred collapse mechanism which the simulation revealed for the examined bi-tube structure. As Figure 75 depicts, the developed model of bi-tube B crushes by initially formulating a concertina fold at the edge of its bottom and continuing by being formulated in 2-lobe diamond mode. In fact, both internal steel tube and external ertalon tube deform by initially formulating a ring fold and continue to collapse by formulating 2-lode diamond folds, as Figure 76 and Figure 77 show.

Thus, the numerical simulation study reveals that a mixed collapse mode appears to be the dominant failure mechanism during the collapse of the examined bi-tube specimen as both ring and 2-lobe diamond convolutions are formulated. Further, both internal and external tubes collapse in mixed mode too. In addition, Figure 78 illustrates the fully collapsed bi-tube B as the numerical simulation reveals it, while Figure 79 shows a cut view of previous figure. As shown, the simulation predicts the collapse mechanism of bi-tube B, and also it reveals that the adhesion is lost in the areas of the specimen in which folds are not developed. However, in the areas where folds are formulated, the convolution of external softer tube (ertalon) partially maintains the adhesion with the developed folds of internal harder tube (steel), as the softer tube convolutions often enclose the folds of internal harder tube.

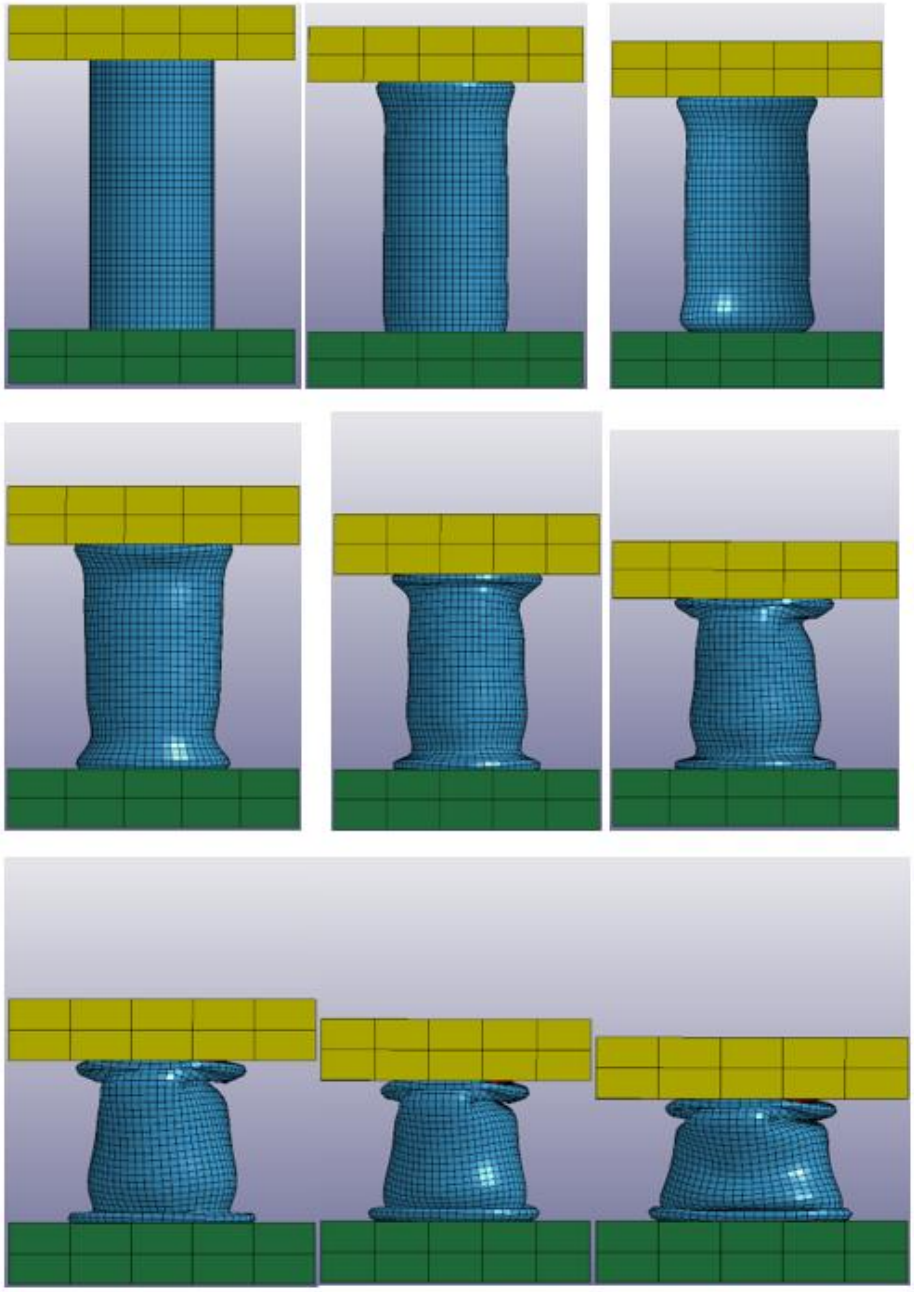

Figure 75 States of axial collapse from numerical simulations of bi-tube B

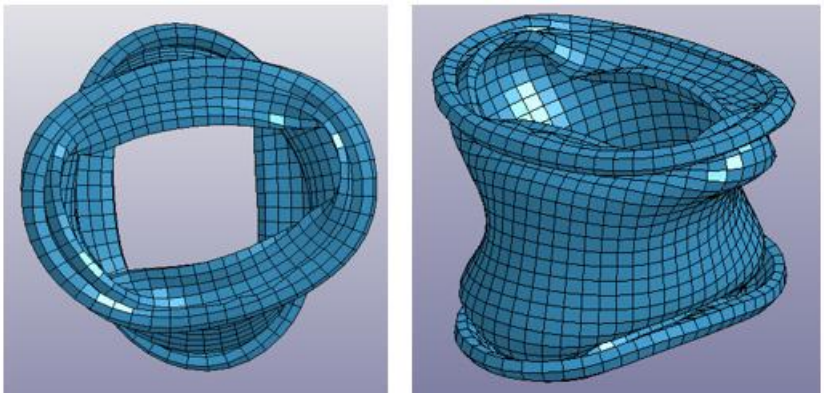

Figure 76 Fully collapsed external ertalon tube of bi-tube B

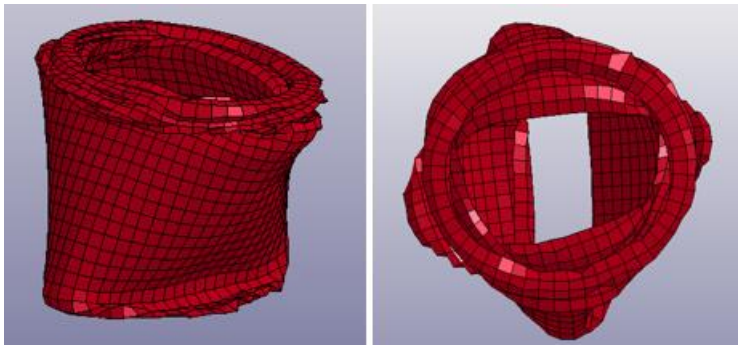

Figure 77 Fully collapsed internal steel tube of bi-tube B

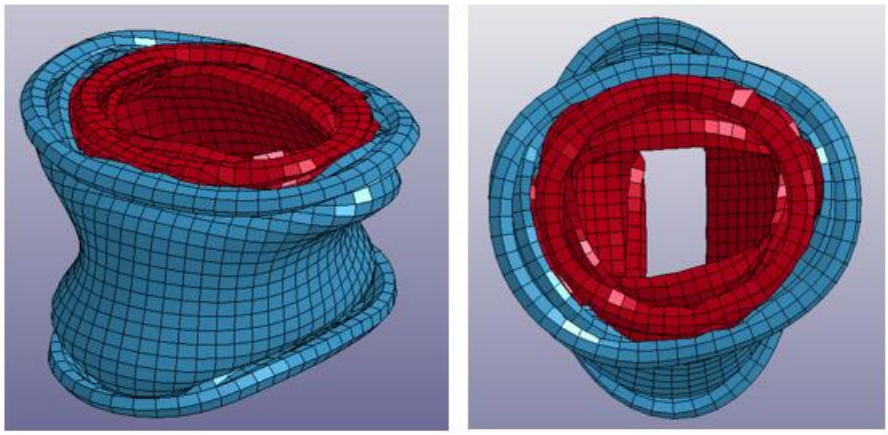

Figure 78 Fully collapsed bi-tube B

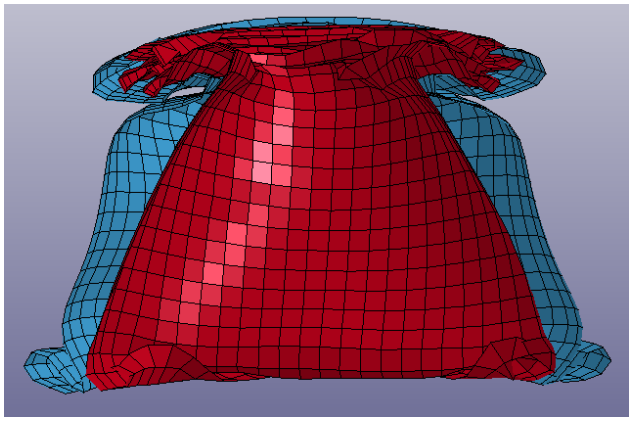

Figure 79 Cut structure of fully collapsed bi-tube B

5.3.3 Bi-tube Specimen C

The model of bi-tube specimen C is simulated under axial compression with 0.5 mm/msec crushing speed. Additionally, the internal and external tubes, from which the bi-tube consists of, are also simulated in this case too. The provided load-deflection curves of bi-tube specimen and its internal/external tubes are illustrated in Figure 80. As observed in the same figure, the bi-tube F-s curve is greater than the ones of the two tubes, while the steel F-s curve is placed upper than the one of ertalon as expected. For the numerical simulation results processing, the response characteristics of bi-tube crashworthiness behavior can be computed. Specifically, peak crushing force, mean sustained load, specific energy absorption and amount of absorbed energy are the computed parameters to assess the crashworthiness behavior of the bi-tube structure. Table 12 presents the values of critical parameters for crashworthiness assessment as the numerical F-s curve data processing revealed them.

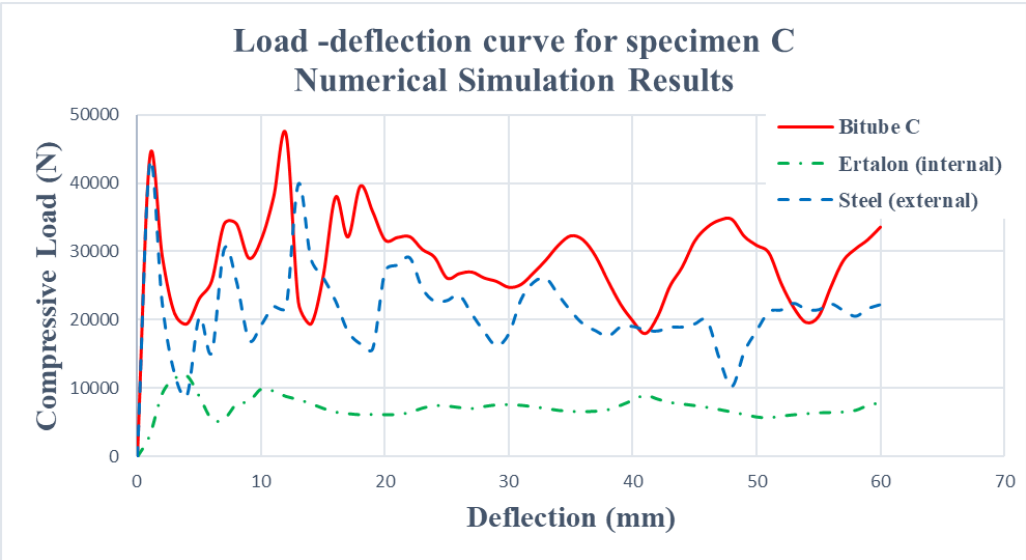

Figure 80 Numerical results for load-deflection curve of bi-tube C and its tube components

Numerical Simulation Results	
Bi-tube Specimen C	
Peak Crushing Force (kN)	47.22
Mean Sustained Load (kN)	28.61
Energy Absorption (J)	1716.32
Specific Energy Absorption (J/kg)	13376.20

Table 12 Numerical Simulation Results for bi-tube C crashworthiness assessment

Except from the response characteristics calculation, the simulated model of crushed bi-tube specimen provides also critical conclusions for the occurred collapse mechanism which the simulation revealed for the examined bi-tube structure. As Figure 81 depicts, the developed model of bi-tube C crushes by initially formulating a concertina fold at its bottom and top edges and continuing by deforming in 3-lobe diamond mode. In fact, both internal steel tube and external ertalon tube deform by initially formulating a ring fold – at the top edge for the ertalon tube and at both edges for the steel tube - and continue to collapse by formulating 3-lode diamond folds, as Figure 82 and Figure 83 show.

Thus, the numerical simulation study reveals that a mixed collapse mode appears to be the main failure mechanism during the collapse of the examined bi-tube specimen as both concertina initially, and 3-lobe diamond convolutions at next, are formulated. Further, both internal and external tubes collapse in mixed mode too. In addition, Figure 84 illustrates the fully collapsed bi-tube C as the numerical simulation reveals it, while Figure 85 shows a cut view of previous figure. As shown, the simulation predicts the collapse mechanism of bi-tube C, and also it reveals that the adhesion between internal/external tubes is maintained, as the folds of the softer (ertalon) internal tube are trapped maintaining full contact with the convolutions of the harder (steel) external tube.

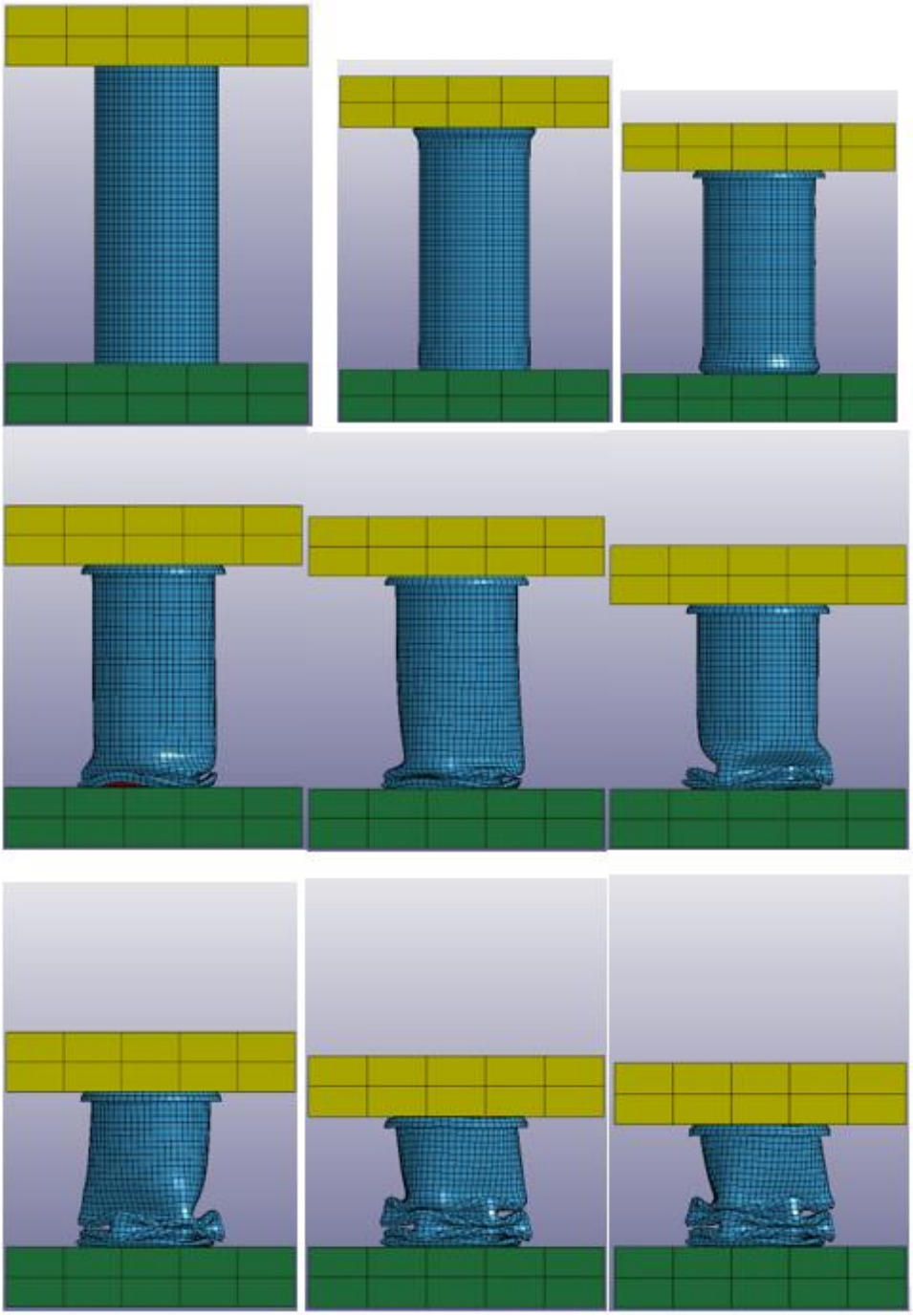

Figure 81 States of axial collapse from numerical simulations of bi-tube C

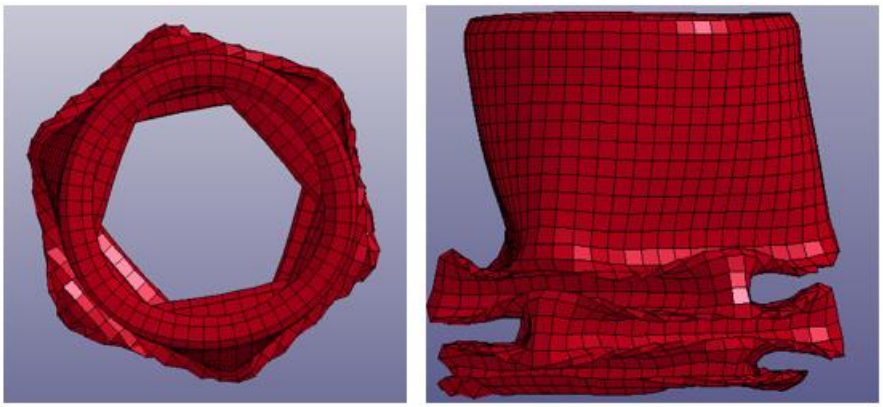

Figure 82 Fully collapsed internal ertalon tube of bi-tube C

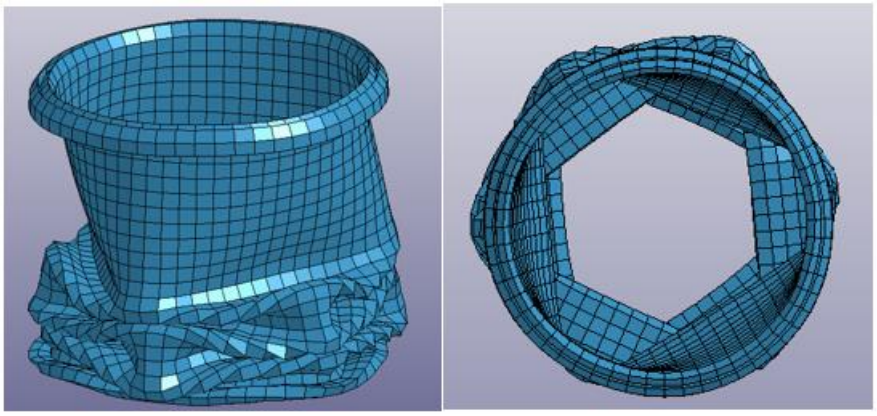

Figure 83 Fully collapsed external steel tube of bi-tube C

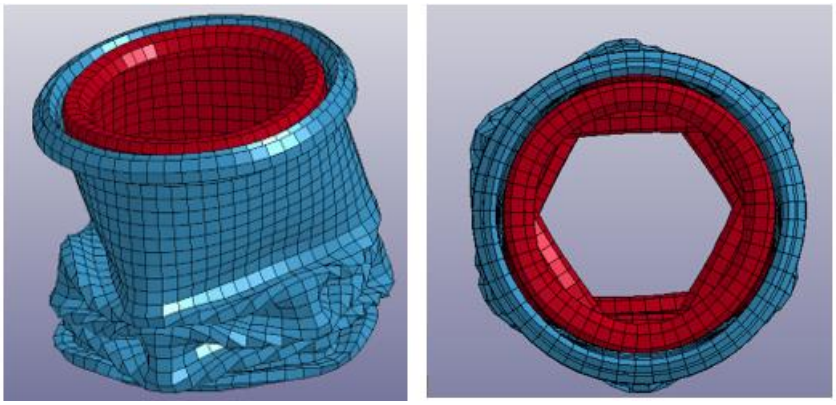

Figure 84 Fully collapsed bi-tube C

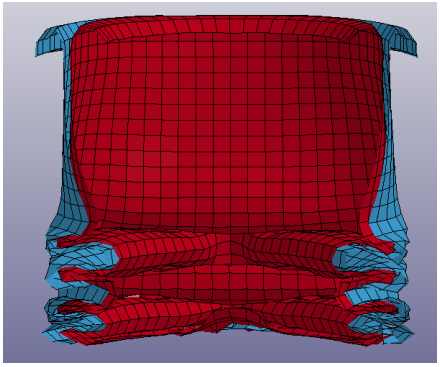

Figure 85 Cut structure of fully collapsed bi-tube C

5.3.4 Bi-tube Specimen D

The model of bi-tube specimen D is simulated under axial compression with 0.5 mm/msec crushing speed. Additionally, the internal and external tubes, from which the bi-tube consists of, are also simulated in this case too. The provided load-deflection curves of bi-tube specimen and its internal/external tubes are illustrated in Figure 86. As observed in the same figure, the bi-tube F-s curve is greater than the ones of the two tubes, while the steel F-s curve is placed upper than the one of ertalon as expected. For the numerical simulation results processing, the response characteristics of bi-tube crashworthiness behavior can be computed. Specifically, peak crushing force, mean sustained load, specific energy absorption and amount of absorbed energy are the computed parameters to assess the crashworthiness behavior of the bi-tube structure. Table 13 presents the values of critical parameters for crashworthiness assessment as the numerical F-s curve data processing revealed them.

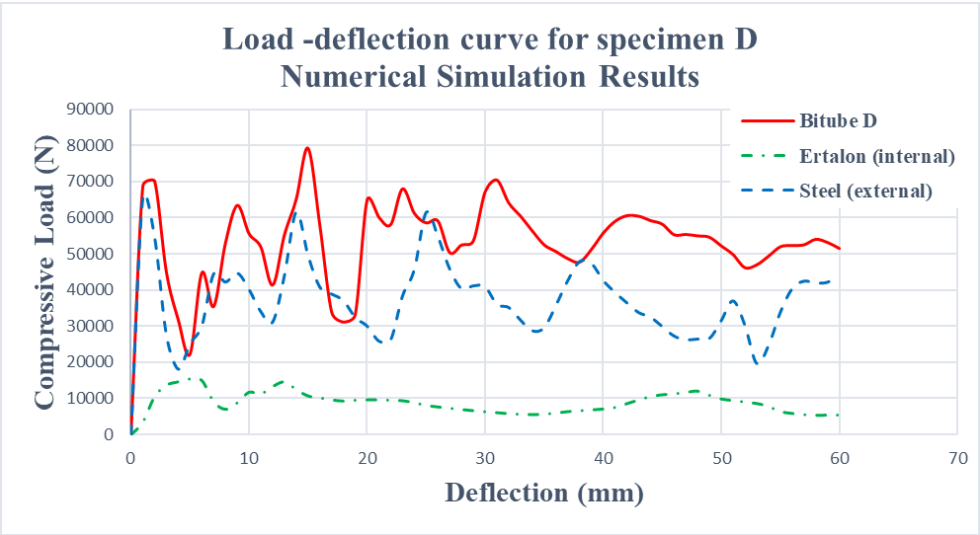

Figure 86 Numerical results for load-deflection curve of bi-tube D and its tube components

Numerical Simulation Results	
Bi-tube Specimen D	
Peak Crushing Force (kN)	79.14
Mean Sustained Load (kN)	53.38
Energy Absorption (J)	3202.73
Specific Energy Absorption (J/kg)	17558.40

Table 13 Numerical Simulation Results for bi-tube D crashworthiness assessment

Except from the response characteristics calculation, the simulated model of crushed bi-tube specimen provides also critical conclusions for the occurred collapse mechanism which the simulation revealed for the examined bi-tube structure. As Figure 87 depicts, the developed model of bi-tube D crushes by initially formulating a concertina fold at both bottom and top edges and continuing by deforming in 3-lobe diamond mode. In fact, both internal steel tube and external ertalon tube deform in mixed collapse mode as they develop initially a ring fold and continue to collapse by formulating 3-lobe diamond mode, as Figure 88 and Figure 89 show.

Thus, the numerical simulation study suggests that a mixed collapse mode appears to be the main mechanism which is occurred during the collapse of the examined bi-tube specimen as both concertina initially, and 3-lobe diamond convolutions at next, are formulated. Further, both internal and external tubes collapse in mixed mode too, as the bi-tube specimen does. In addition, Figure 90 illustrates the fully collapsed bi-tube D as the numerical simulation reveals it, while Figure 91 shows a cut view of previous figure. As shown, the simulation predicts the collapse mechanism of bi-tube D, and also it reveals that the adhesion between internal/external tubes is maintained, as the folds of the softer (ertalon) internal tube are trapped into the convolutions of the harder (steel) external tube, maintaining in that way full contact.

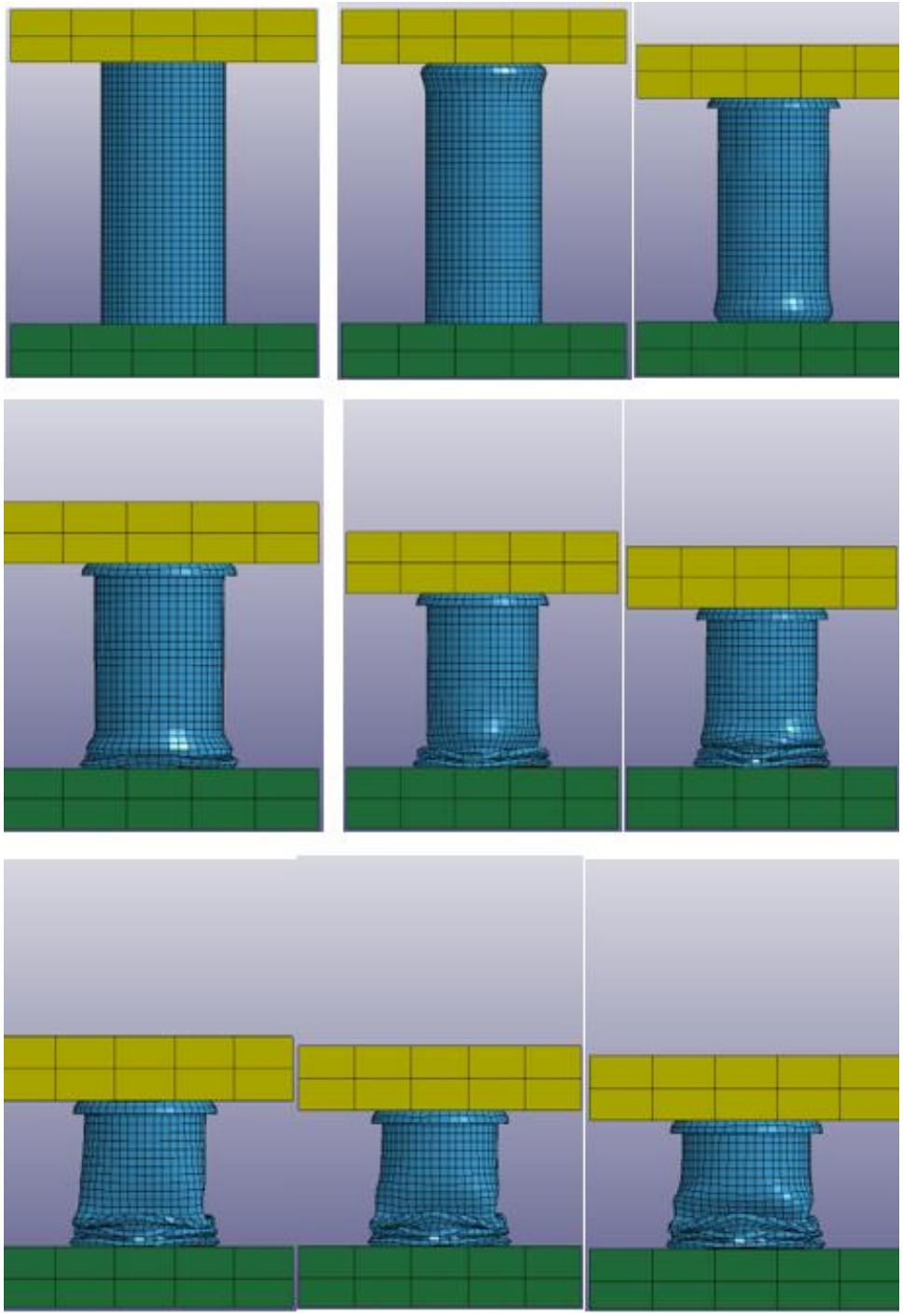

Figure 87 States of axial collapse from numerical simulations of bi-tube D

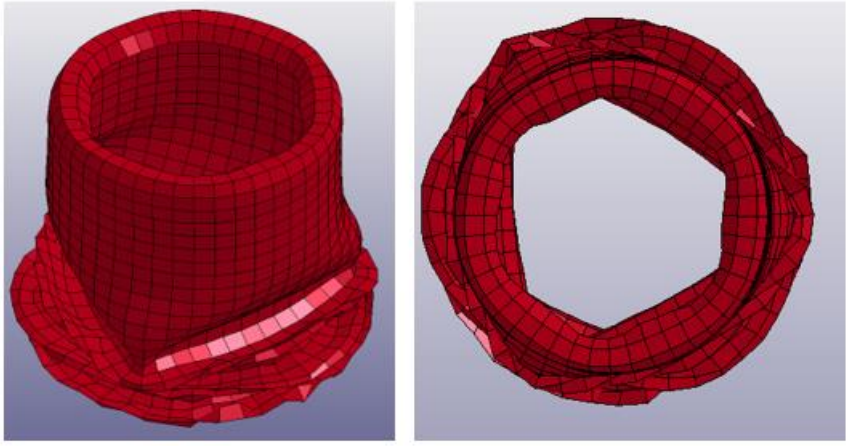

Figure 88 Fully collapsed internal ertalon tube of bi-tube D

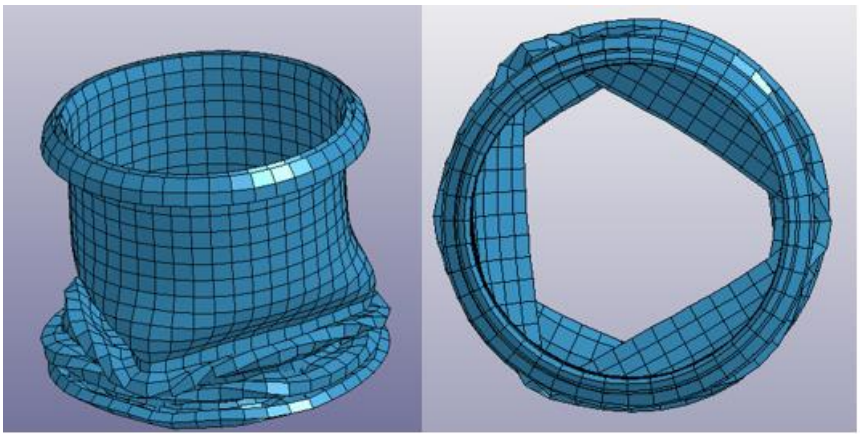

Figure 89 Fully collapsed external steel tube of bi-tube D

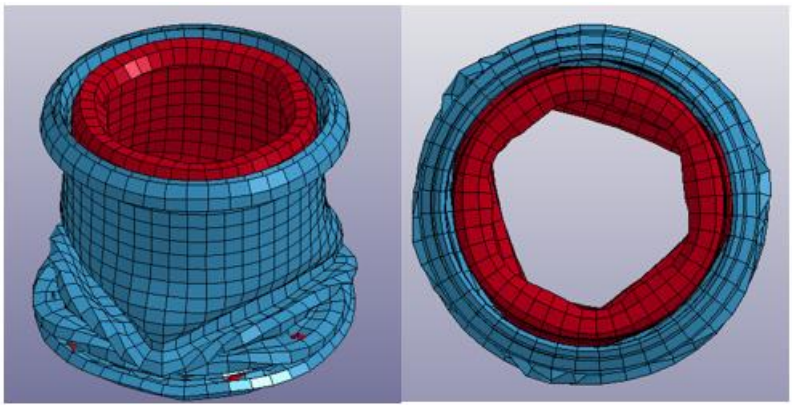

Figure 90 Fully collapsed bi-tube D

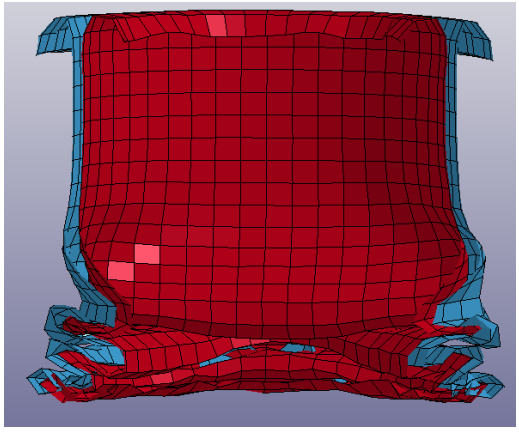

Figure 91 Cut structure of fully collapsed bi-tube D

5.4 Conclusions

By summarizing the provided results from the numerical simulations, critical conclusions can be extracted for the crashworthiness response of examined bi-tube structure models. Especially, the results show that in both occasions of hard/soft or soft/hard as internal/external tubes respectively, the bi-tube models of higher thickness reveal greater energy absorption capability (B&D bi-tube models). In fact, increasing bi-tube thickness results in greater peak force, sustained load and energy absorption capability as Figure 92 depicts. The same trend is confirmed from the provided results for the bi-tube external diameter. More specifically, as the outter diameter of the bi-tube increases, the energy absorption capability increases too, providing a more crashworthy structure. The above conclusions totally agree with the suggestion made by both Alexander [19] and Mamalis et al. [17], according to the mean sustained load varies proportionally to external diameter and thickness as showing below.

$$\bar{P} \sim t^{1.5} D^{0.5} \tag{25}$$

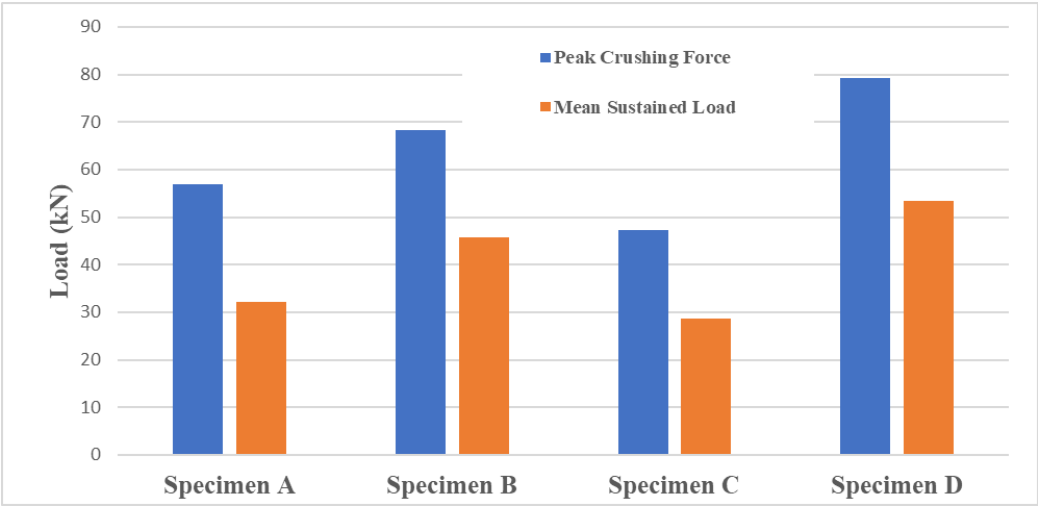

Figure 92 Numerical simulation results for peak force and sustained load of the examined bi-tube models

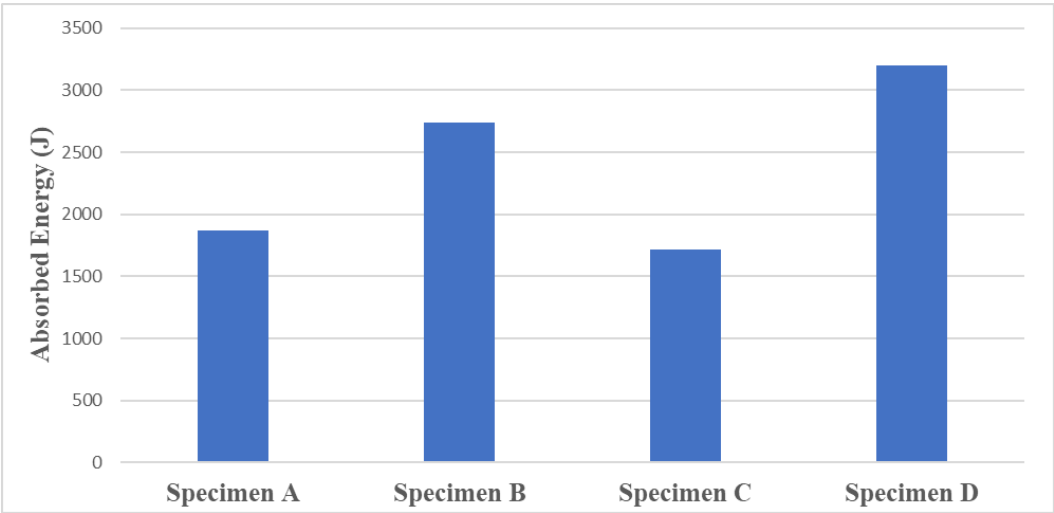

Figure 93 Numerical simulation results for energy absorption capability of the examined bi-tube models

Observing Figure 94, bi-tube D reveals the greater energy absorption capability and so structure D is the most sufficient one in terms of crashworthiness behavior. Further, considering that the external diameter of bi-tube D is lower than the one of bi-tube B, it is easily concluded that the results in comparison could be even more beneficial for bi-tube D in terms of energy absorption capability.

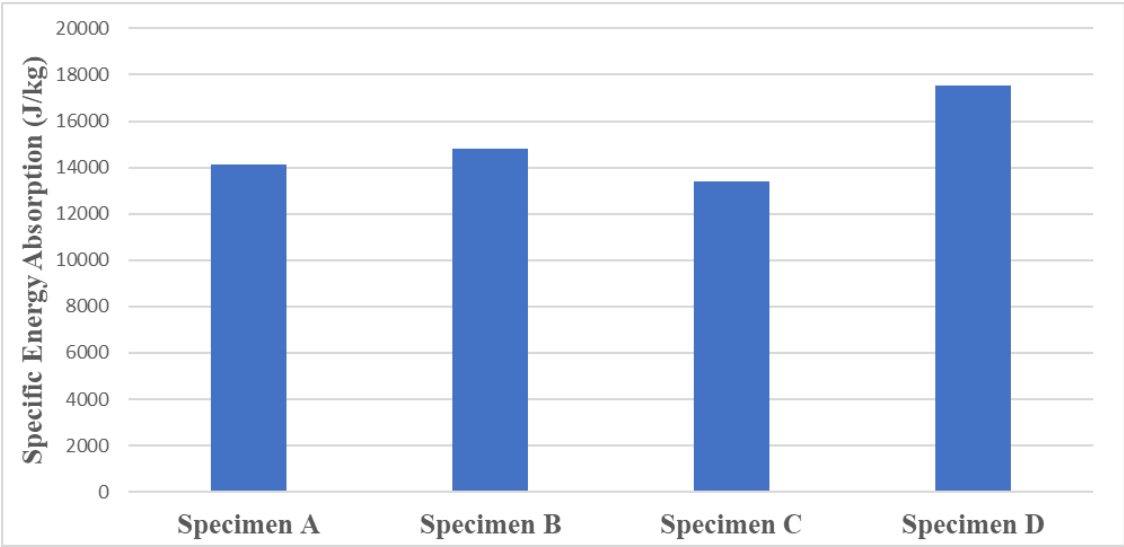

Figure 94 Numerical simulation results for specific energy absorption of the examined bi-tube models

Finally, observing the cut structures of each crushed bi-tube model, it is concluded that the adhesion between the internal/external tubes is more likely to be maintained when the tube thickness increases. In addition, in the case of harder external tube, such as the steel one, the adhesion is almost fully maintained, as the folds of the softer internal tube are trapped into the formulated convolution of the external harder tube. In contrast, in the case of softer external tube (ertalon), the adhesion is lost, except from the bi-tube areas which deform by formulating convolution. In such areas, the adhesion is partially maintained, as some folds are kept in contact with each other, while other not. The second occasion is usually observed when a convolution of the external softer tube contains internally two smaller folds of the internal harder tube.

6. Experimental vs. Numerical Simulation Results

6.1 Introduction

This chapter presents the comparison between the experimental results and the ones provided by the numerical simulations. Also, a comparison against theoretical analytical expression for the mean sustained load of bi-tube crushed structures, is carried out too. Each comparison is made in terms of load-deflection D-s curve, crushing response characteristics (peak force and mean sustained load), energy absorption capability (absorbed energy and specific energy absorption) and occurred collapse mechanism. In each case, the above comparison cases are carried out for each examined bi-tube. Finally, the mean sustained load is also compared against calculations provided by analytical expressions.

6.2 Comparison of Experimental and Simulation Results

In this section, the crashworthiness response characteristics are available for comparison between the numerical simulation and the experimental results. In particular, the F-s diagram and critical response characteristics of a collapsed structure, such as peak force, sustained load, absorbed energy and specific energy absorption, are set for comparison for each examined bi-tube structure separately. Specifically, as will be presented below, the mean sustained load for each examined bi-tube specimen is depicted in Table 14 as computed from the experimental tests, numerical simulation studies and theoretical analytical expression (Equation 16). As shown, the calculation of sustained load offers a similar to simulations accuracy only in the case of bi-tube A, where the revealed relative error is almost 14.85% against the experimental data. Further, it is observed that the use of the analytical expression for calculating the mean sustained load offers more accurate results in lower thicknesses for both occasions of hard/soft or soft/hard combinations of internal/external tube respectively.

Mean Sustained Load (kN)				
	Bi-tube A	**Bi-tube B**	**Bi-tube C**	**Bi-tube D**
Experiment	34.69	41.78	30.98	51.09
Simulation	32.2	45.66	28.61	53.38
Analytical Expression	40.74	67.55	38.93	64.54

Table 14 Mean sustained load predictions

In the following sections, a more detailed comparison between experimental and simulation results is presented for each examined bi-tube separately in terms of both response characteristics under axial crushing and occurred collapse mechanism.

6.2.1 Bi-tube Specimen A

The comparison of provided results from numerical simulations against the experimental data revealed the load-deflection curves for bi-tube specimen A, as depicted in Figure 95. As Table 15 reveals, the simulation tends to underestimate the energy absorption capability of bi-tube A, predicting its load-deflection curve at lower force levels. More specifically, the sustained load is predicted with sufficient accuracy to be 7.2% lower than the one which experiment revealed, while a mean deviation of almost 10% is observed between experimental data and simulation results regarding to predictions in peak load and energy absorption capability.

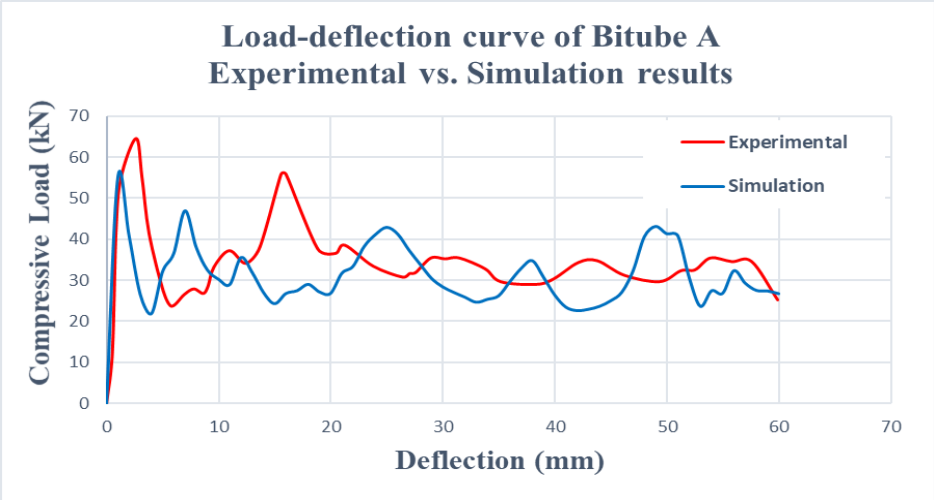

Figure 95 Experimental vs. Simulation load-deflection curve for bi-tube A

Bi-tube A			
	Experimental	**Simulation**	**Error (%)**
Peak Crushing Force (kN)	64.46	56.8	11.88
Sustained Load (kN)	34.69	32.20	7.18
Energy Absorption (J)	2081.11	1872.23	10.04
Specific Energy Absorption (J/kg)	15689.01	14114.30	10.04

Table 15 Relative errors of experimental against simulation results for bi-tube A

Further, both numerical simulations and experimental tests predict the same collapse mechanism for the crushed bi-tube specimen A, which is a mixed collapse mode, as both concertina initially and then 3-lobe diamond folds are observed during the axial collapse. However, the simulated model does not predict accurately the number of formulated folds, as it reveals less developed folds than the ones which are actually formulated. Finally, the experimental tests provide a crushed bi-tube structure in which the adhesion between the two tubes is more maintained. In other words, the simulation fails to predict that the adhesion is partially maintained between all formulated convolutions, but it correctly predicts that the adhesion is almost lost in the areas where no folds have been formulated yet.

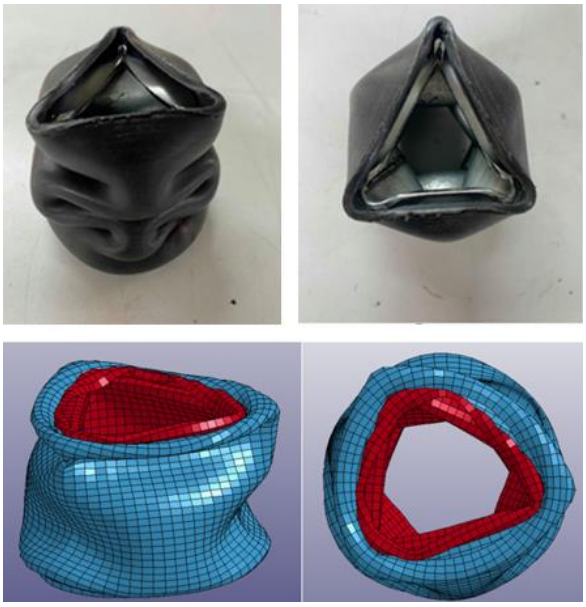

Figure 96 Collapsed structure of bi-tube A (experimental vs. simulation results)

Figure 97 Cut structures of bi-tube A (experimental vs. simulation results)

6.2.2 Bi-tube Specimen B

The comparison of provided results from numerical simulations against the experimental data revealed the load-deflection curves for bi-tube specimen B, as depicted in Figure 98. As Table 16 reveals, the simulation tends to predict sufficiently the peak force by deviating from the experimental results by almost 9.4%. In the same trend, the deviation in sustained load and in consequence the specific energy absorption is predicted at almost 9.3% between the experimental results and the simulation ones.

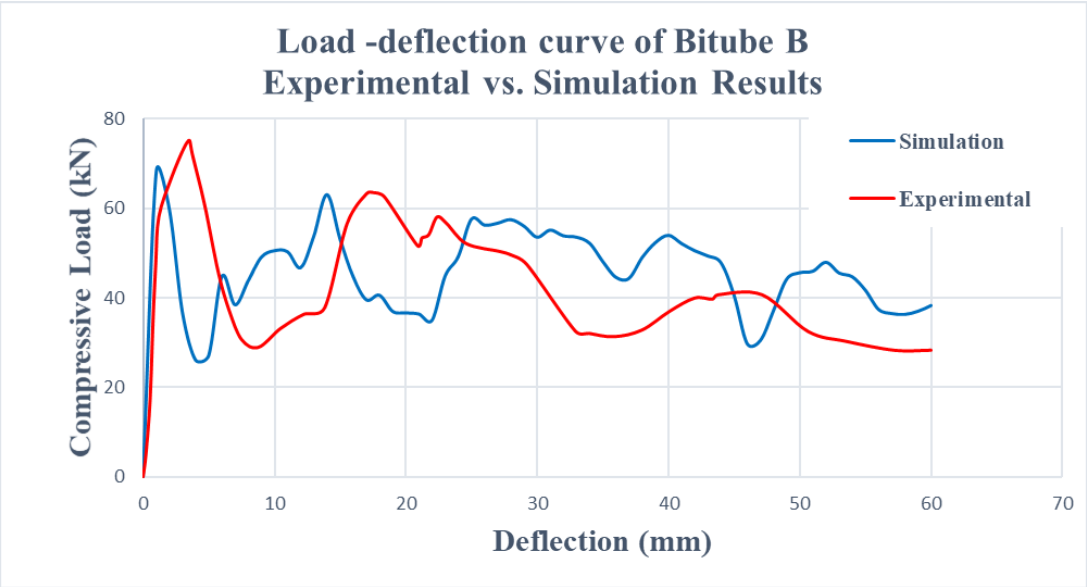

Figure 98 Experimental vs. Simulation load-deflection curve for bi-tube B

Bi-tube B			
	Experimental	**Simulation**	**Error (%)**
Peak Crushing Force (kN)	75.28	68.20	9.40
Sustained Load (kN)	41.78	45.66	9.29
Energy Absorption (J)	2507.06	2739.78	9.28
Specific Energy Absorption (J/kg)	13548.70	14806.70	9.29

Table 16 Relative errors of experimental against simulation results for bi-tube B

Additionally, both numerical simulations and experimental tests predict the same collapse mechanism for the crushed bi-tube specimen B, which is a mixed collapse mode, as both concertina initially and then diamond folds are observed to be formulated during the axial collapse. However, the experimental tests

reveal a 3-lobe diamond collapse after the initial shortening, while the simulation predicts a 2-lobe diamond collapse in which the bi-tube B model continues to deform to, after the initial ring fold formulation. More, the simulated model does not predict accurately the number of formulated folds, as it reveals less developed folds than the ones which are actually formulated. Finally, the experimental tests provide a crushed bi-tube structure in which the adhesion between the two tubes is more maintained than the one provided by the simulation. In other words, the bi-tube B model reveals a final crushed structure in which the adhesion is not maintained in the level that it actually does.

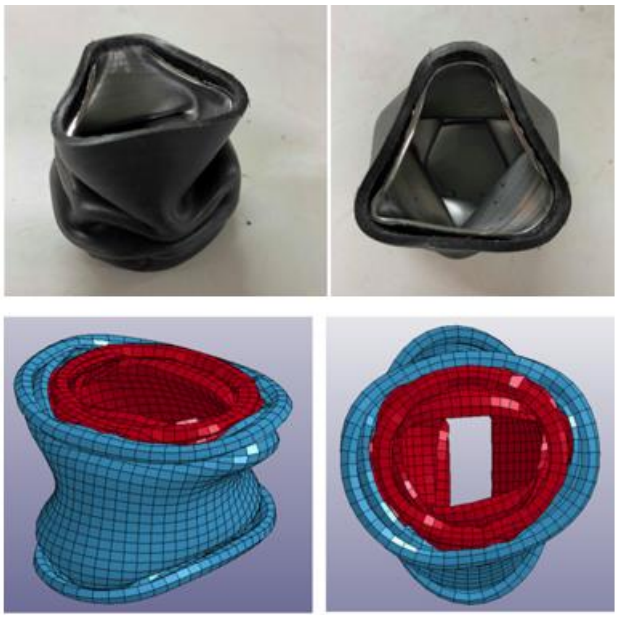

Figure 99 Collapsed structure of bi-tube B (experimental vs. simulation results)

Figure 100 Cut structures of bi-tube B (experimental vs. simulation results)

6.2.3 Bi-tube Specimen C

The comparison of provided results from numerical simulations against the experimental data revealed the load-deflection curves for bi-tube specimen C, as depicted in Figure 101. As Table 17 reveals, the simulation predicts sufficiently the experimental F-s curve, except from the initial peak load. In fact, sustained load, specific energy absorption and absorbed energy are computed with less than 8% deviation between the experimental and numerical simulation results.

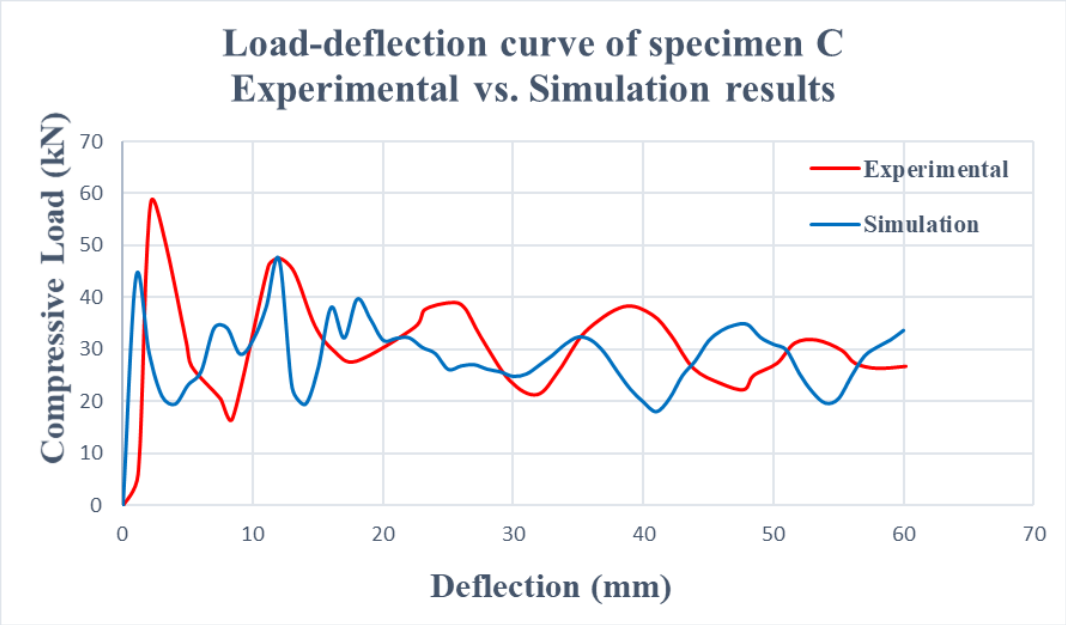

Figure 101 Experimental vs. Simulation load-deflection curve for bi-tube C

Bi-tube C			
	Experimental	**Simulation**	**Error (%)**
Peak Crushing Force (kN)	58.83	47.22	19.7
Sustained Load (kN)	30.98	28.61	7.7
Energy Absorption (J)	1858.73	1716.32	7.7
Specific Energy Absorption (J/kg)	14486.99	13376.20	7.7

Table 17 Relative errors of experimental against simulation results for bi-tube C

Additionally, both numerical simulations and experimental tests predict the same collapse mechanism for the crushed bi-tube specimen C, which is a mixed collapse mode, as both concertina initially and then diamond folds are observed to be formulated during the axial collapse. In fact, the developed model of bi-

tube C predicts also the number of formulated diamond folds, which in specific are four folds. However, the experimental test reveals that the folds which are formulated as the bi-tube specimen continues to collapse in diamond mode, are 2-lobe folds, while the simulation reveals a formulation of 3-lobe folds. Finally, both experimental and simulation results predict that the adhesion between internal and external tubes is almost completely maintained.

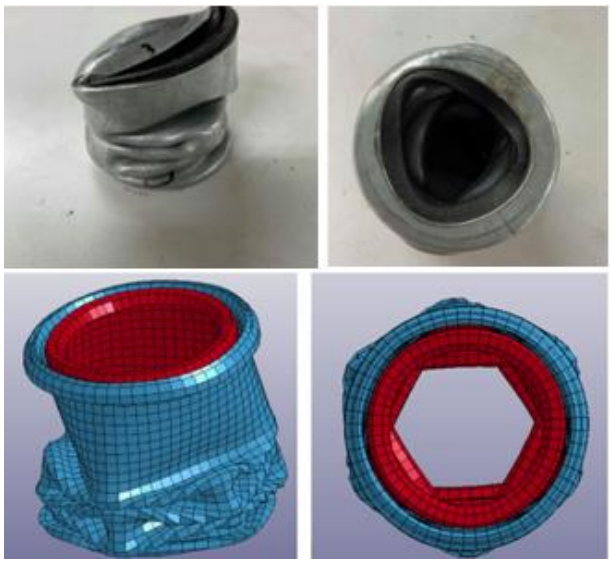

Figure 102 Collapsed structure of bi-tube C (experimental vs. simulation results)

Figure 103 Cut structures of bi-tube C (experimental vs. simulation results)

6.2.4 Bi-tube Specimen D

The comparison of provided results from numerical simulations against the experimental data revealed the load-deflection curves for bi-tube specimen D, as depicted in Figure 104. As Table 18 reveals, the simulation predicts sufficiently the experimental F-s curve, except from the initial peak load where is occurred the maximum deviation of 10.6%. In fact, sustained load, specific energy absorption and absorbed energy are computed with less than 4.5% deviation

providing a sufficient matching between the experimental and the numerical simulation results.

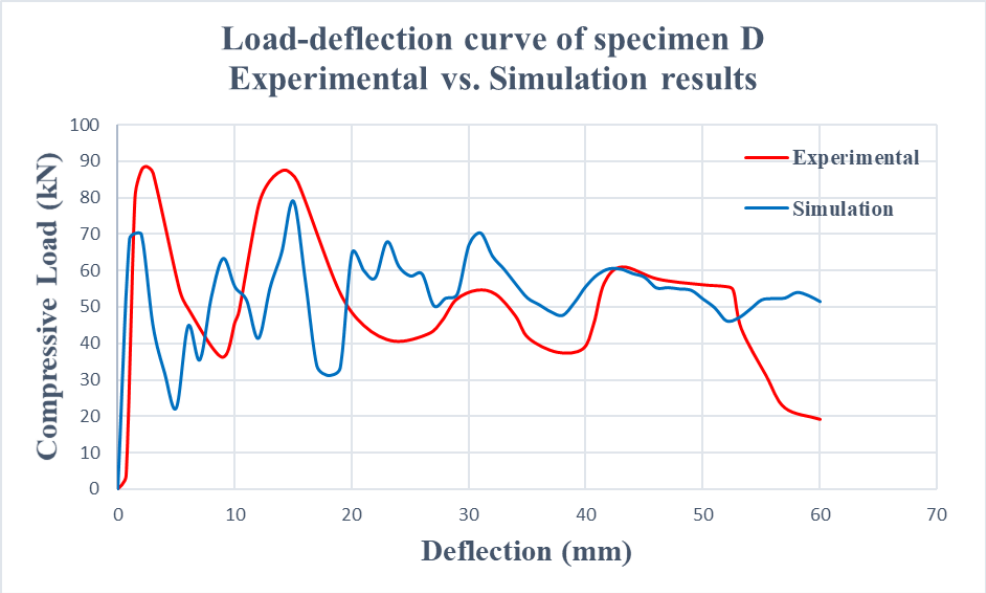

Figure 104 Experimental vs. Simulation load-deflection curve for bi-tube D

Bi-tube D			
	Experimental	**Simulation**	**Error (%)**
Peak Crushing Force (kN)	88.51	79.14	10.6
Sustained Load (kN)	51.09	53.38	4.48
Energy Absorption (J)	3065.62	3202.73	4.47
Specific Energy Absorption (J/kg)	16806.77	17558.40	4.47

Table 18 Relative errors of experimental against simulation results for bi-tube D

Additionally, both numerical simulations and experimental tests predict the same collapse mechanism for the crushed bi-tube specimen D, which is a mixed collapse mode, as both concertina initially and then diamond folds are observed to be formulated during the axial collapse. In fact, the developed model of bi-tube D predicts also the number of formulated diamond folds, which in specific are three folds. However, the experimental test reveals that the folds which are formulated as the bi-tube specimen continues to collapse in diamond mode, are 2-lobe folds, while the simulation reveals a formulation of 3-lobe folds. Finally, both experimental and simulation results predict that the adhesion between internal and external tubes is completely maintained.

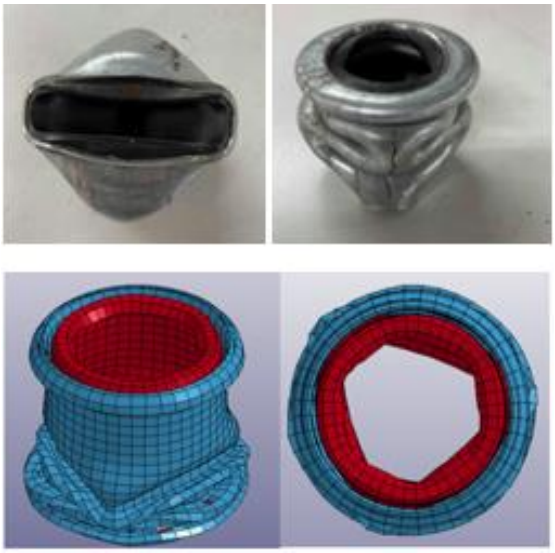

Figure 105 Collapsed structure of bi-tube D (experimental vs. simulation results)

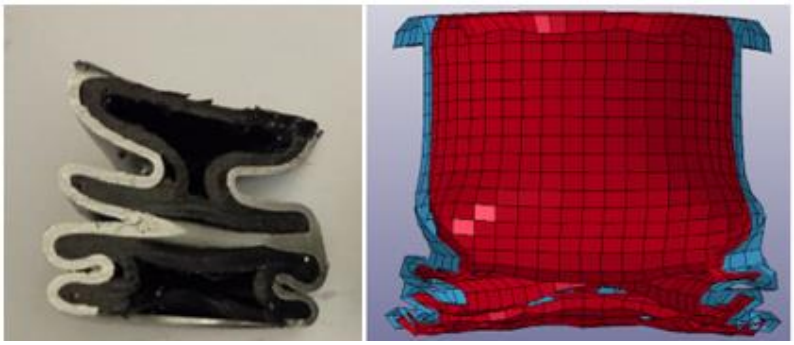

Figure 106 Cut structures of bi-tube D (experimental vs. simulation results)

6.3 Models Accuracy Assessment and Conclusions

By taking into account the above results as the comparison between the experiments and simulations revealed them, critical conclusions can be extracted firstly for the assessment of the validity of the developed bi-tube models in LS-DYNA, but also for the crashworthiness behavior and response of the examined bi-tube structures.

In particular, regarding to the accuracy of the developed bi-tube models, the peak crushing force is the parameter which among the others, appeared to be the most difficult to predict. In contrast, sustained load, absorbed energy and specific energy absorption can be predicted more sufficiently in most cases by the simulations in LS-DYNA. An important although factor which increases the deviations between the simulation results and the experimental ones, is the different examined loading rate (or crushing speed) which is adjusted to the

simulation and the experimental tests. However, a more representative comparison would require the implementation of a dynamic crush test.

Additionally, the crashworthiness behavior and response characteristics of the bi-tube structures which consist of a hard (steel) external tube and soft (ertalon) internal tube, like bi-tube C&D, are more sufficiently predicted. Furthermore, for a certain combination of soft/hard tubes as internal and external tubes, like bi-tubes A&B and C&D, the bi-tubes with greater thickness (like specimen B and D) are predicted more accurately in crush response characteristics.

As for the bi-tubes deformation during their axial collapse, all developed models predict correctly the mixed collapse mode as the main collapse mechanism observed in all four examined bi-tubes. The mixed mode represents in fact a combination of concertina and diamond mode, which are both observed in each one of the bi-tubes collapses. More specifically, all examined bi-tubes start to be compressed and formulating initially a concertina fold, while they continue to collapse by formulating diamond folds resulting in a mixed collapse mode. Although the developed models predicted correctly the mixed collapse mode, they failed to predict absolutely correct the diamond collapse mechanism in the case of specimens C&D. In fact, for the diamond mode occurred after the initial shortening, the simulated models revealed a formulation of 3-lobe diamond folds, while the experimental tests deform the bi-tube specimens by formulating 2-lobe diamond folds. However, for the specimens A&B, the 3-lobe diamond folds of the mixed collapse mode are accurately predicted. Further, in the case of bi-tube specimens C&D, the number of formulated folds is also accurately predicted. Finally, the adhesion maintenance for the bi-tube specimens C&D is accurately predicted too, while for the specimens A&B it is correctly suggested that the adhesion is lost in the areas where no folds are formulated. However, in the folded area of the bi-tubes A&B, the adhesion is not predicted sufficiently to be maintained as it actually does.

7. Summary, Conclusions and Recommendation for Future Work

7.1 Summary and Conclusions

The purpose of current diploma thesis is to study the crashworthiness behavior of circular thin-walled bi-tubes under axial crushing loads. For the needs of this study, four different bi-tube specimens initially constructed. Two of the four bi-tubes consist of an external ertalon tube and an internal steel tube, while the other two bi-tube specimens contain an external steel tube and an internal ertalon tune. Further, different thickness and outter diameters were selected to be examined in order to assess their impact on crashworthiness behavior and response.

Initially, the four constructed bi-tube specimens were tested in axial compression with a loading rate of 10 mm/min. In each test case, the appropriate data were recorded and images of the collapsing specimen were captured. The recorded data used for the calculation of the crashworthiness response characteristics of each bi-tube specimen. More specifically, the F-s curve, the peak crushing force, the mean sustained load, the amount of absorbed energy and the specific energy absorption are computed by the data processing for each one of the bi-tubes.

At next, the model of each bi-tube structure was developed in LS-DYNA software with the finite element modelling approach. The bi-tubes were modelled as thin-walled tubes by adjusting the appropriate mechanical properties of each material (ertalon and steel). The contact interfaces between the two tube components of the bi-tube structure and the two plates were also considered and taken into account properly. At each examined bi-tube model, a crushing speed of 0.5 mm/msec was adjusted to assess their crashworthiness response and behavior.

The results revealed that the bi-tube consisted of the combination of a harder (steel) external tube and a softer (ertalon) internal tube is a more efficient structure in terms of crashworthiness, or in other words it behaves in a more a crashworthy way during its collapse, as it is characterized by greater energy absorption capability. Further, increasing the bi-tube thickness results in greater amounts of absorbed energy, while the same trend is observed increasing the bi-tube external diameter.

Furthermore, all examined configurations deformed during their compression in a mixed collapse mode by initially formulating a single concertina fold and continued to collapse by formulating diamond folds. In the case of bi-tubes with hard (steel) external tube and soft (ertalon) internal one, the adhesion between the two tubes was fully maintained, while in the case of bi-

tube specimens of soft (ertalon) external and hard (steel) internal tubes, the adhesion was lost in the areas where no folds had been formulated. In fact, only in the area where folds had been formulated, the adhesion was partially maintained between some convolutions.

Regarding to the revealed matching between the experimental and the simulation results, it was concluded that the crashworthiness behavior and response characteristics of bi-tubes C&D was predicted in the most sufficient way by providing errors between 4.5% and 7.7% in mean sustained load and specific energy absorption, while the respective ones for bi-tubes A&B were lying about 10%. In addition, the bi-tubes of higher thickness also seemed to be predicted more accurately by the simulated models in LS-DYNA. Finally, all models predicted correctly the mixed collapse mode which was observed in the experimental tests too, while the fully maintained adhesion between the two tubes in the collapsed bi-tubes C&D was also predicted.

7.2 Recommendation for Future Work

Some research fields which are recommended for future work are:

- Modelling of bi-tubes with solid elements in order to obtain the differences in the predicted response under axial crushing loads, crashworthiness characteristics and observed collapse mechanism.
- Assessment of different types of element formulation by adjusting different formulas as the LS-DYNA software offers a large amount of options. Different selections may be proved quite important as different degrees of freedom in the finite elements deformation will may allow to capture more complicated phenomena during specimen collapse.
- Considerations for assessing the impact of strain rate as it differs from the one adjusted to the simulation and the one with which the experimental tests were carried out.
- Examination of lateral crushing loading conditions or different bi-tube components geometry (windowed tubes or multi-cell tubes).

8. Εκτεταμένη Περίληψη στα Ελληνικά

8.1 Εισαγωγή

Οι σύγχρονες σχεδιαστικές τάσεις συχνά περιορίζονται σήμερα από αυστηρές προδιαγραφές ασφαλείας οι οποίες αποσκοπούν στην μείωση της επίδρασης που επιφέρει η κρούση στη συγκρότηση/δομή μια κατασκευής, ιδίως μάλιστα όταν πρόκειται για κατασκευή μεταφοράς επιβατών, όπου το κριτήριο πλέον αποτελεί η ελαχιστοποίηση της επίδρασης της κρούσης στους επιβάτες. Επομένως, τα κριτήρια σχεδιασμού έναντι κρουστικής καταπόνησης αποσκοπούν στην επίτευξη των παρακάτω στόχων:

- Αύξηση της απορρόφησης ενέργειας κατά την κρούση, η οποία επιτυγχάνεται με την επιβολή πλαστικών παραμορφώσεων όπου πλέον η κινητική ενέργεια της κρούσης δαπανάται στην πλαστικοποίηση της κατασκευής (έργο παραμόρφωσης) χωρίς να μεταβαίνετε στους επιβάτες.
- Μείωση της επίδρασης της κρούσης στους επιβάτες, ώστε να αποφεύγονται θανάσιμοι ή μη τραυματισμοί
- Διατήρηση ικανοποιητικής δομής της κατασκευής κατόπιν της κρούσης, π.χ. σε επίπεδο μέγιστων επιτρεπτών παραμορφώσεων ή ελάχιστου αναγκαίου απαιτούμενου όγκου/χώρου κλπ.
- Περιορισμός των μεταβιβαζόμενων δυνάμεων προς τους επιβάτες, καθώς η απορρόφηση αυτών από τη δομή της κατασκευής θα τις εξουδετερώσει δαπανώντας τις στην πλαστική παραμόρφωσή της.
- Διατήρηση ασφαλούς και επαρκούς όγκου της κατασκευής, ώστε π.χ. να εξασφαλίζεται η ασφαλής έξοδος των επιβατών.

Η επίτευξη όλων των παραπάνω προδιαγραφών είναι επιθυμητό να συνδυάζεται με μια ελεγχόμενη και προοδευτική κατάρρευση της κατασκευής κατά την κρούση. Οι συσκευές/εξαρτήματα που σχεδιάζονται έναντι κρουστικής καταπόνησης ώστε να απορροφούν την ενέργεια της κρούσης ονομάζονται απορροφητές ενέργειας. Οι τελευταίοι κατασκευάζονται συνήθως από μέταλλα (χάλυβας, αλουμίνιο κ.ά.), πολυμερή, σύνθετα υλικά ή τέλος δι-στρωματικά υλικά (bi-materials). Συγκεκριμένα, η χρήση διπλοκέλυφων υλικών έχει αποκτήσει ευρύ χαρακτήρα τα τελευταία χρόνια, καθώς συνδυάζουν αυξημένη ικανότητα απορρόφησης ενέργειας υπό χαμηλό βάρος κατασκευής.

Στην ίδια κατεύθυνση εμπεριέχονται και οι λεπτότοιχες δομές οι οποίες συνδυάζουν επίσης αυξημένη ικανότητα απορρόφησης ενέργειας υπό χαμηλό μάλιστα βάρος. Συγκριτικά δε με τις συμπαγείς κατασκευές, οι λεπτότοιχες είναι μεν ελαφρύτερες λόγω μικρότερης διατομής, ενώ παρουσιάζουν δε αυξημένη ικανότητα απορρόφησης της κινητικής ενέργειας της κρούσης καθώς η πλαστικοποίηση της λεπτότοιχης διατομής είναι πιο εφικτή από της συμπαγούς,

γεγονός που σημαίνει αυξημένο εσωτερικό έργο παραμορφώσεων και άρα απορρόφηση κρουστικής ενέργειας.

Ως εκ τούτου, οι θεσπισμένοι κανονισμοί ασφαλείας και διάφοροι εμπειρικοί κανόνες από παρελθόντα ή πρόσφατα συμβάντα, είναι αυτοί οι οποίοι θέτουν τις αντίστοιχες προδιαγραφές σχεδιασμού έναντι κρουστικής καταπόνησης.

Ο σκοπός της παρούσας διπλωματικής εργασίας είναι η ανάλυση και διερεύνηση της συμπεριφοράς και της απόκρισης λεπτότοιχων διπλοκέλυφων σωλήνων κυκλικής διατομής έναντι κρουστικής αξονικής καταπόνησης. Για το λόγο αυτό, τόσο πειραματικές διαδικασίες, όσο και κατάλληλες αριθμητικές προσομοιώσεις στο λογισμικό πεπερασμένων στοιχείων LS-DYNA λαμβάνουν χώρα. Τέσσερα δοκίμια διπλοκέλυφων σωλήνων εξετάστηκαν τόσο στα πειράματα, όσο και στις προσομοιώσεις. Τα δυο από αυτά αποτελούνταν από χαλύβδινο εσωτερικό σωλήνα και πλαστικό (ertalon/ PA6) εξωτερικό σωλήνα, ενώ τα άλλα δυο περιέχουν έναν εξωτερικό χαλύβδινο σωλήνα και έναν πλαστικό εσωτερικό (ertalon/ PA6). Διαφορετικά πάχη και εξωτερικοί διάμετροι επιλέχθηκαν για τα εξεταζόμενα δοκίμια, ώστε να ληφθεί υπόψιν και η επίδραση των δυο παραπάνω μεγεθών στην αντοχή έναντι κρούσης.

Έτσι λοιπόν, στο κεφάλαιο 2 της παρούσας εργασίας παρουσιάζονται αρχικά κάποια βασικά στοιχεία/μεγέθη περί της συμπεριφοράς και της απόκρισης μια κατασκευής έναντι κρουστικής καταπόνησης. Επίσης, οι ενδεχόμενοι μηχανισμοί κατάρρευσης παρουσιάζονται και αναλύονται, μαζί προσθέτως και με τις δυνατές πειραματικές δοκιμές που μπορούν να επιτευχθούν. Τέλος, παρουσιάζεται μια σύντομη σύνοψη των κυριότερων αντίστοιχων μελετών της βιβλιογραφίας που συνάπτονται στο παρών αντικείμενο.

Ακόμη, στο κεφάλαιο 3 παρουσιάζονται πλεονεκτήματα, χρήσεις και εφαρμογές των διμεταλλικών υλικών, ενώ το κεφάλαιο 4 παραθέτει την διαδικασία κατασκευής των τεσσάρων δοκιμίων διπλοκέλυφων σωλήνων που εξετάστηκαν. Ακολουθούν οι διαδικασίες διεξαγωγής των πειραματικών δοκιμών και η παρουσίαση των σχετικών αποτελεσμάτων.

Πρόσθετα, το κεφάλαιο 5 παρουσιάζει τη διαδικασία μοντελοποίησης των τεσσάρων δοκιμίων στο λογισμικό LS-DYNA με τη μέθοδο των πεπερασμένων στοιχείων. Έπειτα, παραθέτονται τα αποτελέσματα των προσομοιώσεων των αντίστοιχων μοντέλων, ενώ στο κεφάλαιο 6 παρουσιάζονται συγκριτικά αποτελέσματα μεταξύ προσομοιώσεων και πειραματικών δοκιμών. Τέλος, στο κεφάλαιο 7 επισυνάπτεται μια σύντομη σύνοψη/περίληψη και σχολιασμός των συμπερασμάτων της εργασίας, ενώ προτείνονται παράλληλα και προτάσεις προς μελλοντική διερεύνηση.

8.2 Μηχανική Συμπεριφορά έναντι Κρουστικής Καταπόνησης

Ο σχεδιασμός κατασκευών έναντι κρουστικής καταπόνησης αποσκοπεί κυρίως στην βελτίωση της ικανότητας απορρόφησης της ενέργειας που παράγεται κατά την κρούση. Μια τυπική απόκριση/συμπεριφορά μια κατασκευής έναντι κρουστικής καταπόνησης απεικονίζεται στην Εικόνα 1 μέσω της καμπύλης φορτίου-μετατόπισης (βράχυνσης). Από την καμπύλη κρουστικού αξονικού φορτίου-μετατόπισης (F-s), μερικά κρίσιμα μεγέθη μπορούν να ορισθούν και τα οποία εν τέλει χαρακτηρίζουν την συμπεριφορά και την αντοχή μιας κατασκευής έναντι κρουστικής καταπόνησης.

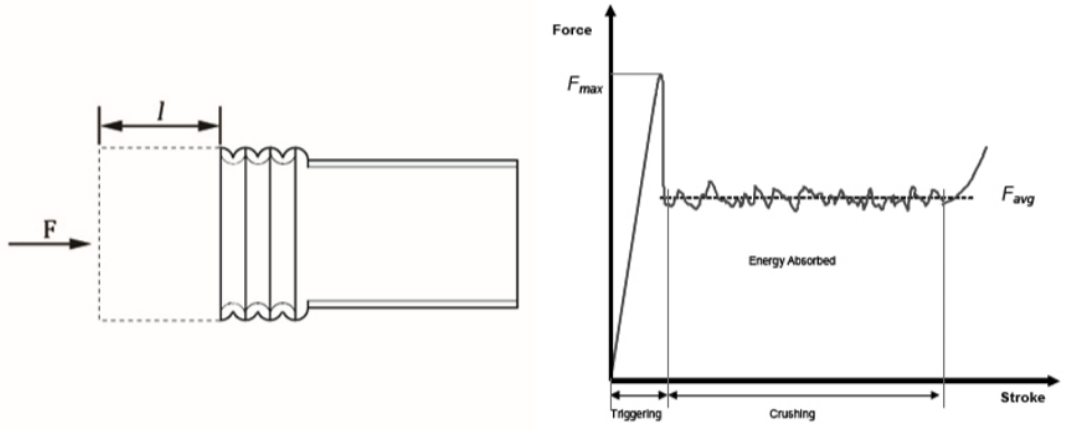

Εικόνα 1 Τυπική απόκριση μιας κατασκευής έναντι κρουστικής καταπόνησης

Διακρίνουμε λοιπόν τις παρακάτω παραμέτρους, οι περισσότερες εκ των οποίων μάλιστα παριστάνονται στην .

- Μέγιστο φορτίο κρούσης (F_{max}), το οποίο είναι το μέγιστο παρατηρούμενο φορτίο της καμπύλης δύναμης-μετατόπισης F-s.

- Μέσο παραμένων φορτίο κατάρρευσης (F_{avg}), το οποίο είναι το παραμένων φορτίο κατάρρευσης της κατασκευής έπειτα από το μέγιστη φόρτιση, και το οποίο επιφέρει την ίδια απορρόφηση ενέργειας εάν ασκούταν κατά αποκλειστικότητα.

$$F_{avg} = \frac{1}{s} \cdot \int_0^s F \cdot ds$$

- Ομοιομορφία φόρτισης (LU), η οποία είναι ο λόγος του παραμένοντος φορτίου κατάρρευσης προς το μέγιστο παρατηρούμενο φορτίο της κατασκευής.

$$LU = \frac{F_{avg}}{F_{max}}$$

- Απορρόφηση ενέργειας κρούσης (EA), η οποία ορίζεται ως το μέγεθος της παραγόμενης ενέργειας κατά την κρούση το οποίο απορροφάτε από την κατασκευή και αναλώνεται στην πλαστικοποίησή της υπό τη μορφή εσωτερικού έργου παραμόρφωσης. Διαφορετικά, εκφράζεται ως το εμβαδόν κάτω από την καμπύλη δύναμης-μετατόπισης F-s.

$$EA = \int_0^s F \cdot ds = F_{avg} \cdot s$$

5. Ειδική απορρόφηση ενέργειας (SEA), η οποία εκφράζεται ως η ικανότητα απορρόφησης ενέργειας ανά μονάδα μάζας, μετρημένη σε J/g.

$$SEA = \frac{\int_0^s F \cdot ds}{m} = \frac{EA}{\rho \cdot A \cdot l}$$

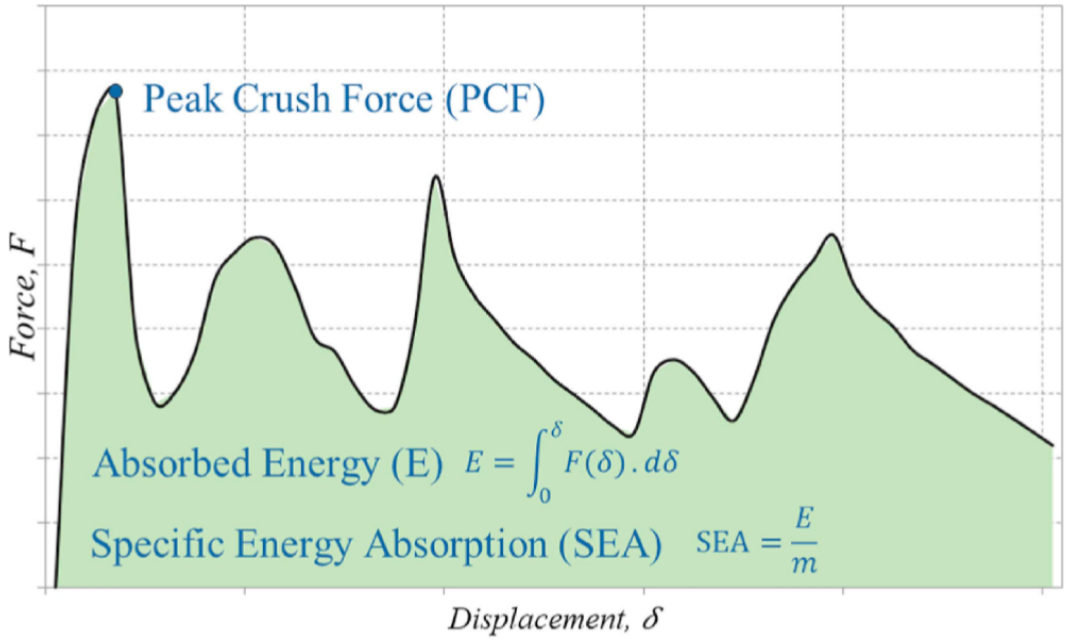

Εικόνα 2 Χαρακτηριστικά συμπεριφοράς μιας κατασκευής έναντι κρουστικής καταπόνησης

Πιο συγκεκριμένα, αναφορικά με το μέγιστο φορτίο κατά την κατάρρευση, αυτό επιδρά αναλογικά στην δυνατότητα απορρόφησης ενέργειας από την κατασκευή, καθώς όσο αυξάνεται, τόσο η καμπύλη δύναμης-μετατόπισης μετατοπίζεται προς τα πάνω, και αυξάνεται το εμβαδό κάτω από αυτήν. Έτσι, υψηλά μέγιστα φορτία κατάρρευσης συχνά επιφέρουν υψηλό παραμένων φορτίο και άρα υψηλά επίπεδα ενέργειας απορρόφησης κατά την κρούση. Ωστόσο, από μια τιμή και πάνω, η περαιτέρω αύξηση του μέγιστου φορτίου κατάρρευσης

επιδρά ανασταλτικά στη δυνατότητα απορρόφησης ενέργειας της κατασκευής, καθώς εξαιρετικά υψηλό μέγιστο φορτίο επιφέρει τον κίνδυνο το φορτίο κρούσης να μην υπερβεί τη τιμή του μέγιστου φορτίου κατάρρευσης και άρα η κατασκευή να μην προλάβει να πλαστικοποιηθεί. Σε μια τέτοια περίπτωση, το εσωτερικό έργο παραμόρφωσης θα ήταν εξαιρετικά μικρό, και κατ' επέκταση η δυνατότητα της κατασκευής να απορροφήσει την παραγόμενη ενέργεια κατά την κρούση.

Πρόσθετα, αναφορικά με το μέσον παραμένων φορτίο κατά την κατάρρευση, η αύξηση του μετατοπίζει την καμπύλη δύναμης-μετατόπισης προς τα άνω, αυξάνοντας έτσι το εμβαδόν υπό της καμπύλης και συνεπώς την απορροφώμενη ενέργεια της κρούσης.

Ακόμη, η ειδική ενέργεια απορρόφησης είναι ενδεικτική της ικανότητας της κατασκευής να αντιστέκεται έναντι κρούσης, ενώ παρουσιάζεται ως το πλέον κατάλληλο μέγεθος προς αξιολόγηση της αντίστασης των κατασκευών έναντι κρούσης, καθώς αποτελεί ανηγμένο μέγεθος ως προς τη μάζα της κατασκευής.

Ως εκ τούτου, ένας ιδανικός απορροφητής ενέργειας χαρακτηρίζεται από υψηλή ειδική ενέργεια απορρόφησης, μοναδιαία ομοιομορφία φορτίου (LU=1), τη μέγιστη δυνατή βράχυνση της κατασκευής, ή αλλιώς την ιδανική/μέγιστη βράχυνση έως και του αρχικού της μήκους, και ένα υψηλό μέγιστο φορτίο κατάρρευσης το οποίο ωστόσο εντοπίζεται εντός λογικών ορίων ώστε να επιτρέπει την πλαστικοποίηση της κατασκευής.

Τέλος, η επίδραση της ταχύτητας κρούσης ή ισοδύναμα της ταχύτητας επιβολής του φορτίου στην απορροφώμενη ενέργεια είναι ομόσημη της επίδρασης του ρυθμού παραμόρφωσης στην καμπύλη τάσης-παραμόρφωσης σ-ε. Εναλλακτικά, όσο αυξάνεται η ταχύτητα επιβολής του κρουστικού φορτίου (ταχύτητα κρούσης), τόσο αυξάνεται η ενέργεια που απορροφάται κατά την κρούση από την κατασκευή προς πλαστικοποίησή της.

8.2.1 Μηχανισμοί Κατάρρευσης

Μια κατασκευή η οποία υπόκειται σε αξονικά θλιπτικά φορτία κρούσης αστοχεί σύμφωνα με συγκεκριμένους μηχανισμούς κατάρρευσης. Οι μηχανισμοί κατάρρευσης που εμφανίζονται μπορεί να είναι ελεγχόμενοι και προοδευτικοί ή καταστροφικοί και ασταθής. Προφανώς, μια κατασκευή η οποία καταρρέει υπό κρουστική φόρτιση, είναι επιθυμητό να καταρρέει κατά ελεγχόμενο και προοδευτικό τρόπο, εφόσον αυτός είναι που εξασφαλίζει ελεγχόμενη αστοχία αλλά και μεγαλύτερα ποσά απορροφώμενης ενέργειας κατά την κρούση, εφόσον το έργο παραμόρφωσης τότε θα είναι μεγαλύτερο. Σύμφωνα με τους Farley και Jones (1989), οι μηχανισμοί κατάρρευσης είναι οι εξής τέσσερις:

1. *Εγκάρσια διάτμηση και θρυμματισμός*
   Χαρακτηρίζεται από διατομή με παράλληλες στρώσεις με ενδοστρωματικές διαμήκης ρωγμές μικρού μήκους οι οποίες σχηματίζουν μερικώς δέσμες στρώσεων. Ο κύριος μηχανισμός απορρόφησης ενέργειας

κατά την κρούση οφείλεται στην θραύση των δεσμών των στρώσεων κατά την έναρξη του θρυμματισμού. Παρατηρείται σε κατασκευές μικρού μήκους, ενώ η αντοχή των στρωματικών δεσμών σε κάμψη είναι αυτή που καθορίζει και ελέγχει την διαδικασία της κρουστικής κατάρρευσης. Στην περίπτωση δε των σύνθετων υλικών, η αντοχή των στρώσεων σε κάμψη εξαρτάται από την ελαστικότητα και την αντοχή των ινών.

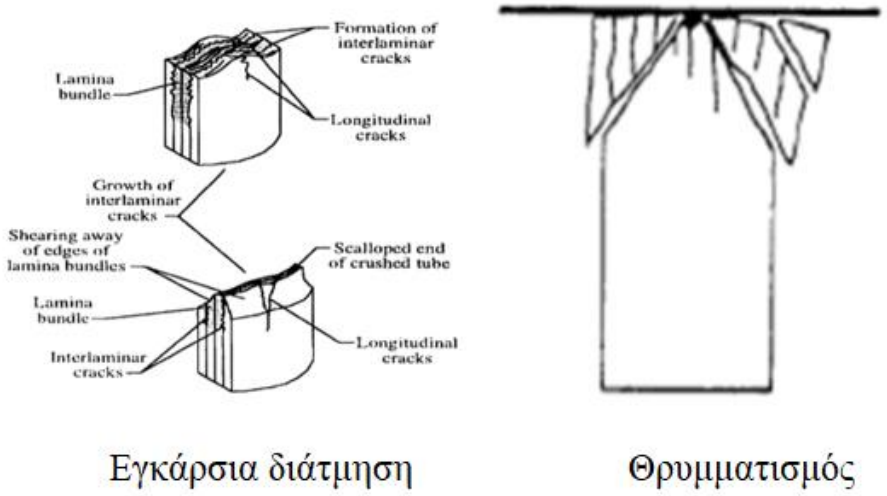

Εικόνα 3 Εγκάρσια διάτμηση και θρυμματισμός

2. *Ψαθυρή θραύση*

Ο μηχανισμός κατάρρευσης της ψαθυρής θραύσης παρουσιάζει τα ίδια χαρακτηριστικά με αυτά του θρυμματισμού τα οποία έγκειται στην αστοχία των δεσμών στρώσεων. Στην ψαθυρή θραύση, όταν αστοχήσει η πρώτη δέσμη στρώσεων, η ανακατανομή του φορτίου στις εναπομείναντες δέσμες συμβάλλει στην εξέλιξη των ρωγμών και κατ' επέκταση στην αστοχία περαιτέρω δεσμών στρώσεων. Οι παράμετροι που ελέγχουν τον μηχανισμό κατάρρευσης της ψαθυρής θραύσης στην περίπτωση των σύνθετων υλικών είναι η ελαστικότητα της μήτρας και η αντοχή σε εφελκυσμό των δεσμών στρώσεων. Πιο συγκεκριμένα, η πρώτη παράμετρος ελέγχει την ανάπτυξη και την εξέλιξη των ρωγμών που εκτείνονται παράλληλα στην διεύθυνση των ινών, ενώ η δεύτερη την αστοχία των δεσμών στρώσεων.

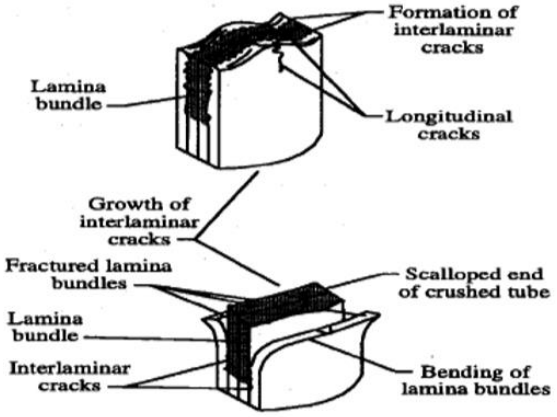

Εικόνα 4 Ψαθυρή θραύση

3. *Κάμψη και αναδίπλωση στρώσεων*

Η κάμψη και η αναδίπλωση των δεσμών των στρώσεων χαρακτηρίζονται από επιμήκεις ρωγμές που αναπτύσσονται ενδιάμεσα και παράλληλα των στρώσεων οι οποίες ωστόσο δεν αστοχούν σε αυτήν την περίπτωση. Ο μηχανισμός απορρόφησης ενέργειας εδώ έγκειται στην ανάπτυξη των ρωγμών, οι οποίες εκτείνονται εις μήκος τουλάχιστον δεκαπλάσιο του πάχους των στρώσεων. Έτσι, όταν η κατάρρευση συνοδεύεται από αναδίπλωση των στρώσεων, οι τελευταίες εμφανίζουν σημαντική κάμψη χωρίς ωστόσο να αστοχούν. Στην περίπτωση δε των σύνθετων υλικών, η αντοχή της μήτρας είναι αυτή που ελέγχει το μηχανισμό κατάρρευσης καθώς ελέγχει την ανάπτυξη των ρωγμών.

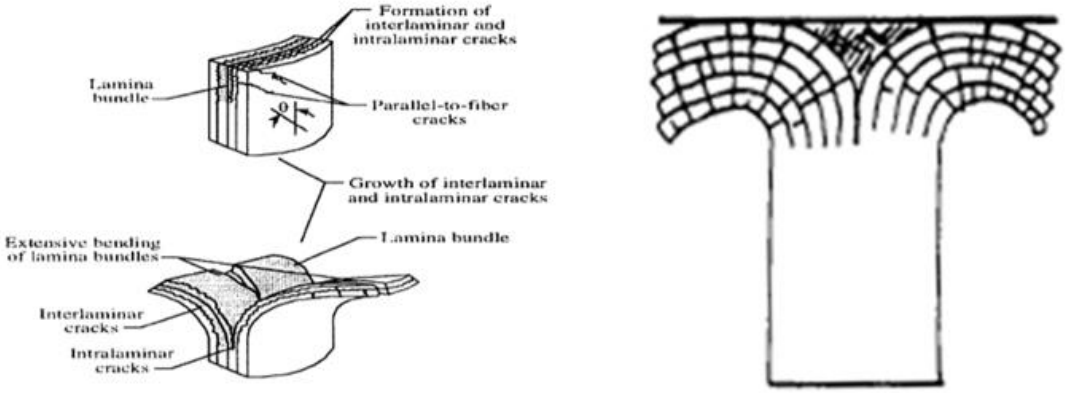

Εικόνα 5 Μηχανισμός κατάρρευσης με κάμψη και αναδίπλωση στρώσεων

4. *Τοπικός λυγισμός και προοδευτικός σχηματισμός πτυχώσεων*

Ο συγκεκριμένος μηχανισμός κατάρρευσης συναντάται τόσο σε όλκιμα όσο και σε ψαθυρά υλικά. Αρχικά εκδηλώνεται τοπικός λυγισμός σε περιοχές του υλικού, ο οποίος εξελίσσεται εν συνεχεία στον σχηματισμό

προοδευτικών διαδοχικών πτυχώσεων/αναδιπλώσεων. Οι μηχανισμοί που ελέγχουν τη προοδευτική κατάρρευση υπό σχηματισμό πτυχώσεων/αναδιπλώσεων είναι η πλαστική διαρροή των ινών ή/και της μήτρας σε περίπτωση σύνθετων υλικών. Μάλιστα δε, στην περίπτωση ψαθυρών υλικών, η κατάρρευση υπό τοπικό λυγισμό καθορίζεται από τη μη-γραμμική συμπεριφορά τάσεων-παραμορφώσεων της μήτρας, ενώ αντιθέτως στην περίπτωση των όλκιμων υλικών, η ελαστικότητα των ινών ή της μήτρας είναι αυτή που καθορίζει την ανάπτυξη τοπικού λυγισμού και διαδοχικών πτυχώσεων/αναδιπλώσεων.

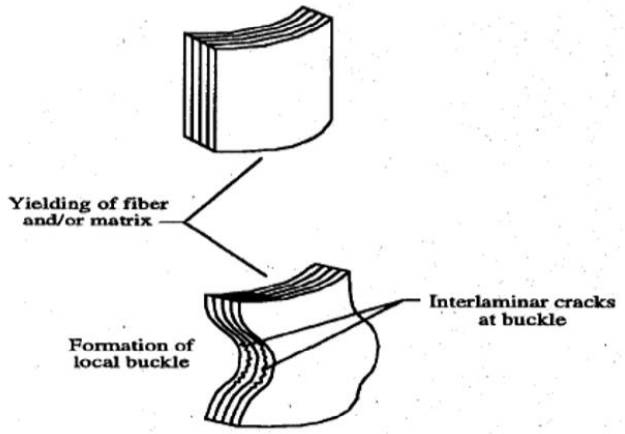

Εικόνα 6 Τοπικός λυγισμός και ανάπτυξη πτυχώσεων/αναδιπλώσεων

Εξετάζοντας τον μηχανισμό κατάρρευσης μιας κατασκευής και την προσφερόμενη σε αυτήν ικανότητα απορρόφησης ενέργειας κατά την κρούση, σύμφωνα με τη βιβλιογραφική πηγή [11], η κατάρρευση υπό μικροθρυμματισμό είναι εκείνη που αποδίδει τα μεγαλύτερα ποσά απορροφώμενης ενέργειας, ωστόσο σε περίπτωση υπερβολικού θρυμματισμού, η ενέργεια απορρόφησης μπορεί να κυμανθεί σε μικρότερα επίπεδα εξαιτίας του περιορισμού βράχυνσης της κατασκευής λόγω των θρυμματισμένων αποβλήτων. Έπειτα, η κατάρρευση υπό τοπικό λυγισμό και προοδευτικό σχηματισμό πτυχώσεων και αναδιπλώσεων προσφέρει μεσαία επίπεδα ικανότητας απορρόφησης ενέργειας από μια κατασκευή, ενώ η κατάρρευση υπό ψαθυρή θραύση προσφέρει τα μικρότερα ποσά απορροφώμενης ενέργειας ως μη ελεγχόμενος και καταστροφικός τρόπος κατάρρευσης. Πρόσθετα, αναφορικά με την επίδραση εξωγενών παραμέτρων στην ικανότητα απορρόφησης ενέργειας από μια κατασκευή, υψηλές ταχύτητες κρούσης ευνοούν την απορρόφηση της ενέργειας που παράγεται κατά την κρούση, σε αντίθεση ωστόσο με την θερμοκρασία περιβάλλοντος, η οποία καθώς αυξάνεται μειώνει το όριο διαρροής, το μέτρο ελαστικότητας και την αντοχή μιας κατασκευής, μετατοπίζοντας προς τα κάτω την καμπύλη σ-ε. Ως εκ τούτου, το εμβαδό υπό τη καμπύλη σ-ε μειώνεται και άρα η ικανότητα της κατασκευής να απορροφήσει την ενέργεια της κρούσης μετατρέποντάς την σε εσωτερικό έργο παραμόρφωσης για την πλαστικοποίησή της. Τέλος, η ταχύτητα κρούσης επίσης επιδρά αναλογικά στην ικανότητα

απορρόφησης ενέργειας, καθώς μεγάλες ταχύτητες επιβολής φορτίου συνεπάγονται αυξημένους ρυθμούς παραμόρφωσης, και συνεπώς η καμπύλη τάσεων-παραμόρφωσης σ-ε μετατοπίζεται προς τα πάνω και η ενέργεια απορρόφησης αυξάνεται.

Αναφορικά δε με τους τρόπους κατάρρευσης με τοπικό λυγισμό και ανάπτυξη πτυχώσεων και αναδιπλώσεων, διακρίνονται οι εξής τέσσερις κατηγορίες:

- ✓ Αξονοσυμμετρικός τρόπος κατάρρευσης (concertina mode)
- ✓ Μη αξονοσυμμετρικός τρόπος κατάρρευσης (diamond mode)
- ✓ Μικτός τρόπος κατάρρευσης (mixed mode)
- ✓ Λυγισμός Euler (Euler type buckling mode)

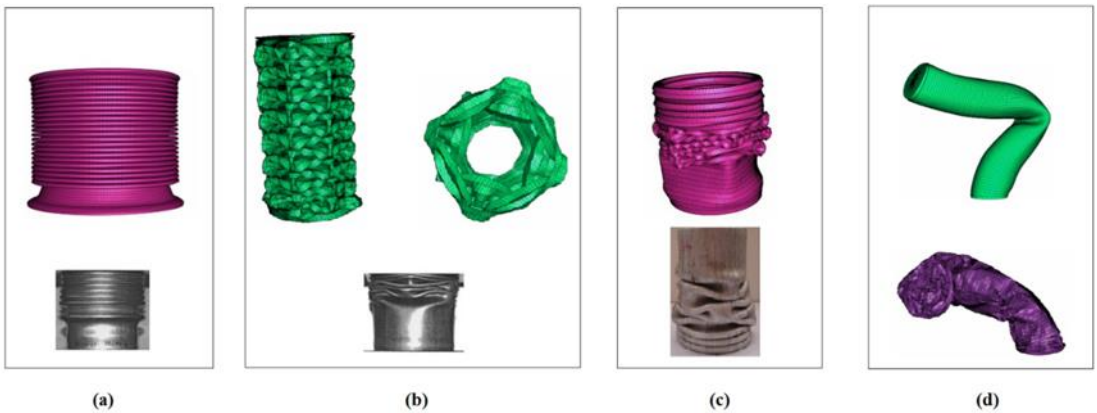

Εικόνα 7 Τρόποι κατάρρευσης με τοπικό λυγισμό και ανάπτυξη πτυχώσεων/αναδιπλώσεων (α:concertina mode, b:diamond mode, c:mixed mode, d:Euler buckling mode)

Πιο αναλυτικά, ο αξονοσυμμετρικός τρόπος κατάρρευσης χαρακτηρίζεται από τον σχηματισμό πτυχώσεων, ή λοβών, κατά εκτατό τρόπο καθώς η επιφάνεια της δομής παραμένει κυκλική με τη περίμετρο της επιφάνειας ωστόσο να αυξάνεται. Είναι ο πλέον επιθυμητός τρόπος κατάρρευσης καθώς αποτελεί έναν ελεγχόμενο τρόπο κατάρρευσης ο οποίος συμβάλλει μάλιστα στην απορρόφηση μεγάλων ποσών ενέργειας κατά την κρούση.

Σχετικά με τον μη αξονοσυμμετρικό τρόπο κατάρρευσης, αποτελεί και αυτός έναν ελεγχόμενο τρόπο κατάρρευσης, ο οποίος ωστόσο επιτρέπει την απορρόφηση μικρότερων ποσών ενέργειας συγκριτικά με την αξονοσυμμετρική κατάρρευση. Εκδηλώνεται με τον σχηματισμό δυο, τριών ή σπανιότερα τεσσάρων λοβών κατά την περιφέρεια της διατομής. Οι λοβοί σχηματίζονται κατά μη εκτατό τρόπο καθώς η περίμετρος της διατομής δεν μεταβάλλεται αλλά αλλάζει η γεωμετρία της (Εικόνα 7b). Επομένως, στην περίπτωση που η αρχικά κυκλική διατομή μετατραπεί σε τριγωνική από την ανάπτυξη τριών λοβών διακρίνουμε 3D μη αξονοσυμμετρική κατάρρευση (3D diamond mode), σε ανάπτυξη αντίστοιχα δυο λοβών διακρίνουμε 2D μη αξονοσυμμετρική κατάρρευση (2D diamond mode) κ.ο.κ. Τέλος, η ανάπτυξη θεωρητικών μοντέλων υπολογισμού αναλυτικών εκφράσεων του φορτίου κατάρρευσης είναι λιγότερο ακριβή σε περίπτωση μη αξονοσυμμετρικής κατάρρευσης.

Επιπλέον, μικτός τρόπος κατάρρευσης δύναται να εμφανισθεί συνδυάζοντας την δημιουργία εκτατών αξονοσυμμετρικών πτυχώσεων συνήθως κατά το αρχικό στάδιο της κατάρρευσης, και συνεχίζοντας με μη αξονοσυμμετρική κατάρρευση.

Η κατάρρευση υπό λυγισμό Euler τέλος αποτελεί μια μη ελεγχόμενη μέθοδος κατάρρευσης καθώς σύμφωνα με αυτήν η κατασκευή αστοχεί χωρίς ωστόσο να έχει υπερβεί το όριο αντοχής της. Γενικά, πρόκειται για ανεπιθύμητο τρόπο κατάρρευσης για μια κατασκευή εξαιτίας τόσο του ασταθούς χαρακτήρα της όσο και των πολύ μικρών ποσών ενέργειας που επιτρέπει να απορροφηθούν.

Επιπρόσθετα, ο μηχανισμός σύμφωνα με τον οποίο καταρρέει μια κατασκευή υπό κρουστική θλιπτική φόρτιση, εξαρτάται ισχυρά από τα γεωμετρικά χαρακτηριστικά της κατασκευής, όπως το μήκος, η διάμετρος, το πάχος τοιχώματος και το γεωμετρικό σχήμα της διατομής. Πιο συγκεκριμένα, όπως παριστάνεται και στην παρακάτω εικόνα, βραχείς σωλήνες μεγάλου πάχους αναμένεται να καταρρεύσουν με αξονοσυμμετρικό μηχανισμό, ενώ για μικρότερα πάχη τοιχώματος μικτός ή μη αξονοσυμμετρικός τρόπος κατάρρευσης ενδέχεται να εμφανιστεί. Ακόμη, λεπτότοιχοι σωλήνες μεγάλου μήκους αναμένεται να καταρρεύσουν υπό ασταθή λυγισμό Euler.

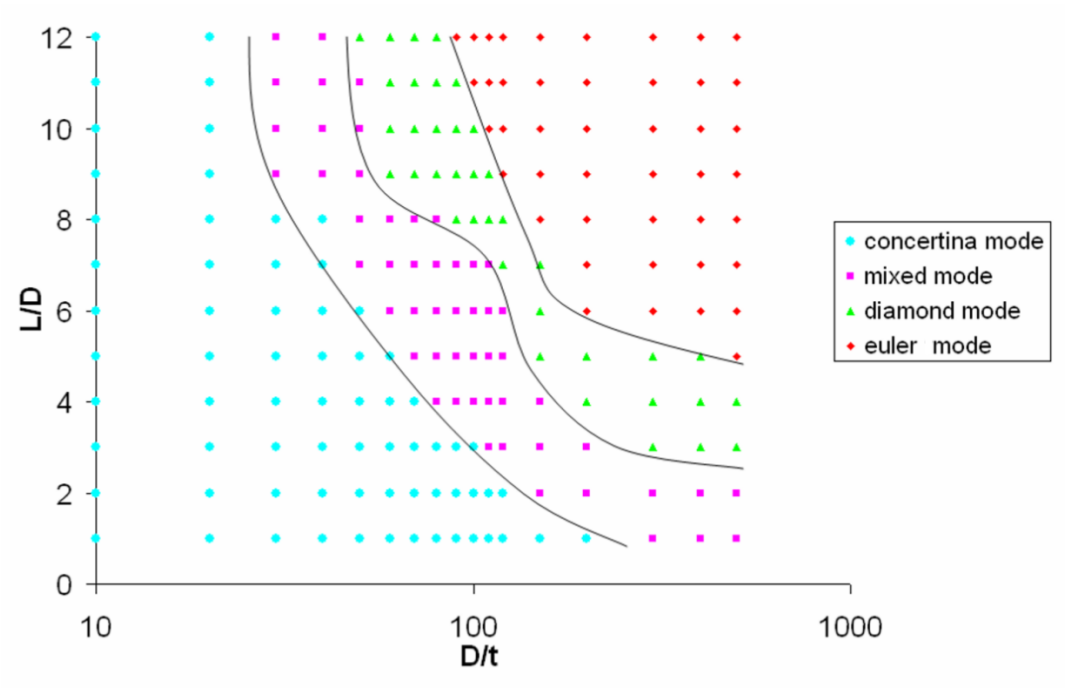

Εικόνα 8 Αναμενόμενοι τρόποι κατάρρευσης για σωλήνες αλουμινίου

Αναφορικά δε με τη επίδραση της διατομής, για απλού σωλήνες, η κυκλική διατομή συμβάλλει στην εμφάνιση αξονοσυμμετρικού μηχανισμού κατάρρευσης, ευνοώντας έτσι την απορρόφηση μεγάλων ποσών κρουστικής ενέργειας. Τέλος δε, η επίδραση των στηρίξεων των άκρων της εξεταζόμενης κατασκευής θεωρείται ως εξίσου σημαντική, καθώς σχετικές μελέτες [13] έδειξαν ότι συμμετρικές στηρίξεις των άκρων θα αποδώσουν συμμετρικό σχηματισμό πτυχώσεων/αναδιπλώσεων. Επίσης, όταν τουλάχιστον ένα άκρο

του συμπιεζόμενου δοκιμίου είναι πακτωμένο, διαπιστώθηκε πως η εμφάνιση αξονοσυμμετρικού μηχανισμού κατάρρευσης είναι πολύ πιθανόν να εμφανιστεί, ενώ τέλος ένα απλά στηριζόμενο άκρο ενός δοκιμίου που καταρρέει υπό τον ασταθή λυγισμό Euler αναμένεται να χάσει την επαφή του με τη στήριξή του.

8.2.2 Δοκιμές Κρούσης

Οι δοκιμές κρούσης είναι πειραματικές δοκιμές που αποσκοπούν στην κατανόηση της συμπεριφοράς και της απόκρισης μιας κατασκευής έναντι κρούσης. Στόχος αποτελεί να παρατηρηθεί ο εμφανιζόμενος μηχανισμός κατάρρευσης, και να εκτιμηθούν σημαντικά χαρακτηριστικά της κατασκευής, όπως το μέγιστο φορτίο κατάρρευσης, η μέγιστη βράχυνση, η απορροφώμενη ενέργεια κατά την κρούση κ.ο.κ.

Οι δοκιμές κρούσης μπορούν να διεξαχθούν τόσο σε ημι-στατικές συνθήκες, όσο και σε δυναμικές. Οι δοκιμές κρούσης που διεξάγονται σε ημι-στατικές συνθήκες πραγματοποιούνται σε ταχύτητες κρούσης πολύ μικρότερες αυτών των πραγματικών συνθηκών κρούσης. Αυτές οι δοκιμές δεν απαιτούν ακριβό εξοπλισμό (στιβαρές μηχανές, κάμερες ταχείας λήψης, καταγραφείς δεδομένων υψηλών συχνοτήτων κλπ.), ωστόσο δεν αντιπροσωπεύουν πλήρως τις εξεταζόμενες συνθήκες κρούσης. Αντιθέτως, οι δοκιμές κρούσης υπό δυναμικές συνθήκες απαιτούν ακριβό εξοπλισμό (στιβαρές μηχανές, κάμερες ταχείας λήψης, καταγραφείς δεδομένων υψηλών συχνοτήτων κλπ.), όμως αντιπροσωπεύουν πλήρως τις πραγματικές συνθήκες κρούσης και για αυτό το λόγο είναι περισσότερο ακριβείς. Ωστόσο, εξαιτίας του κόστους, οι δοκιμές υπό ημι-στατικές συνθήκες επιλέγονται πιο συχνά για την εκτίμηση και διερεύνηση της μηχανικές συμπεριφοράς και του μηχανισμού κατάρρευσης μιας κατασκευής που υπόκειται σε κρουστική φόρτιση.

8.2.3 Σύντομη Βιβλιογραφική Ανασκόπηση

Πλήθος πειραματικών δοκιμών κρούσης και αριθμητικών προσομοιώσεων έχουν διεξαχθεί μέχρι σήμερα από την επιστημονική κοινότητα με σκοπό την ανάλυση και διερεύνηση της μηχανική συμπεριφοράς των κατασκευών έναντι κρουστική καταπόνησης. Συγκεκριμένα, ιδιαίτερο ενδιαφέρον παρουσιάζει ο προσδιορισμός τόσο του μηχανισμού κατάρρευσης όσο και των κύριων χαρακτηριστικών μεγεθών της απόκρισης της κατασκευής, όπως λ.χ. το μέγιστο φορτίο κατάρρευσης (F_{max}), το παραμένων φορτίο κατάρρευσης (F_{avg}), την ομοιομορφία φόρτισης (LU), την ενέργεια απορρόφησης (EA) και την ειδική ενέργεια απορρόφησης (SEA). Η τελευταία δε αποτελεί το πιο χρηστικό μέγεθος προς σύγκριση διαφορετικών κατασκευών ως προς την αντοχή τους έναντι κρούσης, καθώς είναι ανηγμένη προς τη μάζα της κατασκευής.

Έτσι λοιπόν, η μηχανική συμπεριφορά έναντι κρούσης για σύνθετους λεπτότοιχους τετραγωνικούς σωλήνες ενισχυμένους με ίνες άνθρακα, μελετήθηκε [14] συμπεραίνοντας πως η απορροφώμενη ενέργεια εξαρτάται

τόσο από το μηχανισμό κατάρρευσης, όσο και από το πάχος του σωλήνα. Πρόσθετα, παρατηρήθηκε πως κατά την εμφάνιση του μέγιστου φορτίου κατάρρευσης, ρωγμές άρχισαν να εμφανίζονται στις γωνίες της διατομής εξαιτίας συγκέντρωσης τάσεων, οι οποίες ρωγμές αναπτύσσονται έπειτα κατά μήκος του σωλήνα.

Επιπλέον, η πλήρωση των σωλήνων με αφρό στο εσωτερικό τους βρέθηκε πως ενισχύει την αντοχή τους έναντι κρούσης [13], πόρισμα που εξήχθη πραγματοποιώντας αριθμητικές προσομοιώσεις στο λογισμικό πεπερασμένων στοιχείων LS-DYNA. Οι προσομοιώσεις της συγκεκριμένης μελέτης πραγματοποιήθηκαν τόσο με δισδιάστατα επίπεδα πεπερασμένα στοιχεία (shell elements), όσο και με τρισδιάστατα πεπερασμένα στοιχεία (solid elements). Παρατηρήθηκε δε πως και τα δύο είδη πεπερασμένων στοιχείων προέβλεψαν τον μηχανισμό κατάρρευσης, με τα 2D-επίπεδα στοιχεία όμως να προβλέπουν ακριβέστερα τον αριθμό των πτυχώσεων/αναδιπλώσεων.

Ακόμη, έχει διαπιστωθεί πως κυψελοειδής διατομές (Εικόνα 9) αυξάνουν την αντοχή έναντι κρούσης [6], ενώ δε όσο περισσότεροι είναι οι πυρήνες της κυψελοειδούς διατομής τόσο πιο πολύ αυξάνεται η δυνατότητα απορρόφησης ενέργειας από τη δομή της κατασκευής. Επιπροσθέτως, σωλήνες με οπές στην επιφάνειά τους (windowed tubes) παρουσιάζουν χαμηλότερα μέγιστα φορτία κατάρρευσης αλλά και μειωμένα επίπεδα ειδικής απορροφώμενης ενέργειας [4]. Η πρώτη συνέπεια χαρακτηρίζεται ως ευεργετική καθώς συνεπάγεται πως η κατασκευή είναι πολύ πιθανόν να καταφέρει να πλαστικοποιηθεί κατά την κρούση της απορροφώντας ποσά κινητικής κρουστικής ενέργειας, σε αντίθεση με τη δεύτερη συνέπεια, δηλαδή αυτήν της χαμηλής ειδικής ενέργειας απορρόφησης.

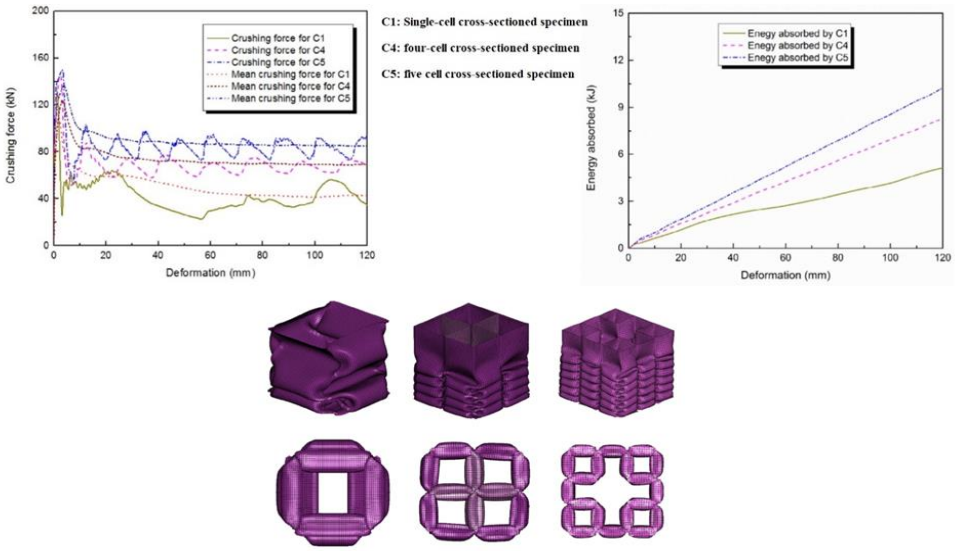

Εικόνα 9 Επίδραση κυψελοειδών διατομών στη μηχανική συμπεριφορά έναντι κρούσης

Στο πεδίο της μηχανικής συμπεριφοράς έναντι κρούσης αναφορικά με τους διπλοκέλυφους σωλήνες, πειραματικές μελέτες [17] έχουν αποφανθεί πως ο εμφανιζόμενος μηχανισμός κατάρρευσης εξαρτάται από το λόγο των ορίων

διαρροής των δύο σωλήνων και το τρόπο κατάρρευσης του σκληρότερου εξ' αυτών στην περίπτωση που ο λόγος παχών είναι περίπου 0,5. Όταν μάλιστα δε, ο ένας σωλήνας είναι αρκετά σκληρότερος από τον άλλον, ο σκληρός σωλήνας είναι αυτός που καθορίζει τόσο τα χαρακτηριστικά κατάρρευσης, όσο και τον τελικό μηχανισμό κατάρρευσης του διπλοκέλυφου σωλήνα. Αναφορικά δε με την διατήρηση της προσκόλλησης των δυο σωλήνων κατά την κατάρρευση της δομής, στην περίπτωση του αξονοσυμμετρικού τρόπου κατάρρευσης, όταν ο εξωτερικός σωλήνας είναι πιο μαλακός, οι πτυχώσεις του σκληρότερου εσωτερικού σωλήνα παγιδεύονται στις πτυχώσεις του μαλακότερου εξωτερικού σωλήνα οι οποίες μάλιστα παύουν αν διατηρούν την προσκόλλησή τους με τις αντίστοιχες εσωτερικές κατά την κατάρρευση (Εικόνα 10). Αντιθέτως, στην περίπτωση των διπλοκέλυφων σωλήνων με εξωτερικά σκληρότερο σωλήνα και εσωτερικά πιο μαλακό, η προσκόλληση φαίνεται να διατηρείται σε μεγαλύτερο βαθμό κατά την κατάρρευση (Εικόνα 11). Τέλος, η μηχανική συμπεριφορά έναντι κρούσης, τα χαρακτηριστικά της και η καμπύλη δύναμης-μετατόπισης F-s επίσης επηρεάζονται από το σκληρότερο σωλήνα. Επομένως, ο σκληρότερος σωλήνας είναι αυτός που καθορίζει περισσότερο τόσο τον μηχανισμό κατάρρευσης, όσο και τα χαρακτηριστικά και την συμπεριφορά της κατασκευής έναντι κρούσης.

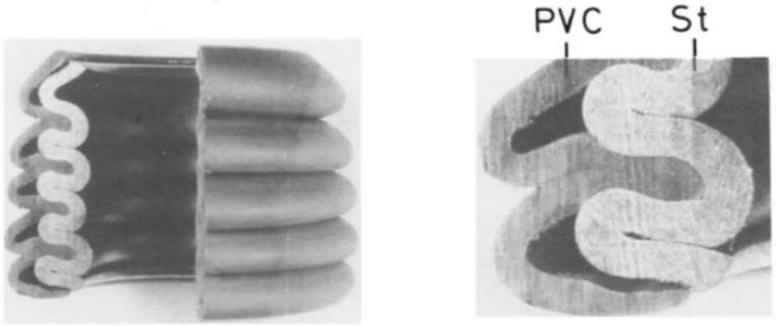

Εικόνα 10 Απώλεια προσκόλλησης σε διπλοκέλυφο σωλήνα (εξωτερικά PVC/εσωτερικά St)

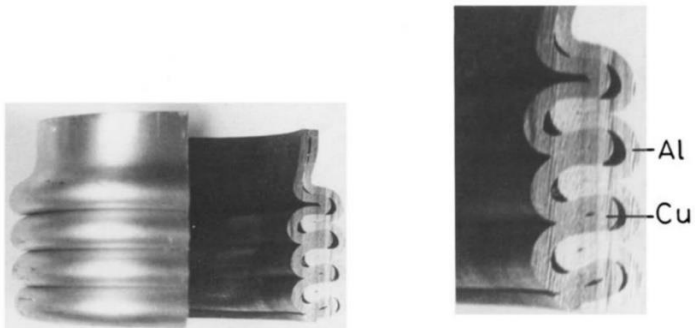

Εικόνα 11 Απώλεια προσκόλλησης σε διπλοκέλυφο σωλήνα (εξωτερικά Al/εσωτερικά Cu)

8.2.4 Αναλυτικός Υπολογισμός Μέσου Φορτίου Κατάρρευσης

Θεωρώντας έναν διπλοκέλυφο σωλήνα εξωτερικής διαμέτρου D, ο οποίος αποτελείται από έναν εσωτερικό και έναν εξωτερικό σωλήνα, με πάχη t_1,t_2 και όρια διαρροής Y_1 και Y_2, το μέσον παραμένων φορτίο κατάρρευσης προκύπτει εξισώνοντας το εξωτερικό έργο φόρτισης (W_e) με το εσωτερικό έργο παραμόρφωσης (W_i), $W_e = W_i = W_1+W_2$. Οι δείκτες 1 και 2 είναι τέτοιοι ώστε $Y_1 t_1 < Y_2 t_2$, και έστω ο λόγος παχών $t_r=t_1/t_2$ και λόγος ορίων διαρροής $k= Y_1/Y_2$. Στην εξίσωση δε των έργων, το εσωτερικό έργο παραμόρφωσης αποτελεί υπέρθεση του έργου που δαπανάται στην κάμψη του τοιχώματος (W_1) και του έργου που δαπανάται στον σχηματισμό των πτυχώσεων/αναδιπλώσεων (W_2).

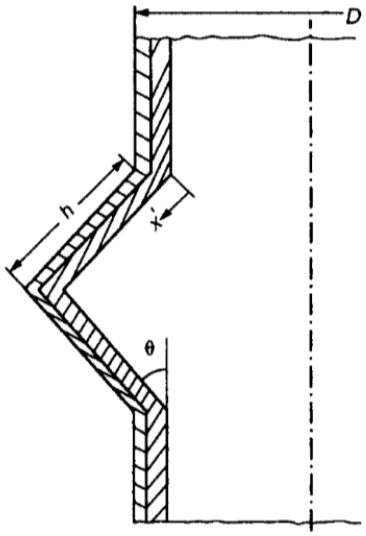

Εικόνα 12 Διπλοκέλυφος σωλήνας υπό κατάρρευση

Τα παραπάνω αναφερθείσα έργα υπολογίζονται ως εξής.

$$W_1 = 2M_p\{\pi D\frac{\pi}{2} + \int_0^{\frac{\pi}{2}} \pi(D \pm 2h \cdot sin\vartheta)\,\delta\vartheta\}$$
$$= 2M_p\pi(\pi D \pm 2h)$$

$$W_2 = \sum_{i=1}^{2} 2\int_0^h Y_i \pi D_i\, t_i\, \frac{2x \cdot sin\vartheta}{D_i} \cdot dx = 2\pi h^2(Y_1 t_1 + Y_2 t_2)$$

$$W_e = \bar{P} \cdot 2h = W_i = W_1 + W_2$$

Εξισώνοντας λοιπόν το εξωτερικό έργο φόρτισης με το εσωτερικό έργο παραμόρφωσης, για την περίπτωση μιας προοδευτικής και ελεγχόμενης

κατάρρευσης, προκύπτει η αναλυτική έκφραση του μέσου παραμένοντος φορτίου κατάρρευσης .

$$\bar{P} = \pi^{1.5} t^{1.5} D^{0.5} Y_2 \frac{\sqrt{(1 + 2kt_r + 2kt_r^2 - k^2 t_r^2)(1 + kt_r)}}{(1 + t_r)^{1.5}}$$

Παρατηρείται λοιπόν, πως τόσο το πάχος του διπλοκέλυφου σωλήνα, όσο και η εξωτερική του διάμετρος, αλλά και το όριο διαρροής, επιδρούν αναλογικά στον φορτίο κατάρρευσης, καθώς η αύξησή τους συνεπάγεται ταυτόχρονη αύξηση και του φορτίου κατάρρευσης.

8.3 Διμεταλλικά Υλικά

Τα σύνθετα υλικά έχει αποδειχθεί πως προσφέρουν τη δυνατότητα απορρόφησης μεγάλων ποσών ενέργειας με μάλιστα χαμηλό ειδικό βάρος. Τα σύνθετα υλικά κατατάσσονται σε:

- ✓ Σύνθετα με κόκκους
- ✓ Σύνθετα με ίνες
- ✓ Στρωματικά σύνθετα

Στην τελευταία κατηγορία, τα σύνθετα στρώσεων κατηγοριοποιούνται σε διμεταλλικά υλικά, πολυστρωματικά υλικά και υλικά sandwich. Στα πλαίσια της παρούσας διπλωματικής εργασίας, μελετώνται οι λεπτότοιχοι διπλοκέλυφοι σωλήνες. Οι ιδιότητες αυτών των σωλήνων είναι ανάλογες των κλασματικών όγκων των ιδιοτήτων των σωλήνων. Τα διμεταλλικά υλικά αποτελούν ουσιαστικά διπλοκέλυφους σωλήνες που απαρτίζονται από μεταλλικούς εσωτερικούς και εξωτερικούς σωλήνες. Τα πλεονεκτήματα των διμεταλλικών που καθιστούν την χρήση τους συχνά ευνοϊκή είναι:

- ✓ Χαμηλή θερμική διαστολή
- ✓ Αντοχή σε φορτίσεις με παράλληλη διατήρηση χαμηλών τάσεων στην κατασκευή
- ✓ Υψηλή θερμική αγωγιμότητα
- ✓ Αντοχή σε διάβρωση, οξείδωση και τριβή
- ✓ Αντοχή σε κόπωση
- ✓ Χαμηλό βάρος
- ✓ Υψηλή διάρκεια ζωής

Τα διμεταλλικά υλικά δύναται δε να κατασκευασθούν με τους εξής παρακάτω τρόπους:

- ✓ Συγκόλληση πίεσης με ψυχρή έλαση
- ✓ Συγκόλληση τριβής
- ✓ Εκρηκτική συγκόλληση
- ✓ Διέλαση

Τέλος, μερικές τυπικές εφαρμογές των διμεταλλικών υλικών συναντώνται στις εξής περιπτώσεις:

- ✓ Ναυπηγική
- ✓ Ηλεκτρική, χημική, πυρηνική και αυτοκινητιστική βιομηχανία
- ✓ Φίλτρα, σωλήνες, θερμοστάτες, εναλλάκτες θερμότητας
- ✓ Δοχεία υψηλής πίεσης και υδραυλικά συστήματα
- ✓ Αεροναυπηγική

8.4 Πειραματική Διερεύνηση της Κρουστικής Καταπόνησης Διπλοκέλυφων Σωλήνων

Για την διερεύνηση ης μηχανικής συμπεριφοράς των διπλοκέλυφων σωλήνων έναντι αξονικής κρουστικής καταπόνησης, αρχικά διεξήχθησαν πειραματικές δοκιμές συμπίεσης προσομοιώνοντας έτσι δοκιμές κρούσης υπό ημι-στατικές συνθήκες. Για το λόγο αυτό επομένως, τέσσερα δοκίμια διπλοκέλυφων σωλήνων παρασκευάστηκαν, συνδυάζοντας έναν χαλύβδινο και έναν πλαστικό (πολυαμίδιο/ertalon PA6) σωλήνα. Τα τέσσερα δοκίμια επιλέχθηκε να κατασκευαστούν σε δυο συνδυασμούς, ώστε να παραχθούν τελικά δυο διπλοκέλυφοι σωλήνες με χαλύβδινο εσωτερικά σωλήνα και πλαστικό εξωτερικά σωλήνα (δοκίμια Α και Β) και δυο διπλοκέλυφοι σωλήνες με χαλύβδινο εξωτερικά σωλήνα και πλαστικό εσωτερικά σωλήνα (δοκίμια Γ και Δ). Μάλιστα, διαφορετικά πάχη και εξωτερική διάμετρος επιλέχθηκε για κάθε συνδυασμό εσωτερικού/εξωτερικού σωλήνα ώστε να διαπιστωθεί η επίδραση των παραγόντων αυτών στον εμφανιζόμενο μηχανισμό κατάρρευσης αλλά και στα χαρακτηριστικά της μηχανικής συμπεριφοράς της κατασκευής έναντι κρούσης. Τα τέσσερα δοκίμια διπλοκέλυφων σωλήνων που παράχθηκαν προς δοκιμή απεικονίζονται στην παρακάτω εικόνα, ενώ όλα εξ αυτών είναι μήκους 100 mm. Για την κατασκευή των τεσσάρων δοκιμίων, οι σωλήνες που τα απαρτίζουν κατασκευάστηκαν αρχικά με τόρνευση και έπειτα δημιουργήθηκε η απαραίτητη σύνδεσή τους με την επίτευξη συναρμογής σύσφιξης μέσω υποβολής της απαραίτητης πίεσης.

Κατόπιν της κατασκευής των δοκιμίων προς εξέταση, κάθε ένα από αυτά συμπιέστηκε αξονικά κατά 60 mm σε πρέσσα με ταχύτητα φόρτισης 10 mm/min έως το τελικό μήκος των 40 mm. Παρακάτω παρουσιάζονται τα αποτελέσματα αναφορικά τόσο με τα χαρακτηριστικά της μηχανικής συμπεριφοράς των δοκιμίων έναντι κρούσης, όσο και με τον εμφανιζόμενο μηχανισμό κατάρρευσης.

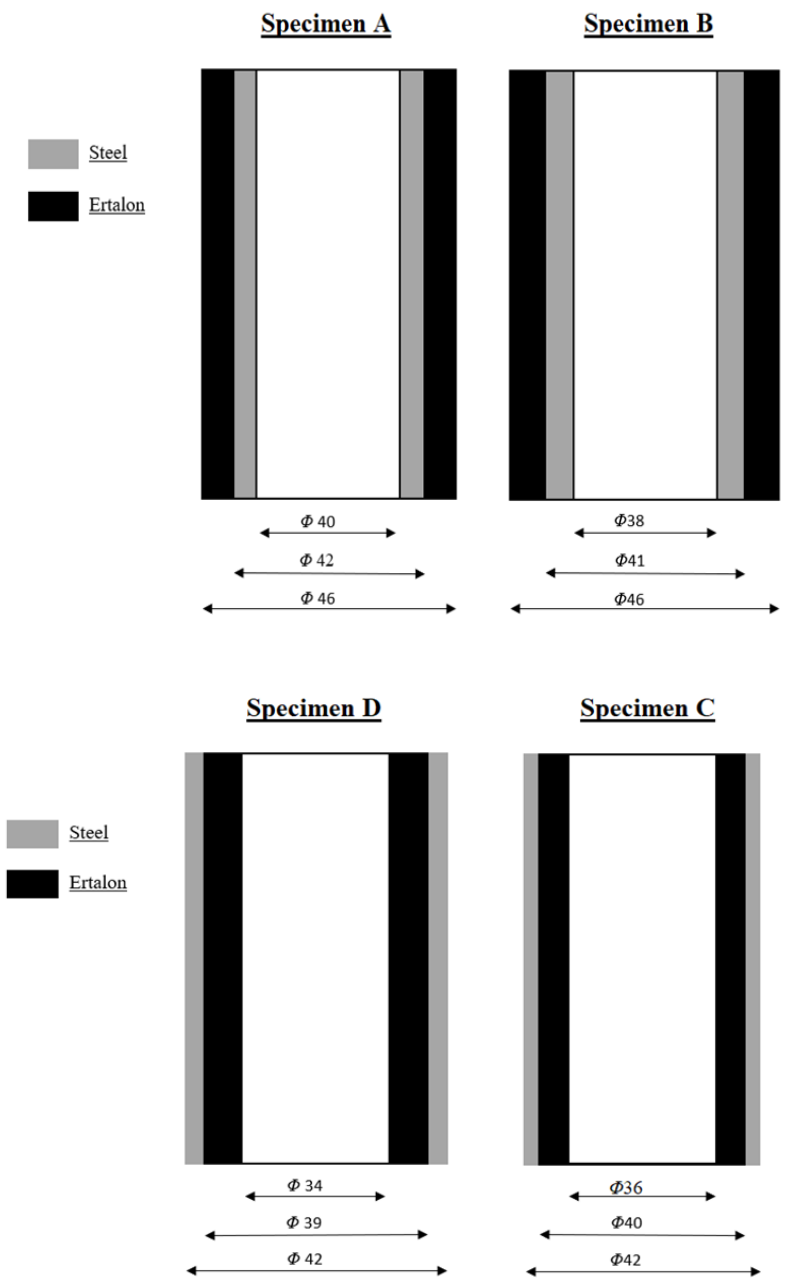

Εικόνα 13 Δοκίμια διπλοκέλυφων σωλήνων προς διερεύνηση της συμπεριφοράς τους έναντι κρουστικής καταπόνησης

8.4.1 Πειραματικά Αποτελέσματα

Η συμπίεση των δοκιμίων απέδωσε τα παρακάτω αποτελέσματα αναφορικά με το διάγραμμα φορτίου συμπίεσης – βράχυνσης, των οποίων η επεξεργασία των μετρήσεων επέτρεψε τον υπολογισμό κρίσιμων χαρακτηριστικών της μηχανικής συμπεριφοράς των δοκιμίων κατά την κρούσης τους, όπως το μέγιστο

φορτίο κατάρρευσης, το μέσο παραμένων φορτίο κατάρρευσης, της απορροφώμενης ενέργειας της κρούσης και της ειδικής ενέργειας απορρόφησης.

Πιο συγκεκριμένα, οι πειραματικές δοκιμές συμπίεσης των τεσσάρων δοκιμίων διπλοκέλυφων σωλήνων απέδωσε τα παρακάτω διαγράμματα δύναμης-βράχυνσης, ενώ η επεξεργασία των μετρήσεων επέφερε τα αποτελέσματα που απεικονίζονται στον Πίνακα 1.

Εικόνα 14 Πειραματικά διαγράμματα δύναμης-μετατόπισης δοκιμίων Α και Β

Εικόνα 15 Πειραματικά διαγράμματα δύναμης-μετατόπισης δοκιμίων Γ και Δ

Αποτελέσματα Πειραματικών Δοκιμών				
	Δοκίμιο Α	**Δοκίμιο Β**	**Δοκίμιο Γ**	**Δοκίμιο Δ**
Μέγιστο Φορτίο (kN)	64.46	75.28	58.83	88.51
Μέσο Παραμένων Φορτίο (kN)	34.69	41.78	30.98	51.09
Ενέργεια Απορρόφησης (J)	2081.11	2507.06	1858.73	3065.62
Ειδική Ενέργεια Απορρόφησης (J/kg)	15689.01	13548.99	14486.99	16806.77

Πίνακας 1 Πειραματικά αποτελέσματα χαρακτηριστικών συμπίεσης εξεταζόμενων δοκιμίων

Όπως παρατηρείται, τα δοκίμια διπλοκέλυφων σωλήνων με το μεγαλύτερο πάχος (δοκίμια Β και Δ) παρουσιάζουν μεγαλύτερη ικανότητα απορρόφησης ποσών κρουστικής ενέργειας εφόσον συνοδεύονται από μεγαλύτερα φορτία κατάρρευσης, γεγονός που διαπιστώνεται παρατηρώντας τόσο τις αντίστοιχες καμπύλες δύναμης-μετατόπισης, όσο και τα σχετικά αποτελέσματα του παραπάνω πίνακα.

Επιπλέον, και τα τέσσερα δοκίμια παραμορφώθηκαν κατά τη συμπίεση υπό μικτό μηχανισμό κατάρρευσης, εφόσον αρχικά δημιουργήθηκε μια πτύχωση/αναδίπλωση αξονοσυμμετρικού τύπου ενώ η κατάρρευσή τους συνεχίστηκε με τον σχηματισμό μη αξονοσυμμετρικών λοβών. Στη περίπτωση δε που ο μαλακότερος σωλήνας ήταν ο εξωτερικός (δοκίμια Α και Β) ο μη αξονοσυμμετρικός τρόπος κατάρρευσης εμφανίσθηκε με σχηματισμό τριών περιφερειακά λοβών (3D diamond), ενώ στην αντίθετη περίπτωση (δοκίμια Γ και Δ) ο μη αξονοσυμμετρικός τρόπος κατάρρευσης εκδηλώθηκε με σχηματισμό δυο περιφερειακά λοβών (2D diamond).

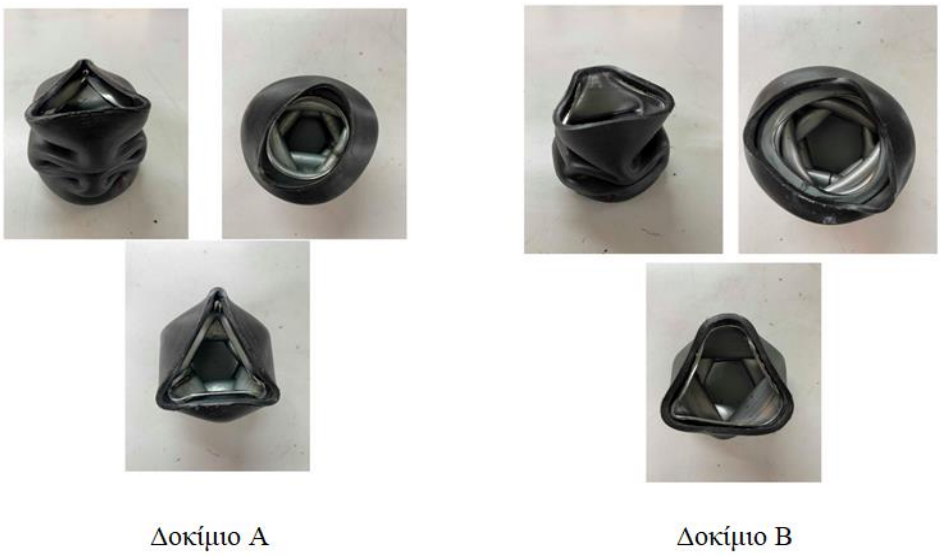

Εικόνα 16 Παραμορφωμένη μορφή δοκιμίων Α και Β έπειτα από το πέρας της κατάρρευσης

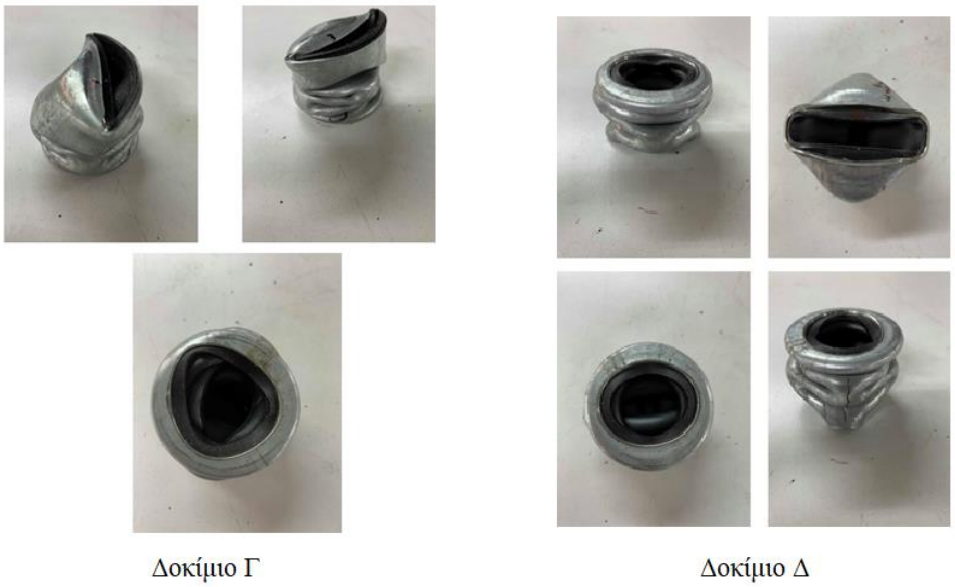

Εικόνα 17 Παραμορφωμένη μορφή δοκιμίων Γ και Δ έπειτα από το πέρας της κατάρρευσης

Τέλος δε, η προσκόλληση μεταξύ των σωλήνων διαπιστώθηκε πως δεν διατηρήθηκε στην περίπτωση που ο μαλακότερος σωλήνας ήταν ο εξωτερικός (δοκίμια Α και Β), ενώ στην αντίθετη περίπτωση (δοκίμια Γ και Δ) η προσκόλληση διατηρήθηκε σχεδόν αποκλειστικά κατά το πέρας της κατάρρευσης.

Δοκίμιο Α Δοκίμιο Β

Εικόνα 18 Άποψη των πλήρως παραμορφωμένων δοκιμίων Α και Β σε τομή

Δοκίμιο Γ Δοκίμιο Δ

Εικόνα 19 Άποψη των πλήρως παραμορφωμένων δοκιμίων Γ και Δ σε τομή

8.5 Μοντελοποίηση Κρουστικής Συμπεριφοράς Διπλοκέλυφων Σωλήνων μέσω Πεπερασμένων Στοιχείων και Αποτελέσματα Προσομοίωσης

Για την μελέτη και ανάλυση της μηχανικής συμπεριφοράς και του μηχανισμού κατάρρευσης έναντι κρούσης αναφορικά με τους διπλοκέλυφους σωλήνες, διεξήχθησαν προσθέτως αριθμητικές προσομοιώσεις. Για την διεξαγωγή των προσομοιώσεων, μοντέλα πεπερασμένων στοιχείων αναπτύχθηκαν αρχικά για τους εξεταζόμενους διπλοκέλυφους σωλήνες στο λογισμικό πεπερασμένων στοιχείων LS-DYNA.

Συγκεκριμένα, για την ανάπτυξη κάθε μοντέλου διπλοκέλυφου σωλήνα, αρχικά ορίσθηκαν η γεωμετρία και οι διαστάσεις κάθε σωλήνα, καθώς και των δυο πλακών στήριξης, εκ των οποίων η μία ήταν ακίνητη, ενώ η άλλη κινούμενη κατά το διαμήκη άξονα του διπλοκέλυφου σωλήνα και κατά διεύθυνση μάλιστα ώστε να προκαλεί τη συμπίεση του τελευταίου (Εικόνα 20). Κατόπιν, ορίσθηκε η πυκνότητα του πλέγματος θέτοντας τις διαστάσεις των πεπερασμένων στοιχείων για κάθε σωλήνα και πλάκα. Συγκεκριμένα δε για τους σωλήνες, ιδιαίτερη προσοχή αποδόθηκε στην επιλογή μεγέθους των πεπερασμένων στοιχείων ώστε το μέγεθός τους να είναι τουλάχιστον ίσο με το πάχος του

σωλήνα. Πρόσθετα, οι δύο σωλήνες κάθε δοκιμίου μοντελοποιήθηκαν μέσω δισδιάστατων επίπεδων πεπερασμένων (shell elements) στοιχείων λαμβάνοντας μάλιστα υπόψιν το πάχος καθενός σωλήνα, ενώ οι πλάκες μοντελοποιήθηκαν με τρισδιάστατα πεπερασμένα στοιχεία (solid elements).

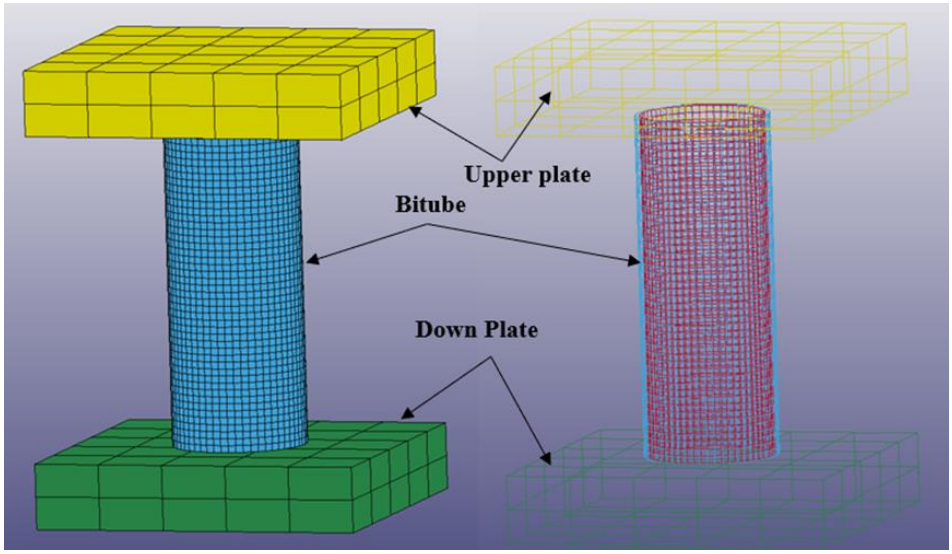

Εικόνα 20 Σχηματική άποψη του μοντέλου προσομοίωσης των εξεταζόμενων διπλοκέλυφων σωλήνων

Έπειτα, το υλικό των σωλήνων (mat_024_piecewise linear plasticity) προσδιορίστηκε δίνοντας κάποιες χαρακτηριστικές ιδιότητές του, όπως πυκνότητα, μέτρο ελαστικότητας, λόγο Poisson και όριο διαρροής, όπως επίσης και τη καμπύλη κράτυνσης του υλικού. Έτσι λοιπόν, σε κάθε ένα από τα δυο υλικά (χάλυβας ή πλαστικό), η πλαστική περιοχή περιγράφεται από οκτώ σημεία τάσης-παραμένουσας πλαστικής παραμόρφωσης. Συγκεκριμένα, για τον προσδιορισμό δε των ιδιοτήτων καθενός υλικού, λήφθηκαν πληροφορίες από την βιβλιογραφία (πυκνότητα και λόγος Poisson), ενώ πρόσθετα πραγματοποιήθηκαν πειράματα εφελκυσμού για τον προσδιορισμό των υπόλοιπων ιδιοτήτων από τα διαγράμματα σ-ε που προέκυψαν (Εικόνα 21 και Εικόνα 22). Αναφορικά δε με τις πλάκες, αυτές θεωρήθηκαν ως χαλύβδινες απαραμόρφωτες άκαμπτες πλάκες (mat_020_rigid) με ιδιότητες (πυκνότητα, μέτρο ελαστικότητας και όριο διαρροής) σύμφωνα με την ανοιχτή βιβλιογραφία. Κάθε ένα από τα δυο πειράματα εφελκυσμού για τον χάλυβα και το ertalon, η ταχύτητα επιβολής του εφελκυστικού φορτίου ήταν 10 mm/min.

Κατόπιν, το επόμενο στάδιο της μοντελοποίησης ήταν ο καθορισμός των οριακών συνθηκών μη εισχώρησης στις διεπιφάνειες τόσο μεταξύ των σωλήνων και των πλακών όσο και μεταξύ των δύο σωλήνων μεταξύ τους, αλλά και μεταξύ των πτυχώσεων/αναδιπλώσεων κάθε σωλήνα με τους γειτονικούς του. Σε κάθε περίπτωση, ο συντελεστής στατικής τριβής λήφθηκε ίσος με 0,2 ενώ αυτός της δυναμικής τριβής ίσος με 0,15.

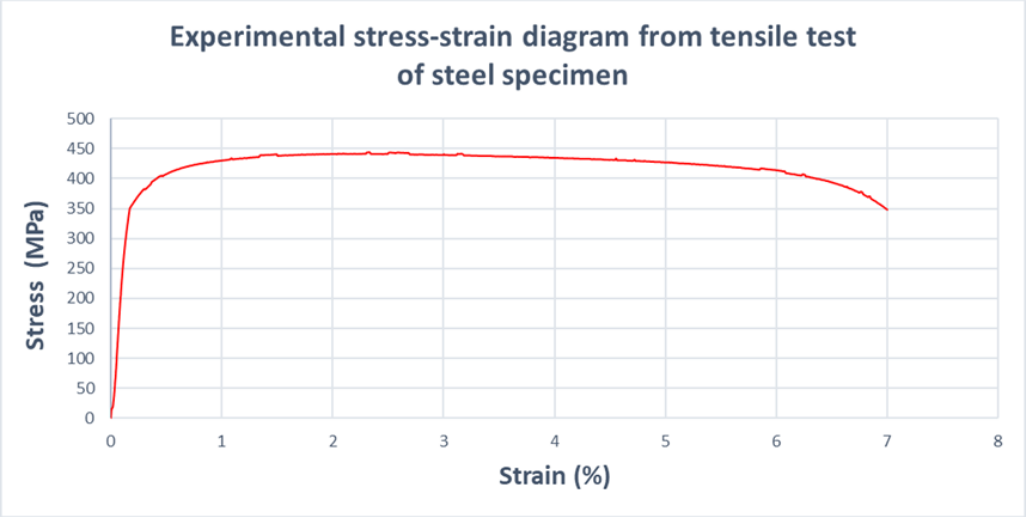

Εικόνα 21 Πειραματικό διάγραμμα σ-ε εφελκυσμού του χάλυβα

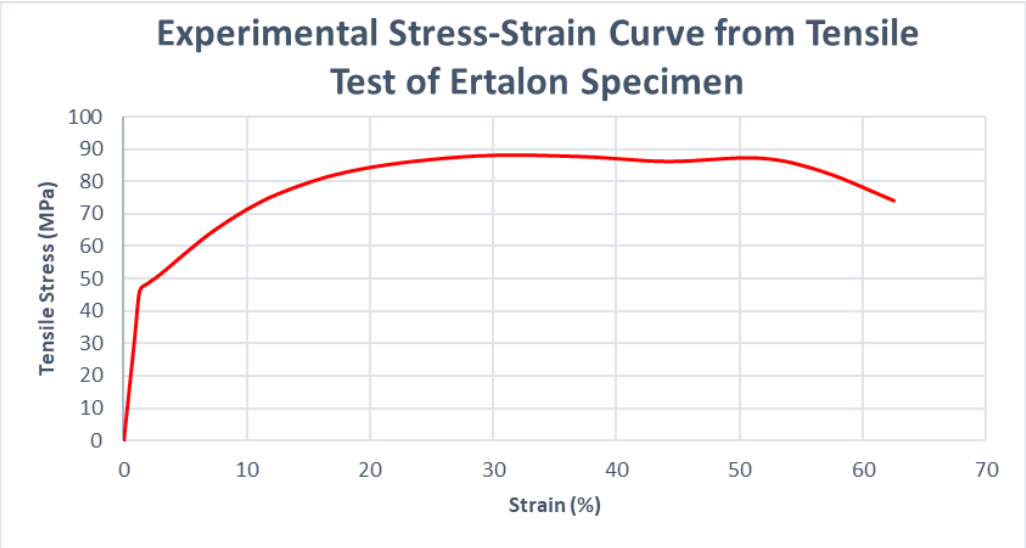

Εικόνα 22 Πειραματικό διάγραμμα σ-ε εφελκυσμού του πλαστικού ertalon

Τέλος, επιβλήθηκε ταχύτητα κίνησης της άνω πλάκας σταθερή και ίση με 0.5 mm/msec ώστε κινούμενη αυτή να συμπιέζει το μοντέλο του διπλοκέλυφου σωλήνα προσομοιώνοντας έτσι την κρουστική καταπόνηση.

8.5.1 Αποτελέσματα Αριθμητικής Προσομοίωσης

Η διεξαγωγή των αριθμητικών προσομοιώσεων στο λογισμικό πεπερασμένων στοιχείων LS-DYNA απέδωσε τα ακόλουθα αποτελέσματα. Η επεξεργασία τους δε επέτρεψε τον υπολογισμό κρίσιμων χαρακτηριστικών της συμπεριφοράς των δοκιμίων έναντι κρούσης, όπως του μέγιστου φορτίου κατάρρευσης, του μέσου παραμένοντος φορτίου κατάρρευσης, της απορροφώμενης κρουστικής ενέργειας προς παραμόρφωση και της ειδικής

ενέργειας απορρόφησης. Πρόσθετα, παρατηρήθηκε ο μηχανισμός κατάρρευσης για κάθε δοκίμιο διπλοκέλυφου σωλήνα, ενώ χρήσιμα συμπεράσματα εξήχθησαν και για την διατήρηση της επαφής μεταξύ εσωτερικού και εξωτερικού σωλήνα κατά την κατάρρευση.

Πιο συγκεκριμένα, οι αριθμητικές προσομοιώσεις αξονικής κρουστικής καταπόνησης των τεσσάρων δοκιμίων διπλοκέλυφων σωλήνων απέδωσε τα παρακάτω διαγράμματα δύναμης-βράχυνσης, ενώ η επεξεργασία των αποτελεσμάτων επέφερε τα χαρακτηριστικά απόκρισης που απεικονίζονται στον Πίνακα 2.

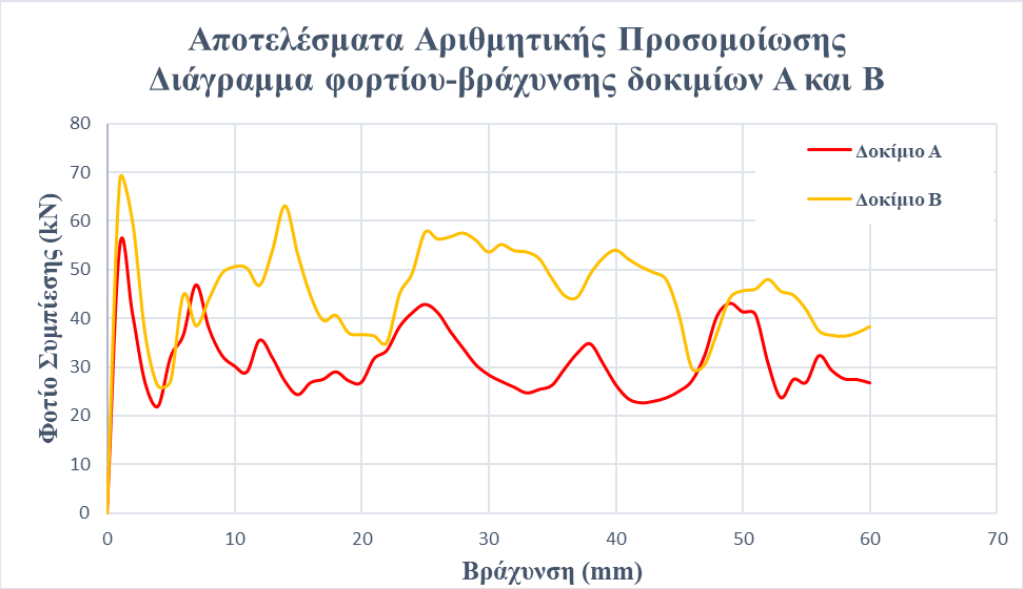

Εικόνα 23 Διάγραμμα δύναμης-μετατόπισης δοκιμίων Α και Β από αριθμητικές προσομοιώσεις στο LS-DYNA

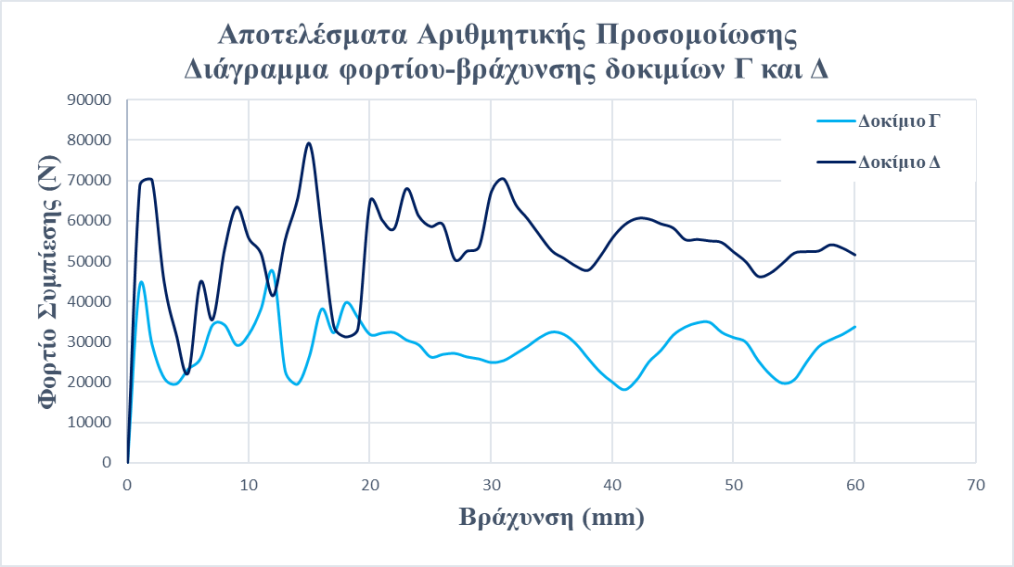

Εικόνα 24 Διάγραμμα δύναμης-μετατόπισης δοκιμίων Γ και Δ από αριθμητικές προσομοιώσεις στο LS-DYNA

Αποτελέσματα Αριθμητικών Προσομοιώσεων				
	Δοκίμιο Α	**Δοκίμιο Β**	**Δοκίμιο Γ**	**Δοκίμιο Δ**
Μέγιστο Φορτίο (kN)	56.8	68.2	47.22	79.14
Μέσο Παραμένων Φορτίο (kN)	32.20	45.66	28.61	53.38
Ενέργεια Απορρόφησης (J)	1872.23	2739.78	1716.32	3202.73
Ειδική Ενέργεια Απορρόφησης (J/kg)	14114.30	13376.1	13376.20	17558.40

Πίνακας 2 Αποτελέσματα προσομοιώσεων των χαρακτηριστικών συμπίεσης εξεταζόμενων δοκιμίων

Όπως παρατηρήθηκε και στην αξιολόγηση των πειραματικών αποτελεσμάτων, οι διπλοκέλυφοι σωλήνες με εξωτερικά σκληρότερο σωλήνα (δοκίμια Γ και Δ), όπως αυτός από χάλυβα στην περίπτωσή μας, παρουσιάζουν μεγαλύτερη αντοχή έναντι κρούσης απορροφώντας μεγαλύτερα ποσά κρουστικής ενέργειας για την παραμόρφωσή τους κατά την κατάρρευση. Ακόμη, οι διπλοκέλυφοι σωλήνες μεγαλύτερου πάχους παρουσιάζουν επίσης μεγαλύτερη αντοχή έναντι κρούσης, όπως άλλωστε διαφαίνεται από την αναλυτική έκφραση υπολογισμού του μέσου φορτίου κατάρρευσης.

Αναφορικά δε με τον προβλεπόμενο μηχανισμό κατάρρευσης, όλα τα δοκίμια προβλέφθηκαν πως καταρρέουν υπό μικτό τρόπο, καθώς αρχικά σχηματίζουν μια αξονοσυμμετρική πτύχωση/αναδίπλωση, ενώ συνεχίζουν την κατάρρευσή τους σχηματίζοντας μη αξονοσυμμετρικές πτυχώσεις. Οι τελευταίες σχηματίζουν 3 λοβούς (3D diamond) περιφερειακά, εκτός από το δοκίμιο Β που προβλέφθηκαν 2 λοβοί (2D diamond).

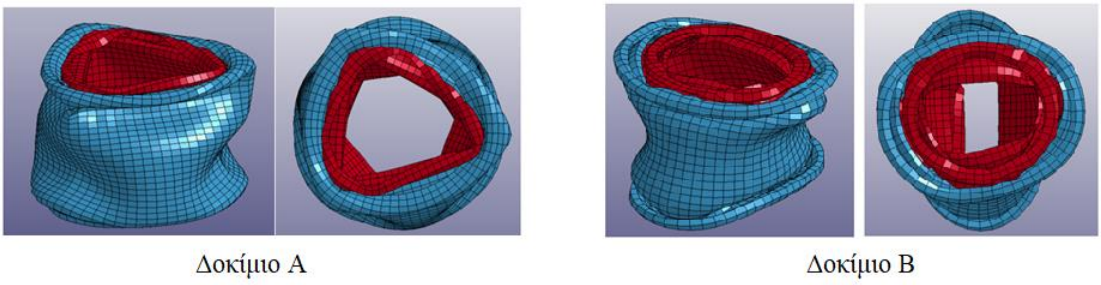

Εικόνα 25 Παραμορφωμένη μορφή δοκιμίων Α και Β έπειτα από το πέρας της κατάρρευσης (προσομοίωση)

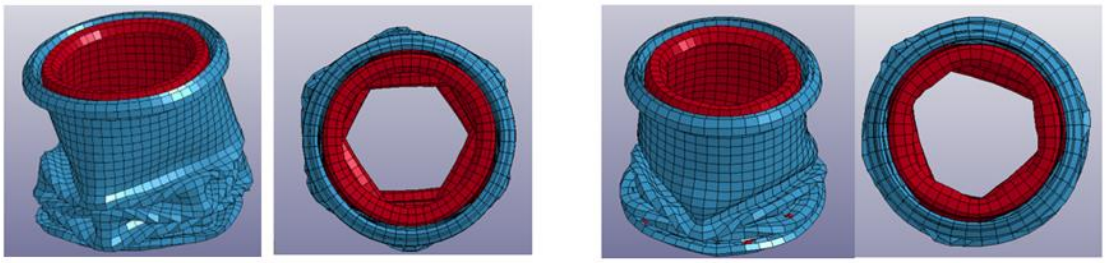

Δοκίμιο Γ Δοκίμιο Δ

Εικόνα 26 Παραμορφωμένη μορφή δοκιμίων Γ και Δ έπειτα από το πέρας της κατάρρευσης (προσομοίωση)

Τέλος, αναφορικά με την διατήρηση της επαφής μεταξύ των σωλήνων κατά την κατάρρευση, συμπεραίνεται πως δεν παραμένει στην περίπτωση που ο μαλακότερος σωλήνας είναι εξωτερικά (δοκίμια Α και Β) ή διατηρείται μερικώς κατά τμήματα, ενώ στην αντίθετη περίπτωση (δοκίμια Γ και Δ) η προσκόλληση διατηρήθηκε σχεδόν αποκλειστικά έως το πέρας της κατάρρευσης.

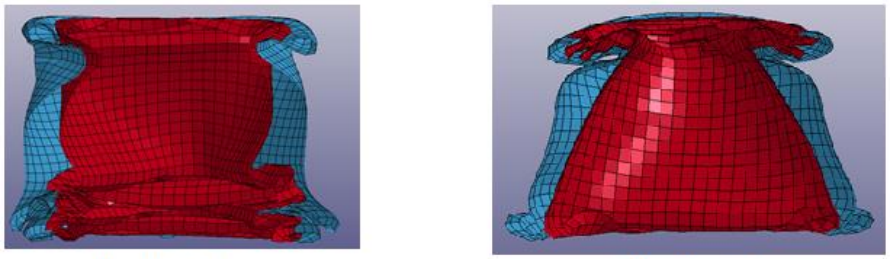

Δοκίμιο Α Δοκίμιο Β

Εικόνα 27 Άποψη των πλήρως παραμορφωμένων δοκιμίων Α και Β σε τομή

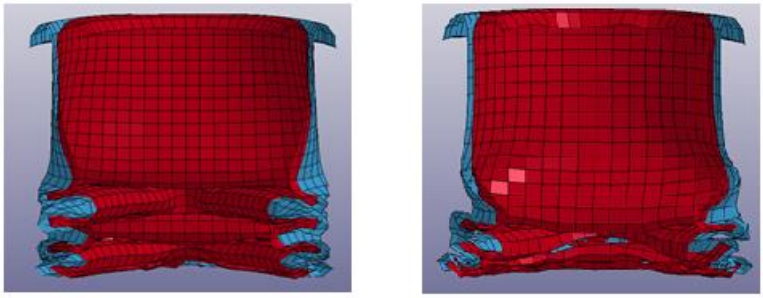

Δοκίμιο Γ Δοκίμιο Δ

Εικόνα 28 Άποψη των πλήρως παραμορφωμένων δοκιμίων Γ και Δ σε τομή

8.6 Σύγκριση και Σχολιασμός

Όπως διαπιστώθηκε από τις συγκρίσεις των διαγραμμάτων δύναμης-μετατόπισης, αναφορικά με τη μηχανική συμπεριφορά των δοκιμίων έναντι κρούσης και των χαρακτηριστικών της, οι διπλοκέλυφοι σωλήνες μεγαλύτερου

πάχους (δοκίμια Β και Δ) προβλέφθηκαν οριακά ακριβέστερα, ενώ όλα τα δοκίμια εμφάνισαν σφάλματα κάτω του 10%.

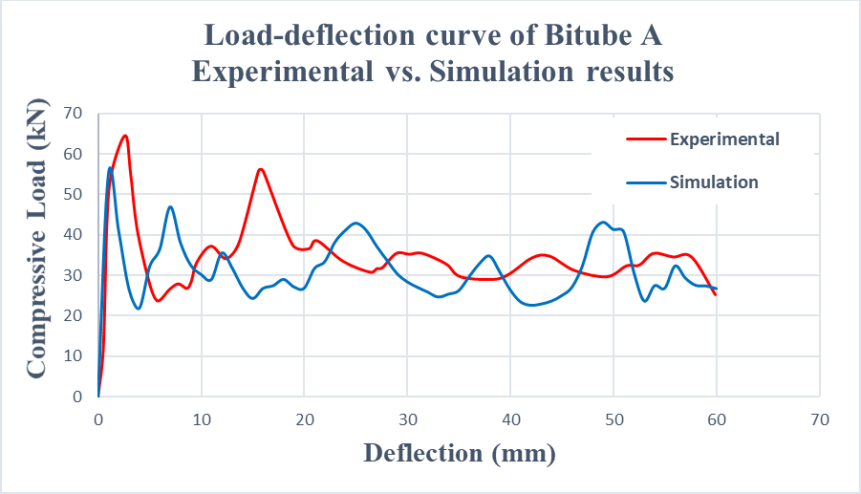

Εικόνα 29 Σύγκριση διαγραμμάτων δύναμης-μετατόπισης δοκιμίου Α

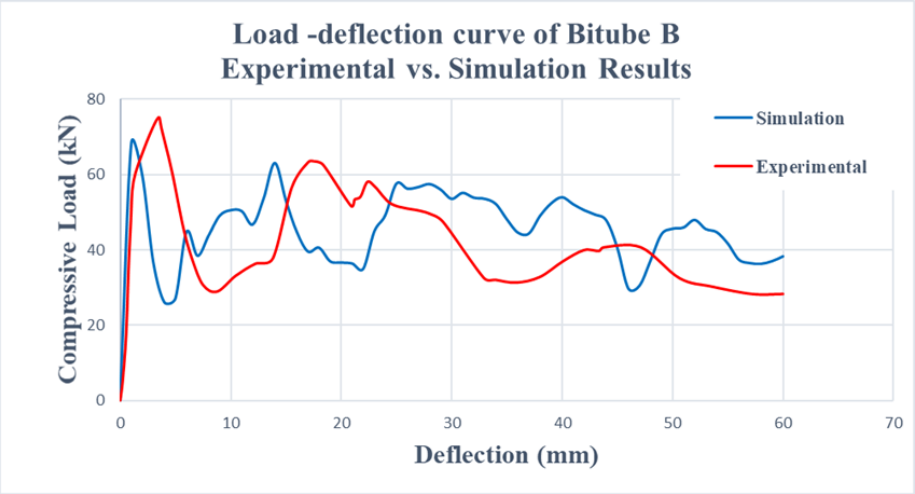

Εικόνα 30 Σύγκριση διαγραμμάτων δύναμης-μετατόπισης δοκιμίου Β

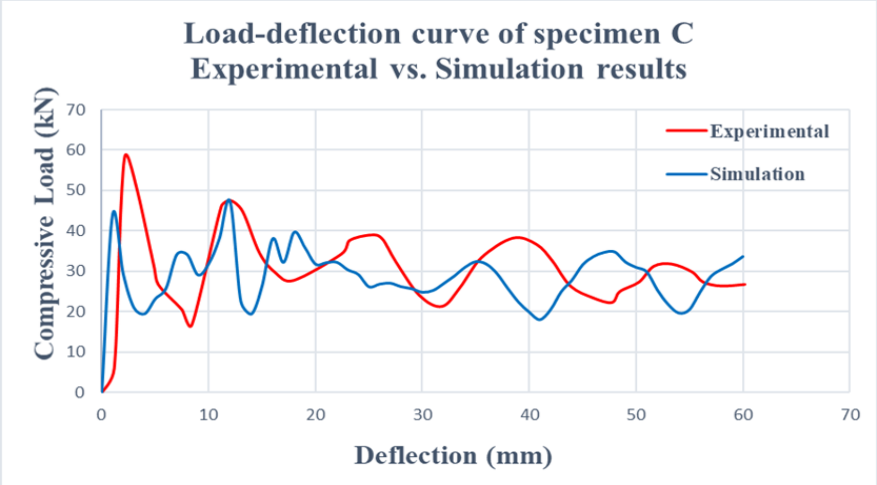

Εικόνα 31 Σύγκριση διαγραμμάτων δύναμης-μετατόπισης δοκιμίου Γ

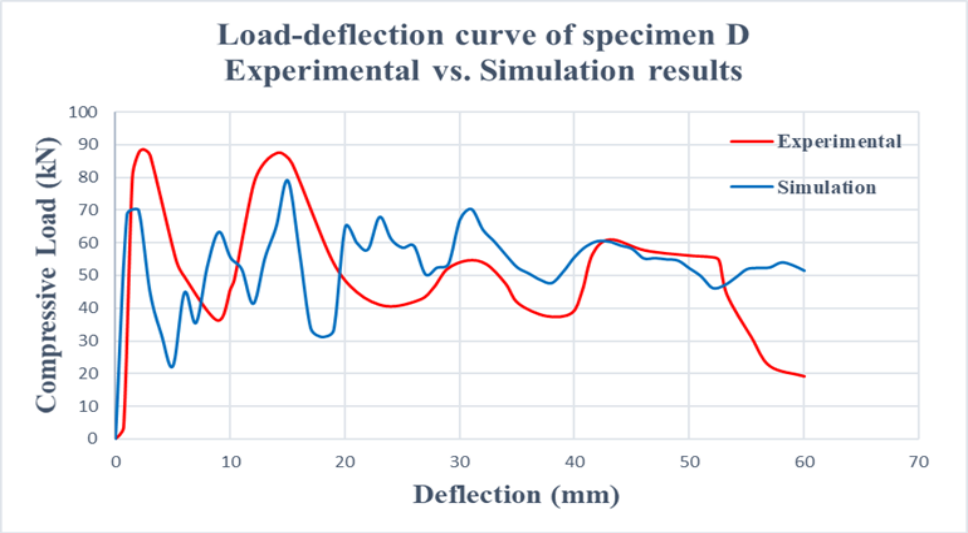

Εικόνα 32 Σύγκριση διαγραμμάτων δύναμης-μετατόπισης δοκιμίου Δ

Πρόσθετα, τα μοντέλα των διπλοκέλυφων σωλήνων Γ και Δ, δηλαδή αυτών με εξωτερικά σκληρότερο σωλήνα, παρουσίασαν μεγαλύτερη ακρίβεια στον υπολογισμό της απορροφώμενης ενέργειας και του μέσου φορτίου κατάρρευσης σημειώνοντας σφάλματα μόλις 7,7% και 4,5% αντίστοιχα, όπως παρατηρείται και από πίνακα 3. Τέλος δε, παρατηρήθηκε πως η πρόβλεψη του μέγιστου φορτίου κατάρρευσης ήταν ακριβέστερη στην περίπτωση των δοκιμίων Α και Β όπου εμφανίστηκαν σφάλματα κοντά στο 10%.

Συγκρίσεις Πειραμάτων και Προσομοιώσεων				
	Δοκίμιο Α	**Δοκίμιο Β**	**Δοκίμιο Γ**	**Δοκίμιο Δ**
		Σχετικό Σφάλμα (%)		
Μέγιστο Φορτίο	11.88	9.4	19.7	10.6
Μέσο Φορτίο	7.18	9.29	7.7	4.48
Ενέργεια Απορρόφησης	10.04	9.28	7.7	4.47
Ειδική Ενέργεια Απορρόφησης	10.04	9.28	7.7	4.47

Πίνακας 3 Σχετικά σφάλματα συγκρίσεων μεταξύ πειραματικών και αριθμητικών αποτελεσμάτων

Αναφορικά με τον προβλεπόμενο από την προσομοίωση και τον παρατηρούμενο κατά τη πειραματική δοκιμή μηχανισμό κατάρρευσης, όλα τα μοντέλα προέβλεψαν σωστά τον μικτό τρόπο κατάρρευσης και για τα τέσσερα δοκίμια, καθώς όλα αρχικά σχημάτισαν έναν αξονοσυμμετρικό λοβό, ενώ συνέχισαν να καταρρέουν υπό μη αξονοσυμμετρικό τρόπο. Ωστόσο, μόνο το μοντέλο του δοκιμίου Α προέβλεψε σωστά τον σχηματισμό των 3 λοβών (3D diamond) περιφερειακά στην έκταση όπου μη αξονοσυμμετρικές πτυχώσεις σχηματίστηκαν.

Τέλος δε, τα μοντέλα των δοκιμίων Γ και Δ προέβλεψαν σωστά πως η προσκόλληση των σωλήνων διατηρείται σχεδόν πλήρως ακόμη και μετά το πέρας της κατάρρευσης, ενώ για τα δοκίμια Α και Β προβλέφθηκε ορθά πως η επαφή των σωλήνων διατηρείται μερικώς μόνο όμως στις περιοχές σχηματισμού πτυχώσεων/αναδιπλώσεων.

8.7 Συμπεράσματα και Προτάσεις προς Μελλοντική Διερεύνηση

Σκοπός της παρούσας διπλωματικής εργασίας αποτελεί η μελέτη και διερεύνηση της μηχανικής συμπεριφοράς και της αντοχής των διπλοκέλυφων σωλήνων έναντι αξονικής κρουστικής καταπόνησης. Η ανάλυση διεξήχθη τόσο μέσω πειραματικών δοκιμών κρούσης όσο και με αριθμητικές προσομοιώσεις στο λογισμικό LS-DYNA. Τέσσερα δοκίμια διπλοκέλυφων σωλήνων εξετάστηκαν, εκ των οποίων δυο αποτελούνταν από χαλύβδινο εξωτερικά σωλήνα και πλαστικό (ertalon) εσωτερικά, και δύο από χαλύβδινο εσωτερικά σωλήνα και πλαστικό (ertalon) εξωτερικά, συνδυάζοντας επίσης διαφορετικά πάχη και εξωτερικές διαμέτρους ώστε να εξεταστεί και η επίδρασή τους στην αντοχή των εξεταζόμενων δοκιμίων έναντι κρούσης. Οι πειραματικές δοκιμές κρούσης διεξήχθησαν υπό ημι-στατικές συνθήκες επιβάλλοντας ταχύτητας

συμπίεσης των δοκιμίων σε πρέσσα ίση με 10 mm/min. Σε αντίθεση, οι αριθμητικές προσομοιώσεις εξέτασαν τα μοντέλα των τεσσάρων δοκιμίων σε αξονική κρούση υπό ταχύτητα φόρτισης 0,5 mm/msec.

Τα αποτελέσματα των προσομοιώσεων επέδειξαν ικανοποιητική ακρίβεια ως προς την πρόβλεψη της ικανότητας απορρόφησης ενέργειας των δοκιμίων, ενώ στην περίπτωση που ο διπλοκέλυφος σωλήνας αποτελούταν από σκληρότερο εξωτερικά σωλήνα (δοκίμια Γ και Δ) το μέγιστο φορτίο κατάρρευσης εμφάνισε μεγαλύτερες αποκλίσεις. Επίσης η ακρίβεια των μοντέλων αποδείχθηκε καλύτερη για τους σωλήνες μεγαλύτερου πάχους. Πρόσθετα, όλες οι προσομοιώσεις πρόβλεψαν ορθά τον εμφανιζόμενο μηχανισμό κατάρρευσης.

Εν κατακλείδι, συμπεραίνεται πως οι διπλοκέλυφοι σωλήνες με σκληρότερο εξωτερικά σωλήνα παρουσιάζουν αυξημένη ικανότητα απορρόφησης κρουστικής ενέργειας προς παραμόρφωσή τους, ενώ δε ευεργετικά επιδρούν ακόμη τα αυξημένα πάχη και οι αυξημένες εξωτερικές διάμετροι των σωλήνων. Επιπλέον, όλα τα εξεταζόμενα δοκίμια παρατηρήθηκε πως κατέρρευσαν υπό μικτό μηχανισμό εφόσον αρχικά σχημάτισαν έναν αξονοσυμμετρικό λοβό, ενώ συνέχισαν σχηματίζοντας μη αξονοσυμμετρικούς λοβούς. Τέλος, η προσκόλληση μεταξύ των σωλήνων διατηρήθηκε σχεδόν πλήρως στο πέρας της κατάρρευσης για τα δοκίμια Γ και Δ όπου οι λοβοί του μαλακότερου εσωτερικού σωλήνα παγιδευτήκαν εντός των λοβών του εξωτερικά σκληρότερου σωλήνα παραμένοντας έτσι σε επαφή μεταξύ τους. Σε αντίθεση, η προσκόλληση μεταξύ των σωλήνων για τα δοκίμια Α και Β σχεδόν χάθηκε καθώς οι λοβοί του μαλακότερου εξωτερικού σωλήνα παραμορφώθηκαν εκτενέστερα περιβάλλοντας μερικές φορές τους λοβούς του εσωτερικά σκληρότερου σωλήνα, διατηρώντας έτσι την επαφή μεταξύ τους τμηματικά αι μόνο στην περιοχή σχηματισμού πτυχώσεων, εφόσον εκτός αυτής η επαφή μεταξύ εσωτερικού/εξωτερικού σωλήνα χάθηκε αποκλειστικά. Προς περαιτέρω μελλοντική διερεύνηση συνίσταται:

- Η μοντελοποίηση των διπλοκέλυφων σωλήνων με τρισδιάστατα πεπερασμένα στοιχεία (solid elements) ώστε να εξεταστεί η πιθανή επίδρασή τους στα προβλεπόμενα αποτελέσματα
- Εξέταση διαφορετικών σεναρίων βαθμών ελευθερίας των πεπερασμένων στοιχείων κατά τη παραμόρφωσή τους, επιτρέποντας εναλλακτικές δυνατότητες μορφοποίησής τους
- Εξέταση της επίδρασης της ταχύτητας παραμόρφωσης στην διεξαγωγή των αριθμητικών προσομοιώσεων, καθώς οι ιδιότητες των υλικών των σωλήνων θεωρήθηκαν διεξάγοντας πειραματικές δοκιμές εφελκυσμού στις οποίες ωστόσο ο ρυθμός παραμόρφωσης ήταν αδύνατον να εξισωθεί με τους αντίστοιχους που συναντώνται σε ρεαλιστικές συνθήκες κρούσης
- Μελέτη πλευρικής κρουστικής φόρτισης για διπλοκέλυφους σωλήνες, οι οποίοι μάλιστα ενδέχεται να περιέχουν σύνθετους σωλήνες ή σωλήνες πιο πολύπλοκης γεωμετρίας ή διατομής.

9. Bibliography

[1] **W.J. Hughes** (2016). "Crushing Behavior of Laminated Composite Structural Elements: Experiment and LS-DYNA Simulations." Federal Aviation Administration, U.S. Department of Transportation, DOT / FAA / TC-15/25

[2] **US Dept. of Transportation FAA** (2009). Advisory Circular 20-107b. pp: 1-37

[3] **F. Garattoni** (2011). "Crashworthiness and composite materials: development of an experimental test method for the energy absorption determination and implementation of the relative numerical model." PhD thesis. University of Bologna

[4] **H. Nikkhah, A. Baroutaji, A. Ghani Olabi** (2019). "Crashworthiness design and optimisation of windowed tubes under axial impact loading." ELSEVIER

[5] **F. Tarlochan, S. AiKhatib** (2017). "Energy absorption capabilities of complex thin walled structures." 4th Internacional Conference of Mechanical Engineering Research. IOP Publishing

[6] **W. Suzhen, Z. Gang, S. Guangyong, L. Qiang, L. Guangyao, L. Qing** (2016). "On design of milti-cell thin-walled structures for crashworthiness." ELSEVIER. Internacional Journal of Impact Engineering

[7] **The Aluminium Automotive Manual** (2013). Applications-Car Body-Crash Management Systems ELSEVIER. Internacional Journal of Impact Engineering. European Aluminium Association

[8] **A.Riccio, S.Saputo, A.Sellitto, A.Russo, F. Di Caprio, L.Di Palma** (2019). "An insight on the Crashworthiness Behavior of a Full-Scale Composite Fuselage Section at Different Impact Angles." Aerospace MDPI

[9] **G.L. Farley, R.M.Jones** (1989). "Energy-absorption capability of compsite tube and beams." NASA Technical Publications. TM 101634. pp: 1-248

[10] **C. Bisagni** (2009). "Experimental Investigation of the Collapse Modes and Energy Absorption Characteristics of Composite Tubes." Internacional Journal of Crashworthiness. Vol.14. No.4. pp: 365-378

[11] **A.G. Mamalis, D.E. Manolakos, M.B. Ioannidis, D.G. Chronopoulos, P.K. Kostazos** (2009). "On the crashworthiness of composite rectangular thin-

walled tubes internally reinforced with aluminium or polymeric foams: Experimental and Numerical simulation." ELSEVIER. Composite Structures

[12] **M. Ptak, P.Kaczynski, F.A.O. Fernandes, R.J. Alves de Sousa** (2017). "Assessing impact velocity and temperature effects on crashworthiness properties od cork material." ELSEVIER. Internacional Journal of Impact Engineering

[13] **P.Florent, Y.Wenyi, W.Cui'e** (2007). "Crushing modes of aluminium tubes under axial compression." 5th Australian Congress on Applied Mechanics. Brisbane Australia

[14] **A.G. Mamalis, D.E. Manolakos, M.B. Ioannidis, D.P. Papapostolou** (2004). "Crashworthy characteristics of axially statically compressed thin-walled square CFRP composite tubes: experimental." ELSEVIER. Composite Structures

[15] **E. Acar, M. Altin, M.A. Guler** (2019). "Evaluation of various multi-cell design conceptsfor crashworthiness design of thin-walled aluminium tubes." ELSEVIER. Thin-walled Structures

[16] **A.G. Mamalis, D.E. Manolakos, G.L. Viegelahn, S.M. Yap, G.A. Demosthenous** (1991). "On the axial crumpling of fibre-reinforced composite thin-walled conical shells." UK Inderscience

[17] **A.G. Mamalis, D.E. Manolakos, G.A. Demosthenous, W.Johnson** (1991). "Axial Plastic Collapse of Thin Bi-Material Tubes as Energy Dissipating Systems." Internacional Journal of Impact Engineering. Vol.11. No.2. pp: 185-196

[18] **U. Afaque, H.K. Bakhtawar, K. Salman, A. Azaz, M. Reyaz-Ur-Rahim** (2018). "Energy absorption, deformation and crushing behavior of bimetallic tubes with different cross-sectional shapes under axial loading." IOP Conference Series: Materials Science and Engineering

[19] **J.M. Alexander** (1960). "An approxiamte analysis of the collapse of thin cylindrical shells under axial loading." Imperial College of Science and Technology

[20] **W.Johnson, P.D. Soden, S.T.S. Al-Hassani** (1997). "Inextensional collapse of thin-walled tubes under axial compression." Journal of Strain Analysis. Vol. 12. No. 4

[21] **R. Uscinowicz** (2013). "Impact of temperature on shear strength of single lap Al-Cu bimetallic joint." ELSEVIER. Composites

[22] **M. Abbasi, A. Karimi Taheri, M.T. Salehi** (2001). "Growth rate of intermetallic compounds in Al/Cu bimetal produced by cold roll welding process." ELSEVIER. Journal of Alloys and Compounds

[23] **Livermore Software Technology Corporation** (2007). "LS-DYNA keyword user's manual." Vol. I. Version 971